

Aus dem Bereich Physiologie
Theoretische Medizin und Biowissenschaften
der Medizinischen Fakultät
der Universität des Saarlandes, Homburg/Saar

Intrazellulärer Interferon-Gamma-Transport und Interferon-Gamma-Sekretion in aktivierten CD8-T Lymphozyten

DISSERTATION

**zur Erlangung des Grades eines Doktors der theoretischen Medizin
der Medizinischen Fakultät
der UNIVERSITÄT DES SAARLANDES
2023**

vorgelegt von **Xuemei Li**
geboren am 23.12.1988 in Chongqing, China

Tag der Promotion: April 19, 2023

Dekan: Univ.-Prof. Dr. med. Michael D. Menger

Berichterstatter: PD. Dr. phil. nat. Elmar Krause

Univ.-Prof. Dr. rer. nat. Markus Hoth

Disclosure

This work was funded by: China Scholarship Council (CSC).

From: Nov. 3rd, 2018 till Nov. 2nd, 2022.

All experiments were supported and performed at the Department of Cellular Neurophysiology (formerly Prof. Dr. Jens Rettig) from Physiology Institute in Center for Integrative Physiology and Molecular Medicine (CIPMM), University of Saarland, 66424 Homburg, Germany.

Eidesstattliche Versicherung

(Erklärung gemäß § 7 Absatz 1 Nr. 2)

Ich erkläre hiermit an Eides statt, dass ich die vorliegende Arbeit ohne unzulässige Hilfe Dritter und ohne Benutzung anderer als der angegebenen Hilfsmittel angefertigt habe. Die aus anderen Quellen direkt oder indirekt übernommenen Daten und Konzepte sind unter Angabe der Quelle gekennzeichnet.

Bei der Auswahl und Auswertung folgenden Materials haben mir die nachstehend aufgeführten Personen in der jeweils beschriebenen Weise unentgeltlich geholfen:

1. Der elektronenmikroskopische Teil wurde von Dr. Claudia Schirra durchgeführt.
2. Die P815-Zielzellen wurden von Nicole Rothgerber gezüchtet.
3. Das Klonen des *pMAX-ifng-linker-mCherry* wurde von Dr. Keerthana Ravichandran durchgeführt.
4. Die WGA- und GzmB-Färbung auf den unterstützten Lipiddoppelschichten wurde von Dr. Hsin-Fang Chang durchgeführt.

Weitere Personen waren an der inhaltlich-materiellen Erstellung der vorliegenden Arbeit nicht beteiligt. Insbesondere habe ich nicht die entgeltliche Hilfe von Vermittlungs- bzw. Beratungsdiensten (Promotionsberaterinnen/Promotionsberater oder anderer Personen) in Anspruch genommen. Außer den Angegebenen hat niemand von mir unmittelbar oder mittelbar geldwerte Leistungen für Arbeiten erhalten, die im Zusammenhang mit dem Inhalt der vorgelegten Dissertation stehen.

Die Arbeit wurde bisher weder im Inland noch im Ausland in gleicher oder in ähnlicher Form in einem anderen Verfahren zur Erlangung des Doktorgrades einer anderen Prüfungsbehörde vorgelegt.

Ich versichere an Eides statt, dass ich nach bestem Wissen die Wahrheit gesagt und nichts verschwiegen habe.

Die Bedeutung der eidesstattlichen Erklärung und die strafrechtlichen Folgen einer unrichtigen oder unvollständigen eidesstattlichen Erklärung sind mir bekannt.

(Ort, Datum)

(Unterschrift der/des Promovierenden)

(Unterschrift der die Versicherung an Eides statt aufnehmenden Beamtin bzw. des aufnehmenden Beamten)

Acknowledgment

First, I would like to express my deepest gratitude and admiration to **Prof. Dr. Jens Rettig** for providing me with an excellent international platform for my Ph.D. studies. He provided me with great help and support during my doctoral studies in terms of scientific proposals and expenses.

I especially thank my supervisor **PD. Dr. Elmar Krause** for his great support and helpful discussions on scientific ideas and methodological issues such as FACS and SIM. With his continued guidance, I was able to complete my Ph.D. work.

I would also like to thank **Dr. Varsha Pattu** for providing me with initial scientific support in my Ph.D. work.

I would like to express my gratitude to **PD. Dr. Ute Becherer** introduced me to TIRF-microscopy and **Dr. Claudia Schirra** for excellent CLEM imaging. I also thank **Dr. Hsin-Fang Chang** for her help with my experiment.

I would like to thank **Anja Ludes, Margarete Klose, Silke Bruns-Engers, Nicole Rothgerber,** and **Katrin Sandmeier** for their excellent technical assistance. Special thanks go to the secretary **Bernadette Schwarz** and the CRC894 coordinator **Andrea Berger**, who kindly supported me in all administrative issues.

Further, thanks go to **Dr. Keerthana Ravichandran, Dr. Micheal Estl, Ibrahim Omnia Mohmed Khamis, Marie-Louise Wirkner,** and other Ph.D. students for scientific discussion and help with protocols.

Last but not least, my gratitude goes to **my beloved family** who gave me the necessary and irreplaceable support, companionship, and an unforgettable time when I study abroad.

Content

List of abbreviations.....	9
List of Figures.....	13
Abstract	15
Zusammenfassung.....	16
1. Introduction.....	18
1.1 Immune system.....	18
1.2 CD8+ T-lymphocytes.....	19
1.2.1 CD8+ T-lymphocytes activation and differentiation.....	19
1.2.2 CD8+ T-lymphocyte effector mechanisms.....	21
1.3 CGs exocytosis and classification.....	22
1.4 Interferon-gamma	24
1.4.1 Interferon-gamma production and function.....	24
1.4.2 Molecular characteristics of IFN γ	27
1.4.3 Interferon-gamma signaling pathway.....	27
1.4.4 Interferon-gamma trafficking and secretion	28
1.5 Major goals of the thesis	30
2. Material and Methods	31
2.1 Material	31
2.1.1 Chemicals	31
2.1.2 Commercial Kits	33
2.1.3 Antibodies.....	33
2.1.4 Medium and solution.....	34
2.1.5 Mouse models.....	35
2.2 Methods.....	35
2.2.1 Isolation of primary CD8+ T-lymphocytes	35
2.2.2 Culture of primary CD8+ T-lymphocytes	35
2.2.3 Electroporation.....	37
2.2.4 P815 cell culture	37
2.2.5 <i>pMax-IFNγ-linker-pHuji</i> Cloning	37
2.2.6 Western blot.....	41
2.2.7 Immunocytochemistry.....	41
2.2.8 Structured illumination microscopy (SIM).....	41
2.2.9 Total internal reflection fluorescence microscopy (TIRF-M).....	42
2.2.10 Correlative light and electron microscopy (CLEM).....	42
2.2.11 Flow cytometry and enzyme-linked immunosorbent assay.....	44

2.2.12 <i>In vitro</i> live cell imaging	47
2.2.13 Data analysis	47
3. Results.....	48
3.1 IFN γ -production needs anti-CD3 ϵ restimulation in activated CTLs	48
3.2 Quantification of activated CTL subsets during restimulation.....	49
3.3 Localization and trafficking of IFN γ in CTLs.....	51
3.3.1 Verification of a homemade <i>pMax-linker-IFNγ-mCherry</i> construct.....	51
3.3.2 Live cell imaging of the conjugation between CTLs and P815 target cells	52
3.3.3 Super-resolution SIM analysis of IFN γ localization in CTLs.....	53
3.4 Subcellular morphology of IFN γ compartments – TEM and CLEM.....	56
3.5 Live cell imaging of IFN γ secretion with TIRF-M.....	58
3.5.1 Usability of a pH-sensitive IFN γ -pHuji expression construct	58
3.5.2 The majority of fusion events at the IS are IFN γ /GzmB joint fusions	60
3.5.3 IFN γ and GzmB are released at the IS by both SCGs and MCGs	62
3.6 IFN γ release from CTLs is strongly regulated by TCR activation and dependent on the SNARE-associated protein Munc13-4.	65
3.6.1 IFN γ secretion is abrogated in Munc13-4 deficient CTLs.....	65
3.6.2 Quantification of IFN γ in the surrounding environment	66
4. Discussion.....	68
4.1 IFN γ expression and release from CTLs are TCR dependent and its release takes place at the IS	68
4.2 Implications on familial haemophagocytic lymphohistiocytosis (FHL).....	69
4.3 IFN γ expression in the endogenous and overexpressing system	70
4.4 IFN γ localization in immune cells	71
5. Outlook	73
6. Reference	74
7. Publication.....	81
8. Curriculum Vitae.....	82

List of abbreviations

	%	Percentage
	°C	Degrees Celsius
	µg	Microgram
	µL	Microliter
	µM	Micromolar
	#, n or N	Number
A	ANOVA	Analysis of variance
	APC	Antigen-presenting cells or Allophycocyanin
B	BSA	Bovine serum albumin
C	CaCl ₂	Calcium chloride
	CD	Cluster of differentiation
	CO ₂	Carbon dioxide
	CTLs	Cytotoxic T-lymphocytes
	CGs	Cytotoxic granules
	CLEM	Correlative fluorescence light and electron microscopy
	cSMAC	Central supra-molecular activation cluster
D	DMSO	Dimethyl sulfoxide
	DPBS	Dulbecco's phosphate-buffered saline
	dSMAC	Distal supra-molecular activation cluster
E	ER	Endoplasmic reticulum
	<i>E. coli</i>	<i>Escherichia coli</i>
	EDTA	Ethylenediaminetetraacetic acid
	ELISA	Enzyme-linked Immunosorbent Assay
	Endo.	Endogenous
	<i>et al.</i>	et alia
F	Fab	Fragment antigen-binding
	FasL	Fas ligand
	FCS	Fetal calf serum
	FHL	Familial hemophagocytic lymphohistiocytosis
H	h	Hour
	HEPES	4-(2-Hydroxyethyl)-1-piperazineethanesulfonic acid
	H+L	Heavy + Light
	HPLC	High-performance liquid chromatography
	HRP	Horseradish peroxidase
	HSC	Hematopoietic stem cells
I	ICAM	Intercellular Adhesion Molecule

	ICC	Immunocytochemistry
	IFN γ / <i>ifng</i>	Interferon-gamma
	IFNGR	Interferon-gamma receptor
	IgG	Immunoglobulin G
	IL	Interleukin
	IP	Immunoprecipitation
	IS	Immunological synapse
	ITAMs	Immunoreceptor tyrosine-based activation motifs
G	GzmB	Granzyme b
K	kb	Kilobase
	KCl	Potassium chloride
	kDa	Kilodalton
	KI	Knockin
	KO	Knockout
L	L	Liter
	LAMP1	Lysosomal-associated membrane protein
	LB	Lysogeny broth
	CGs	Lytic granules
M	m	Mili
	M	mol/L
	MAFA	Multiple Analyte Flow Assay
	MAPK	Mitogen-activated protein kinases
	MCGs	Multiple core granules
	min	Minute
	MHC	Major histocompatibility complex
	MgCl ₂	Magnesium chloride
	MgSO ₄	Magnesium sulfate
	mL	Milliliter
	mm	Millimeter
	mM	Millimolar
	mmol	Millimole
	mTFP	Monomeric-Teal fluorescent protein
	MTOC	Microtubule-organizing center
	Munc13	Mammalian uncoordinated-13
	MW	Molecular weight
N	NaCl	Sodium chloride
	NC	Nitrocellulose
	NH ₄ Cl	Ammonium chloride

	NaHCO ₃	Sodium bicarbonate
	NaH ₂ PO ₄	Monosodium phosphate
	Na ₂ HPO ₄	Disodium phosphate
	NK	Nature killer cell
	nm	Nanometer
	N/n	Number
O	Osm	Osmoles
	Overexp.	Overexpression
P	<i>p</i>	Probability value
	PALS	Periarteriolar lymphoid sheath
	PBS	Phosphate-buffered saline
	PCC	Pearson's correlation coefficient
	PCR	Polymerase chain reaction
	PE	Phycoerythrin
	PFA	Paraformaldehyde
	pH	Potential hydrogen
	pg	picogram
	pmol	Picomole
	prf	Perforin
	pSMAC	Peripheral supra-molecular activation cluster
R	rpm	Revolutions per minute
	RT	Room temperature
S	SA-PE	Streptavidin-phycoerythrin
	SCGs	Single core granules
	SDS	Sodium dodecyl sulfate
	s	Second
	SEM	Standard error of the mean
	SIM	Structure illumination microscopy
	SGs	Secretory granules
	SMAPs	Supramolecular attack particles
	SNAP	Synaptosomal-associated protein
	SNAREs	Soluble N-ethylmaleimide-sensitive factor attachment protein (SNAP) receptor
	StdDev	Standard deviation
T	T-bet	T-box transcription factor TBX21
	TBS	Tris-buffered saline
	TBST	Tris-buffered saline + Tween 20
	TCR	T-lymphocyte receptor
	TEM	Transmission electron microscopy

	TIRF-M	Total internal reflection fluorescence microscopy
	TNF	Tumor necrosis factor
	t-SNARE	Target-SNARE
U	U	Units
	UV	Ultraviolet
V	V	Volt
	VAMP	Vesicle-associated membrane protein
	VS.	Versus
	v-SNARE	Vesicular-SNARE
W	WB	Western blot
	WBC	White blood cell
	WT	Wild-type

List of Figures

Figure 1. Immune cell development.	18
Figure 2. Mouse splenocytes stained for B- and T-lymphocytes.	19
Figure 3. Scheme of CD8+ T-lymphocyte activation, differentiation, and effector mechanism.	20
Figure 4. Development of CD8+ T-lymphocytes from naïve to memory.....	21
Figure 5. Synapse assembly, function, and disassembly in cytotoxic T-lymphocytes.	23
Figure 6. MCG, a newly classified cytotoxic granule, is the source of SMAPs.	24
Figure 7. IFN γ production and signaling.	25
Figure 8. IFN γ action on immune and non-immune cells.....	26
Figure 9. Regulated and constitutive exocytosis of cytokines.	29
Figure 10. Positive isolation of CD8+ T-lymphocytes from mouse spleen and T-lymphocytes culture.	36
Figure 11. Vector map of <i>pMax-ifng-linker-mCherry</i> with restriction enzymes.	38
Figure 12. Sample preparation and operation procedure for the correlative light and electron microscopy.	43
Figure 13. Assay procedure summary for supernatant IFN γ measurement.	45
Figure 14. Assay procedure summary for supernatant IFN γ measurement.	46
Figure 15. Intracellular IFN γ and GzmB in activated CTLs detected by flow cytometry.	49
Figure 16. Effector- and central memory cell populations during restimulation.	50
Figure 17. IFN γ -mCherry detection using Western Blot and immunocytochemistry.	52
Figure 18. Conjugation of CTLs and P815 cells.	53
Figure 19. IFN γ partially colocalizes with GzmB.....	54
Figure 20. IFN γ robustly colocalizes with GzmB at different conditions.	56
Figure 21. IFN γ and GzmB exist in the same compartments.....	57
Figure 22. Validation of a <i>pMax-ifng-linker-pHuji</i> construct.	59
Figure 23. IFN γ and GzmB secretion observed by TIRF-M.....	62
Figure 24. IFN γ and GzmB are released from both SCGs and MCGs.	64
Figure 25. The exocytosis of IFN γ - and GzmB-containing vesicles is abrogated in Munc13-4 KO CTLs.	65

Figure 26. Quantification of IFN γ concentration in CTLs culture. 67

Abstract

CD8⁺ cytotoxic T-lymphocytes (CTLs) are important guardians to protect us from infection and disease by killing viral-infected cells and tumor cells. The effector mechanisms of CTLs are composed of perforin (Prf) and granzyme B (GzmB) causing targets death and Fas/FasL interaction inducing targets apoptosis. Besides the effector function, CTLs have immunosurveillance and immunomodulatory functions by producing and secreting Interferon-gamma (IFN γ). IFN γ and TNF alpha (TNF α) mediated anti-microbe and anti-tumor effects. IFN γ binds to the Interferon-gamma receptors (IFNGRs) on the surrounding cells' surface and triggers the IFN γ -signaling pathway which can induce a series of effects on immune cells. My thesis aims to understand under which conditions IFN γ is produced by CTLs and how it is released to the extracellular space.

We showed that IFN γ was tremendously produced in CTLs upon a few hours of anti-CD3 ϵ restimulation and the more mature the CTLs were, the faster IFN γ was produced. The effector memory and effector T-lymphocytes were the major sources of IFN γ . Though it had been shown that IFN γ was directed to and secreted at the immunological synapse (IS) from T-lymphocytes, the trafficking and secretion process of IFN γ hadn't been well-studied yet in CD8⁺ CTLs.

In my thesis, it was described by quantification of the intracellular and supernatant IFN γ that both IFN γ -production and IFN γ -secretion were regulated by TCR/CD3 ϵ engagement. Most of the IFN γ shared a common secretion process with GzmB upon an anti-CD3 ϵ restimulation as I could show by using structured illumination microscopy (SIM), correlative light and electron microscopy (CLEM), and total internal reflection fluorescence microscopy (TIRF-M). Using GzmB-mTFP KI mice, we found that IFN γ extensively colocalized with GzmB-containing vesicles, most of which compartmentalized in dark core (DC) and amorph vesicles. In addition, we observed that usually IFN γ and GzmB were secreted together by the same vesicle to the IS. IFN γ could be released from multi-core granules (MCGs) besides single-core granules (SCGs) and more interestingly, it was also found in supramolecular-attack-particles (SMAPs). Using a Munc13-4 knockout mouse, we demonstrated that Munc13-4, a SNARE-associated protein involved in CGs trafficking and priming, was also a critical factor for IFN γ secretion. Munc13-4 knockout resulted in a deficiency of IFN γ and GzmB secretion. In summary, I was able to show for the first time that IFN γ has an identical secretion pathway to GzmB and occurs together with GzmB in SMAPs and reclassified MCGs alongside SCGs, and it is released at the IS. In addition to the already known secretion deficiency for GzmB in Munc13-4 knockout mice, to the best of our knowledge, for the first time, IFN γ secretion is also abrogated in Munc13-4 KO mice.

Zusammenfassung

CD8⁺ zytotoxische T-Lymphozyten (CTLs) sind wichtige Wächter des Immunsystems, die uns vor Infektionen und Krankheiten schützen, indem sie virusinfizierte Zellen und Tumorzellen abtöten. Die Effektormechanismen von CTLs bestehen aus der Sekretion der zytotoxischen Substanzen Perforin (Prf) und Granzym B (GzmB) und der Fas Ligand und Fas Rezeptor (Fas/FasL)-Interaktionen, welche die Apoptose der Zielzellen induzieren. Neben der Effektorfunktion haben CTLs Immunüberwachungs- und immunmodulatorische Funktionen, indem sie Zytokine, wie IFN γ produzieren und sezernieren. IFN γ und TNF-alpha (TNF α) haben hierbei anti-mikrobielle und anti-Tumor Wirkungen. IFN γ bindet an die Interferon-Gamma-Rezeptoren (IFNGRs) auf der Oberfläche der umgebenden Zellen und löst den IFN γ -Signalweg aus, welcher eine Reihe von Wirkungen auf Immunzellen hat. Das Ziel meiner Doktorarbeit war es, zu verstehen, unter welchen Bedingungen IFN γ von CTLs produziert wird und wie es in den extrazellulären Raum abgegeben wird.

Wir zeigten, dass IFN γ in CTLs nach einigen Stunden Anti-CD3 ϵ -Restimulation in enormen Mengen produziert wurde. Dabei korrelierte der Reifestand der Lymphozyten positiv mit der Fähigkeit IFN γ zu produzieren. Effektor-Memory oder Effektor Lymphozyten waren die größten Quellen von IFN γ . Obwohl bereits gezeigt wurde, dass IFN γ von T-Lymphozyten zur Immunologische Synapse (IS) geleitet und dort sezerniert wird, war der Transport- und Sekretionsprozess von IFN γ in CD8⁺-CTLs bislang noch nicht gut untersucht.

In meiner Dissertation wurde durch Quantifizierung des intrazellulären und sekretierten IFN γ beschrieben, dass sowohl die IFN γ -Produktion als auch die IFN γ -Sekretion durch TCR/CD3 ϵ -Engagement reguliert werden. Der größte Teil des IFN γ teilte einen gemeinsamen Sekretionsprozess mit GzmB nach einer Anti-CD3 ϵ -Restimulation, wie ich durch die Verwendung von strukturierter Beleuchtungsmikroskopie (SIM), korrelativer Licht- und Elektronenmikroskopie (CLEM) und Fluoreszenzmikroskopie mit totaler interner Reflexion (TIRF-M) zeigen konnte. Unter Verwendung von GzmB-mTFP-KI-Mäusen fanden wir heraus, dass IFN γ überwiegend mit GzmB-enthaltenden Vesikeln kolokalisiert ist. Außerdem beobachteten wir, dass IFN γ und GzmB gemeinsam an der IS sezerniert werden. IFN γ konnte nicht nur aus Single core granules (SCGs), sondern auch aus Multi-Core-Granulen (MCGs) freigesetzt werden und es wurde interessanterweise in „Supramolecular-Attack-Particles“ (SMAPs) gefunden. Durch die Verwendung einer Munc13-4-Knockout-Maus konnte ich zeigen, dass Munc13-4, ein SNARE-assoziiertes Protein, das am Transport und Priming von CGs beteiligt ist, notwendig für die IFN γ -Sekretion ist. Der Knockout von Munc13-4 führte zu einer Reduzierung der IFN γ - und GzmB-Sekretion. Zusammenfassend konnte ich zum ersten Mal zeigen, dass IFN γ einen identischen Sekretionsweg wie GzmB hat und zusammen mit GzmB in SMAPs und reklassifizierten MCGs neben SCGs vorkommt und in der IS freigesetzt wird. Neben dem bereits

bekanntem Sekretionsmangel für GzmB in Munc13-4-Knockout-Mäusen wird unseres Wissens nach erstmals auch die IFN γ -Sekretion in Munc13-4-KO-Mäusen außer Kraft gesetzt.

1. Introduction

1.1 Immune system

The immune system (including innate and adaptive immune systems) is a large complex network of organs, white blood cells (WBCs), proteins (antibodies), and chemicals. The immune organs/tissues include central lymphoid organs (CLOs) and peripheral lymphoid organs (PLOs). CLOs include bone marrow and thymus, places for lymphocyte generation and maturation. PLOs include lymph nodes, spleen, appendix, adenoid, tonsil, skin, mucous membranes, and other first-line defenses for initiating adaptive immune responses and maintaining lymphocytes. The pluripotent hematopoietic stem cells (pHSC) from the bone marrow can differentiate into different WBCs (Figure 1) (Janeway et al., 2001).

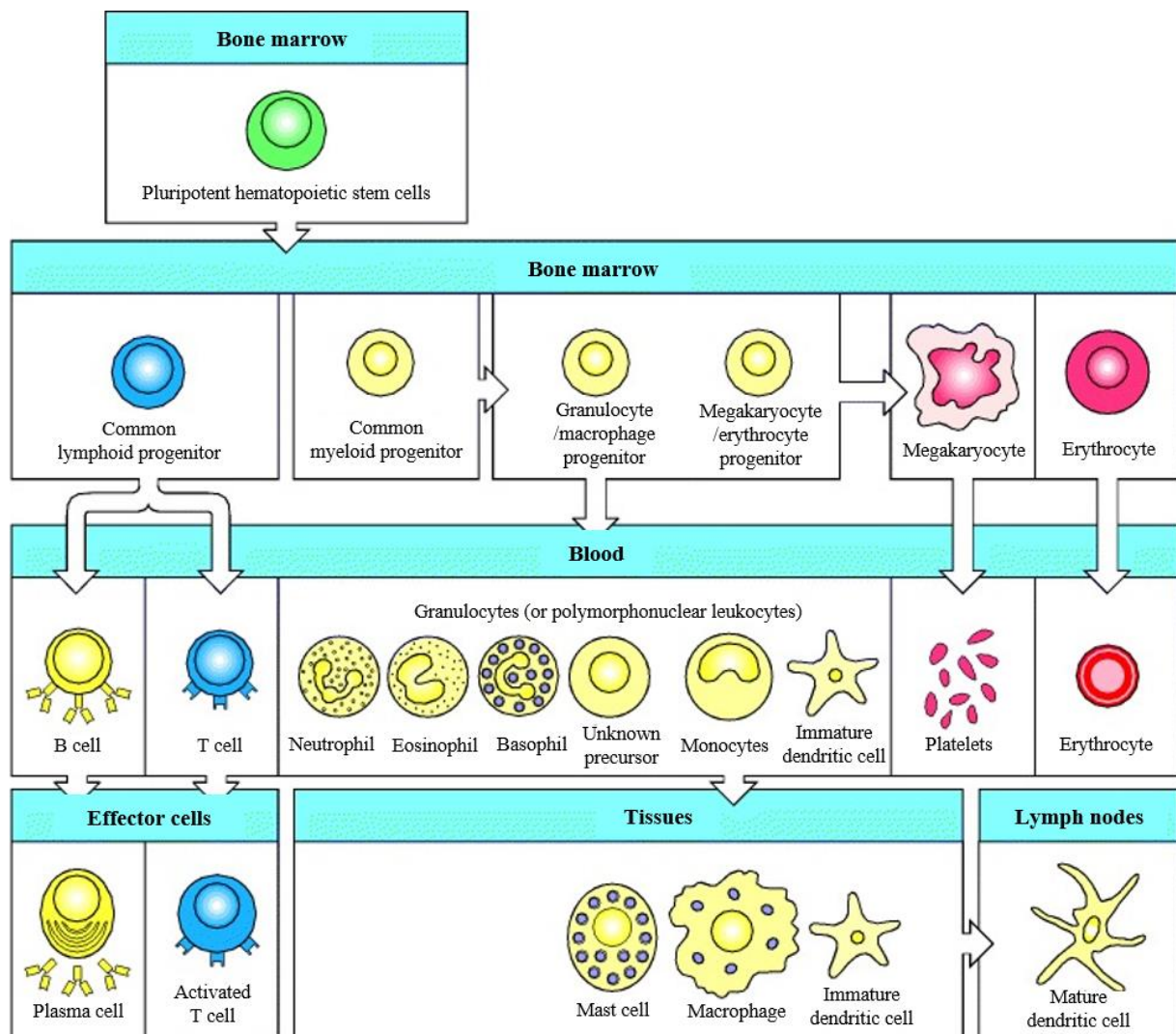


Figure 1. Immune cell development.

All cellular elements of blood, including the lymphocytes, arise from pluripotent hematopoietic stem cells in the bone marrow (scheme from Janeway et al., 2001).

Most T-lymphocytes reside in lymph nodes and part of them is in the spleen. The spleen captures antigens from the blood, gets rid of aged red blood cells, and is composed of red and white pulp. The red pulp disposes of red blood cells, while the white pulp area consists of T and B lymphocytes in its internal region which is compartmentalized as a periarteriolar lymphoid sheath (PALS). After having removed blood cells from the smashed spleen, the rest are splenocytes which mainly contain B- lymphocytes (44-58%) and T-lymphocytes (21-25%), and a few monocytes (3.5-5%), dendritic cells (1-3%), granulocytes (1-2%), natural killer cells (1-2%) and macrophages (1-2%) (Figure 2).

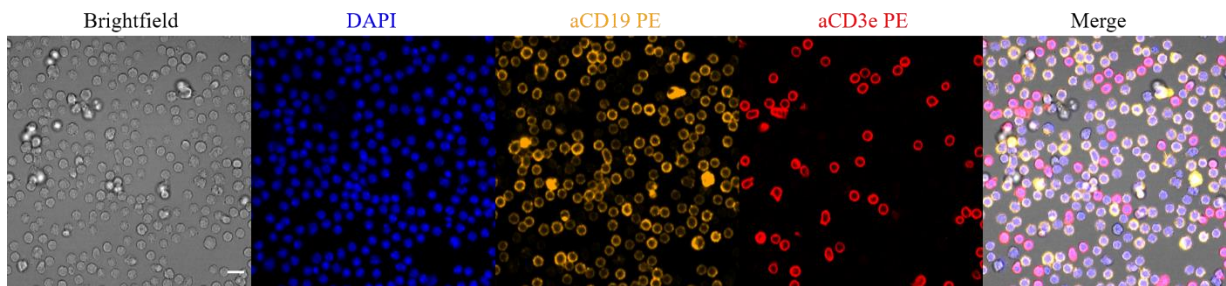


Figure 2. Mouse splenocytes stained for B- and T-lymphocytes.

C57/BL6N splenocytes were stained with DAPI (nuclei), anti-CD19 PE (B cells), and anti- CD3 ϵ Alexa 647 (CD4+ and CD8+ T-lymphocytes) as indicated above images. Scale bar, 10 μ m.

The innate and adaptive immune systems work together to protect us from foreign invaders (bacteria, viruses, parasites, fungi, and abnormal cells) that cause infection and disease. When pathogens invade the body, the body produces WBCs to fight against the infection. The WBCs identify the pathogens through pattern recognition receptors (PRRs), produce antibodies or cytotoxic granules and cytokines to fight against them, and recruit immune or non-immune cell responses. They also have a memory of invading pathogens which is the basis of vaccinations. Vaccination exposes the immune system to a dead or weakened microbe, or protective antigens (i.e. proteins) from the pathogens so that the body can recognize and respond fast to any future exposure to the same microbe. For microbial invasion, B-lymphocytes play a critical role in humoral immunity. For viral infection or tumor cells, natural killer (NK) and CD8+ T-lymphocytes are the major guardians of cellular immunity. Here, we study the biological features of murine CD8+ T-lymphocytes and Interferon-gamma trafficking and secretion in murine CTLs.

1.2 CD8+ T-lymphocytes

1.2.1 CD8+ T-lymphocytes activation and differentiation

Naïve CD8+ T-lymphocytes have few cytoplasmic organelles and condensed nuclear chromatin. The presentation of an antigen by a specialized antigen-presenting cell (APC) is necessary to trigger the

proliferation and differentiation of CTLs to gain effector function (Janeway et al., 2001; Stemberger et al., 2007). Their activation requires three signals from APC (Figure 3). Initially, the T-lymphocyte receptor (TCR) on CD8+ T-lymphocytes recognizes the antigen peptides presented by major histocompatibility complex class I molecules (pMHC-I) from APC. Secondly, costimulatory signals are required, such as the binding of CD80 or CD86 from the APC to the CD28 molecule expressed by the CD8+ T-lymphocyte. Finally, an alarm signal is produced by APC, such as IL-12, IL-18, and type I Interferon (IFN), inducing surrounding naïve CD8+ T-lymphocyte activation and immune response of other cells (Curtsinger et al., 2003 & 2005; Cox et al., 2011).

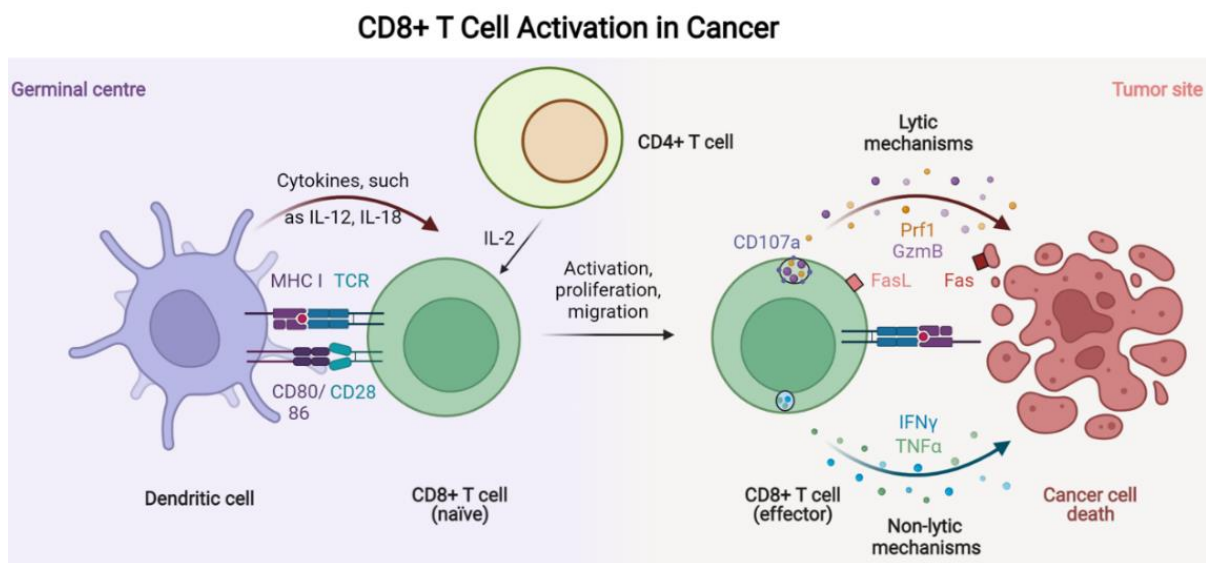


Figure 3. Scheme of CD8+ T-lymphocyte activation, differentiation, and effector mechanism.

Left: Naïve CD8+ T-lymphocytes are activated by the binding of their TCR to the antigen peptide presented by MHC1 together with the binding of CD80/86 surface proteins of dendritic cells (DC) by CD28 receptor from CTLs (co-stimulation). Cytokine release from DC and CD4+ T-lymphocytes is also indispensable for CD8+ T-lymphocyte activation and differentiation. Right: CTLs exert their cytotoxicity mainly by degranulation of cytotoxic substances GzmB and Prf1 to targets, which is accompanied by the appearance of CD107a (LAMP1) on the cell membrane. In addition, Fas/FasL interaction has an effector function. Last, CTLs effector cytokines, such as IFN γ and TNF α , exert various antiviral, antitumor, inflammatory, and immunomodulatory functions.

Accompanying the initial activation, CD8+ T-lymphocytes produce IL-2 along with IL-2R (CD25) immediately and undergo clonal expansion, generating a large pool of effector cells that can produce and release high levels of cytokines and cytotoxic molecules (Figure 3) (Hamann et al., 1997; Wolint et al., 2004; Kaech et al., 2007; Miller et al., 2008). Additionally, effector CD8+ T-lymphocytes (T_E) acquire the ability to migrate to peripheral tissues (Weninger et al., 2002). T_E undergo apoptosis in the contraction phase after clonal expansion (Figure 4). In the later stage of the contraction phase, there is a transient refractory period when CD8+ T-lymphocytes sustain partial effector functions but lose the ability to produce IL-2 (Deeths et al., 1999). T_E need external IL-2 mainly produced by Th1 cells to keep proliferation ongoing and recover full functional ability (Figure 3) (Tham et al., 2002).

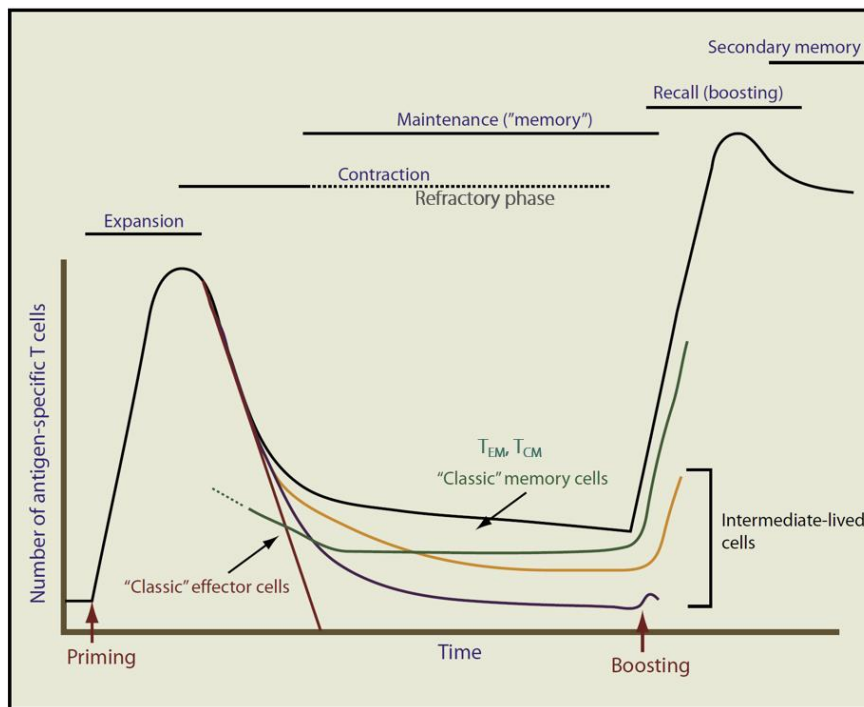


Figure 4. Development of CD8+ T-lymphocytes from naïve to memory.

The scheme of the kinetics of antigen-specific T-lymphocyte-number (black line) at different phases of the acute immune response. During the primary response, the fate of classical effector (dark red line) and memory (green line) cells is shown. The intermediate-lived cells, which may also contribute to protection from reinfection, are shown in blue and orange lines. With a boost, memory cells are recalled and developed more efficiently killing T-lymphocytes (from Jameson & Masopust, 2009).

Finally, only a few activated cells are maintained as long-term memory T-lymphocytes (T_M) which comprise at least two subtypes: central memory (T_{CM}) and effector memory (T_{EM}) T-lymphocyte (Sallusto et al., 1999 & 2004). In the mouse, short-living T_E express some IL-7 receptor alpha chains (CD127) and downregulate L-selectin (CD62L) (Huster et al., 2004). Long-living T_M constitutively expressed CD127. T_{CM} (CD62L^{high}) highly express CD62L and T_{EM} (CD62L^{low}) downregulate CD62L. T_E prefer migrating to nonlymphoid tissues, where some survive as T_{EM} for long periods (Masopust et al., 2001; Reinhardt et al., 2001). T_{EM} can recover effector functions quickly but proliferate poorly upon antigen stimuli. In contrast, most T_{CM} are homing to lymphoid organs and robustly re-expand upon the second attack. This memory phase can last the whole life of the individual (Figure 4) (Lanzavecchia & Sallusto, 2000; Wherry et al., 2004). T_M can differentiate into T_E once they receive activation signals, obtaining a high ability for cytokine production and cytotoxicity (Akondy et al., 2017).

1.2.2 CD8+ T-lymphocyte effector mechanisms

Effector CD8+ T-lymphocytes, also called cytotoxic T-lymphocytes (CTLs) play a critical role in immune surveillance and defense against pathogens and cancer (Zhang & Bevan, 2011). CTLs effector

functions include lytic (cytotoxic granules) and non-lytic (cytokine production) mechanisms (Figure 3) (Perdomo-Celis et al., 2019). The T-bet, Eomes, CRTAM, T-box and Runx families of transcription factors are regulators of CTLs effector functions (Cruz-Guilloty et al., 2009; Takeuchi et al., 2009; Paley et al., 2012). CTLs' killing ability is determined by their cytotoxic granules (CGs) and degranulation capacity (Betts & Koup, 2004). CGs are secretory lysosomes (SGs) containing cytotoxic substances, such as granzymes and perforin (Peters et al., 1991). Granzymes are serine proteases that finally lead to target apoptosis. Perforin is a glycoprotein responsible for pore formation in the cell membranes of targets (Lieberman, 2003). The membrane of CGs is a lipid bilayer containing lysosome-associated membrane glycoproteins (LAMP), including LAMP-1 (CD107a), LAMP-2 (CD107b), and LAMP-3 (CD63) (Fukuda, 1998). During the degranulation, cytotoxic substances are released by exocytosis once the CG membrane fuses with the plasma membrane of the CTLs (Paley et al., 2012). Interestingly, the surface of the resting CD8+ T-lymphocyte doesn't show LAMP molecules making the surface expression of CD107a/b, a quantitative marker for regulated degranulation (Betts & Koup, 2004). In addition, CGs also contain the membrane pore-forming protein granulysin (Stenger et al., 1998), the proteoglycan matrix protein serglycin (Metkar et al., 2002), the perforin inhibitor calreticulin (Dupuis et al., 1993), and the lysosomal enzymes cathepsins (Balaji et al., 1995). Moreover, Fas-ligand (CD95L), an apoptosis-inducer, is stored in specialized SG of CD8+ T-lymphocytes and the degranulation process controls its expression at the cell surface (Bossi & Griffiths, 1999). CD8+ T-lymphocytes express both Fas-receptor (Fas) and FasL on the surface, the interactions of Fas/FasL are a mechanism by which CD8+ T-lymphocytes can kill each other, called CTL-fratricide, to eliminate effector T-lymphocytes during the contraction phase. Last, and most important for my thesis, CTLs effector function is also mediated by the release of IFN γ and TNF α , which exert a variety of antitumor, antimicrobial, and inflammation functions, and IFN γ attends in immunomodulation and can upregulate the Fas expression on the targets (Figure 3).

1.3 CGs exocytosis and classification

The regulated exocytosis of CGs takes place at a specialized CTL-targets interface called the immunological synapse (IS) (Bossi & Griffiths, 1999). The IS formation is transient and requires the transport and assembly of a multiplex of organelles and proteins toward the contact zone. After the recognition of pMHC-I complexes presented on the target cells by TCR, a supramolecular activation cluster consisting of central proteins (cSMAC), peripheral proteins (pSMAC), and distal proteins (dSMAC) is formed (Huppa & Davis, 2003; Griffiths et al., 2010; Dustin et al., 2010). CGs are then transported, along microtubules toward the IS (Stinchcombe et al., 2006; Qu et al., 2011). This process is believed to be organized by the microtubule-organizing center which is localized straightly underneath the IS (Stinchcombe et al., 2011). The CGs are anchored by the docking process and rendered fusion

competent by priming before exocytosis (Fischer et al., 2007). Only primed CGs enter the fusion process and release cytotoxic molecules into the synaptic cleft. The CGs fusion process is regulated by a SNARE complex consisting of the t-SNAREs (Syntaxin11 and SNAP-23) on the target plasma membrane (Stow et al., 2006; Halimani et al., 2013) and a v-SNARE on the CG membrane (Figure 5). The v-SNARE from humane CTLs was identified as the vesicle-associated membrane protein/synaptobrevin 7 (VAMP7/Syb7) (Chitirala et al., 2019) and that from mouse CTLs was VAMP2/Syb2 (Matti et al., 2013). Some more proteins are associated with CGs trafficking and fusion. The interaction of Rab27a with Munc13-4 is involved in the CGs docking and priming process (Figure 5) (Elstak et al., 2011; Johnson et al., 2011). In mouse CTLs, Munc13 isoforms are responsible for the priming process of CGs (Dudenhöffer-Pfeifer et al., 2013), and synaptotagmin 7 (Sy7) serves as a Ca^{2+} sensor and is involved in Ca^{2+} -dependent CGs trafficking and fusion (Figure 5) (Sleiman et al, 2020).

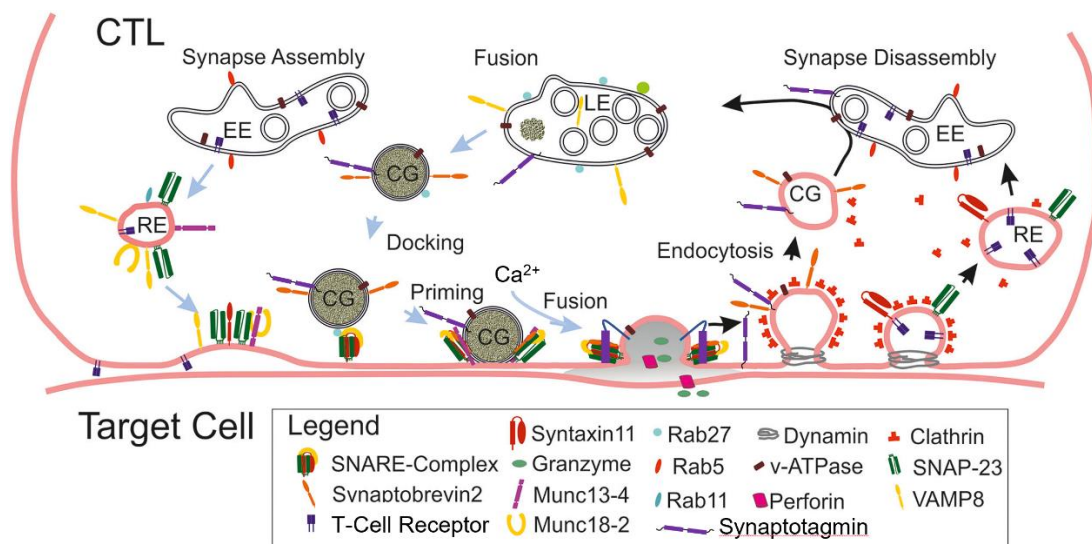


Figure 5. Synapse assembly, function, and disassembly in cytotoxic T-lymphocytes.

The assembly of the immunological synapse (IS) begins with the fission of recycling endosomes (RE) from the early endosomes (EE) (left). The RE is transported to and fuses with the plasma membrane. RE delivers proteins that are required for subsequent docking, priming, and fusion of cytotoxic granules (CGs). After maturation via late endosomes and lysosomes (middle), CGs are delivered to the plasma membrane where they anchor (docking). After priming under the control of Munc13-4 and being mediated by the Ca^{2+} sensor synaptotagmin, the SNARE complex drives membrane fusion. Recycling CGs are returned to the cytoplasm via endocytosis (right) where they fuse with the EE and are then trafficked to the LE (modified from Rettig & Stevens, 2017).

Recently, Chang and her colleagues classified a new class of vesicles that fulfill cytotoxic functions (Chang et al., 2022). According to its appearance in electron microscopy, Chang et al. discriminate single core granule (SCG) from multi-core granule (MCG). SCG and MCG differed in morphologies and proteomics. Transmission and scanning electron microscopy showed that SCG contained a single dense core and had a uniform diameter of 150 nm. MCG contained multiple cores and varying diameters between 200 and 350 nm. Mass spectrometry demonstrated that both granules contained large amounts of GzmB. However, the SCG was lysosomal-like, containing cathepsins, while the MCG was more

heterogeneous, containing endosomal-like proteins (such as Rabs) and supramolecular attack particles (SMAP)-associated proteins. Light microscopic super-resolution images and electron microscopy revealed thrombospondin 1 (TSP1), and GzmB as characteristic content of MCGs while only GzmB is typical for SCGs. Both vesicle types fused at the IS (Figure 6). Chang et al. also found that MCGs were more efficient in the killing of target cells in the long term when compared to SCGs (19 h). In conclusion, it seemed that soluble Prf1 and GzmB are directly released to the targets precisely through the IS via SCGs, while SMAPs are released via MCGs, stay on the surface of targets and keep active for hours. The SMAPs had a cytotoxic core of Prf1, GzmB, and Srgn, dominantly surrounded with a coat of TSP-1 and galectin-1 (Gal-1). In both mice and human CTLs, SMAPs were stored in MCGs and, following release, they were able to kill target cells autonomously and composited chemoattraction through chemokine ligand 5 (CCL5) and immunomodulatory by IFN γ (Balint et al., 2020). Human NK cells could also secrete SMAPs as CTLs but they were larger than CTLs' SMAPs (Ambrose et al., 2020).

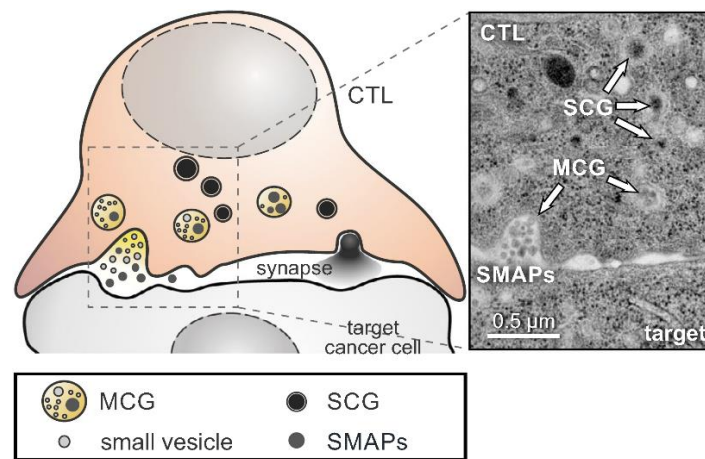


Figure 6. MCG, a newly classified cytotoxic granule, is the source of SMAPs.

Proposed model of cytotoxic T-lymphocytes that contains two classes of CGs (MCG and SCG), both of which can fuse in parallel at the immunological synapse (left). While the SCG content diffuses rapidly after release, MCGs deposit supramolecular attack particles (SMAPs) that retain their integrity in the synaptic cleft. The latter is illustrated in the exemplary electron micrograph on the right (from Chang et al., 2022).

1.4 Interferon-gamma

1.4.1 Interferon-gamma production and function

Interferon-gamma (IFN γ) was first recognized based on its antiviral function in the 1960s (Wheelock, 1965), and it was characterized based on the inducing properties and cell-type expression patterns that differ from the classical virus-induced Interferons. IFN γ is the only member of the type II Interferon family and is unrelated to the Type I Interferons at both the genetic and the protein levels (Gray & Goeddel, 1982). Moreover, IFN γ production is induced by a unique set of stimuli such as cytokines (IL-12 and IL-18) or antigens (Figure 7) (Kambayashi et al., 2003). It is mainly produced by innate lymphoid

cells (ILCs), such as natural killer (NK) cells, and adaptive immune cells, such as T helper 1 (Th1) cells and CD8+ CTLs (Figure 7) (Ivashkiv, 2018). CD8+ T-lymphocytes represent the majority of IFN γ + cells in the lymph nodes (~70%) and the second major population of IFN γ -producing cells in the spleen (~30%).

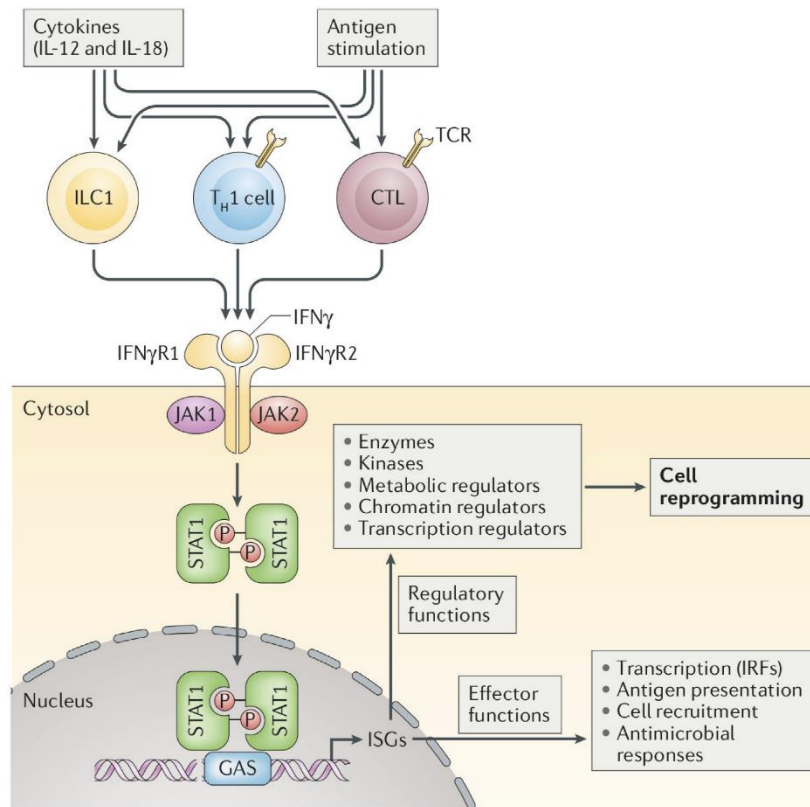


Figure 7. IFN γ production and signaling.

IFN γ is produced by innate-like lymphocytes, including group 1 innate lymphoid cells (ILC1), and by adaptive lymphocytes, including T helper 1 (TH1) cells and cytotoxic T-lymphocytes (CTL), in response to cytokine and antigen stimulation. IFN γ acts on its receptors to induce rapid and transient Janus kinase (JAK)-signal transducer and activator of transcription (STAT) signaling and Interferon-stimulated gene (ISG) induction. Over time, the cellular IFN γ response evolves by impacting the expression and function of various enzymes and regulators of metabolism, chromatin, and transcription to induce a reprogrammed cellular state that is characterized not only by its gene expression profile but also by altered responsiveness to environmental challenges. GAS, IFN γ activation site; IFN γ R, IFN γ receptor; IRF, Interferon regulatory factor; TCR, T-lymphocyte receptor (from Ivashkiv, 2018).

IFN γ is a soluble and pleiotropic protein with anti-microbial (Czarnecki & Sonnenfeld, 1993; Shtrichman & Samuel, 2001; Costa-Pereira et al., 2002; Rhein et al., 2015), immune surveillance (Kaplan et al., 1998; Castro et al., 2018) and immunomodulatory functions (Russell et al., 2009; Su et al. 2015). It has an antitumor function (Lugade, 2008; Gerber et al., 2013; Stromnes et al., 2015) and promotes tumor progression (Jorgovanovic et al., 2020). IFN γ is a proinflammatory cytokine involved in the cytokine storm (Yiu et al., 2012), it activates macrophages to produce and secrete proinflammatory cytokines such

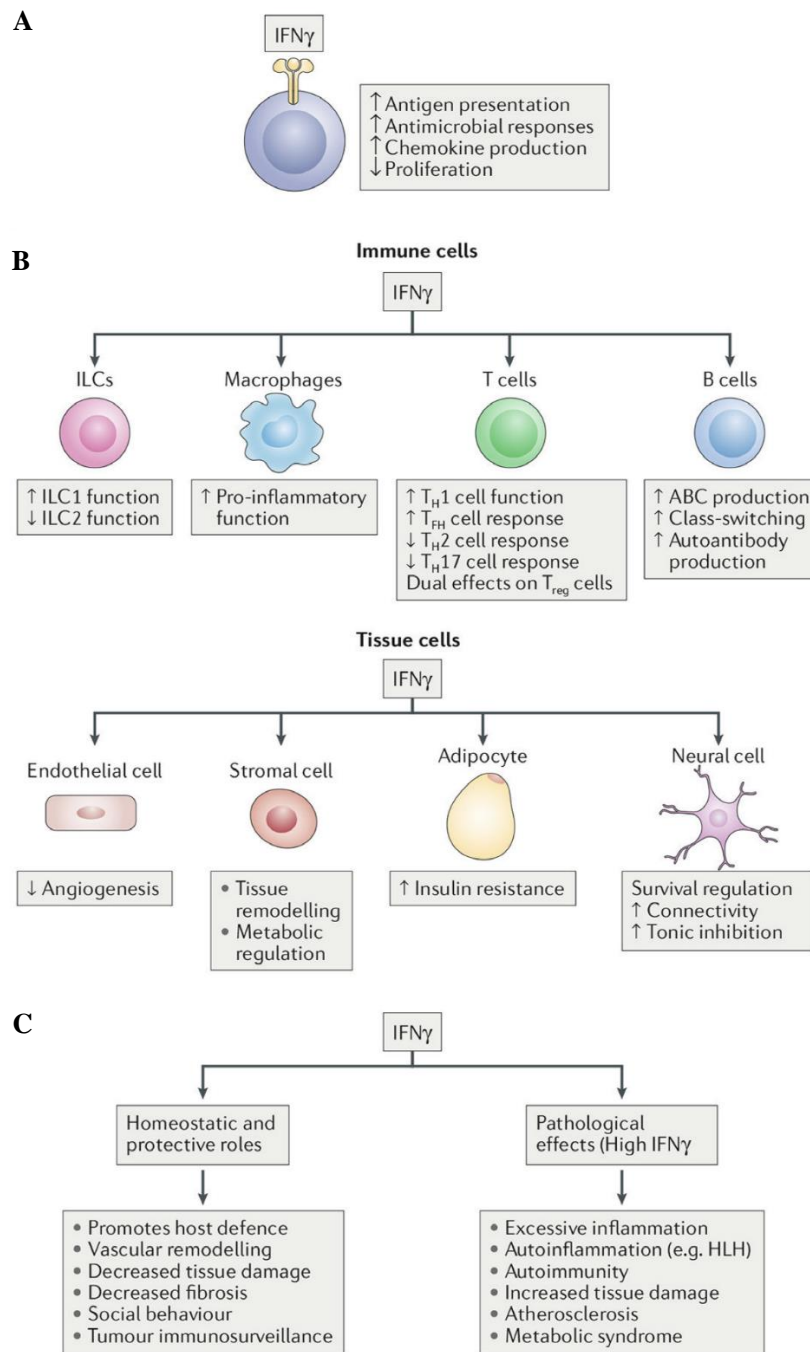


Figure 8. IFN γ action on immune and non-immune cells.

The functional outcomes of IFN γ action on tissues and organs are determined by the integration of its effects on specialized tissue cells and resident or infiltrating immune cells. The effects of IFN γ are context-dependent and can differ under homeostatic or disease conditions; thus, IFN γ can either suppress or promote tissue damage. **A**, IFN γ has general effects on various cells. **B**, IFN γ has effects on different immune cell populations. **C**, IFN γ has homeostatic and pathological effects. ABC, age-associated B cell; HLH, haemophagocytic lymphohistiocytosis; ILCs, innate lymphoid cells; T_{FH} cell, T follicular helper cell; T_H cell, T helper cell; T_{reg} cell, regulatory T-lymphocyte (from Ivashkiv, 2018).

as TNF α and IL-6 (Qiao et al., 2013; Su et al., 2015; Glass & Natoli, 2016). It promotes the progression of steatohepatitis (Luo et al., 2013). It has important effects on immune cells, such as T helper (T_H) cells, T follicular helper (T_{FH}) cells, regulatory T (T_{reg}) cells, B cells, and innate-like lymphocytes (ILs)

(Figures 8A, B) (Hu et al., 2009; Villarino, 2017). IFN γ also plays a role in the tissue-specific functions of non-immune cells (Figures 8A, C). The combined effects of IFN γ on infiltrating immune cells and tissue cells have an important role in tissue homeostasis and pathobiology (Figure 8C).

1.4.2 Molecular characteristics of IFN γ

Gray & Goeddel were the first who cloned the murine IFN γ cDNAs in 1982 (Gray & Goeddel, 1983) and in our days the structure of IFN γ genes and IFN γ protein are well-known. The 6 kb IFN γ gene has four exons and three introns and is located on chromosomes 10 and 12, in mouse and human respectively (Trent et al. 1982; Naylor et al., 1983 & 1984). There is a regulatory element in the IFN γ gene that controls IFN γ expression. The regulatory element comprises binding sites for transcription factors, including Fos, Jun, GATA3, NFAT, nuclear factor (NF)- κ B, and T-bet (Penix et al. 1993 & 1996; Sica et al. 1997; Szabo et al. 2000). Murine IFN γ has 134 amino acids (~15.4 kDa) and exists only as a noncovalent homodimer (Gray & Goeddel, 1983). The polypeptide chains of murine IFN γ contain two independent and different N-linked glycosylation sites, resulting in subunits of different molecular weights. Natural human IFN γ consists of polypeptides that occupy none, one, or two glycosylation sites and displays molecular masses of 17, 20, and 25 kDa respectively (Kelker, et al., 1984; PAN et al., 1987) explaining the molecular weight heterogeneity existing in the fully mature IFN γ homodimer (the molecular weights of natural human and murine IFN γ ranged from 30-50 kDa). Glycosylation is not critical for IFN γ activity. It appears to influence the circulatory half-life of the homodimer (Kelker et al., 1983; Cantell et al., 1986; Rutenfranz et al., 1988). Recent data indicate that both the amino and carboxy-terminal regions play important roles in maintaining protein function.

1.4.3 Interferon-gamma signaling pathway

IFN γ exerts on cells by binding with a heterodimeric receptor consisting of Interferon-gamma receptor1 (IFNGR1) and Interferon-gamma receptor 2 (IFNGR2). Nearly all cells in various body tissues express IFN γ receptors on surfaces (Figure 8A) (Hu & Ivashkiv, 2009). The binding induces oligomerization of the receptor and activation of the receptor-associated Janus kinase (JAK) 1 and 2 via trans-phosphorylation (Figure 7). The activated JAKs phosphorylate the intracellular domain of the receptor (e.g., tyrosine 440 of human IFNGR1) which serves as a docking site for signal transducer and activator of transcription 1 (STAT1). STAT1 is phosphorylated on tyrosine 701, forms dimerization, translocates to the nucleus, and regulates gene expression by binding to gamma-activated sequence (GAS) elements in the promoter of Interferon-stimulated genes (ISGs) (Figure 7) (Poggi & Giuliani, 2016; Gao et al., 2017; Negishi et al., 2017; Villarino et al., 2017). ISGs regulate inflammatory signaling (Liu et al., 2018). Many of them drive the transcription of effector genes, such as Interferon regulatory factor-1

(IRF-1). Activation of IRF-1 induces several kinds of gene expression, which participate in biological processes such as cell cycle regulation, apoptosis, growth inhibition, and tumor suppression (Schroder et al., 2004; Mimura et al., 2018). IRF-1 is the transcription activator of the Interferon-stimulated response element (ISRE), resulting in secondary response gene transcription (Rettino & Clarke, 2013). More importantly, IRF-1 promotes the synthesis of MHC-I and MHC-II, which increases the sensitivity of IFN γ -exposed cells to CTLs attacks (Yang, 2018). In addition, it participates in the activation of suppressors of cytokine signaling-1 (SOCS-1). The SOCS-1 is important to inhibit IFN γ signaling (Alspach et al., 2019). STAT1 can be phosphorylated at serine 727 (Ser727) by a few kinases. Phosphorylation at STAT1 (Ser727) can let STAT1 translocate to the nucleus, but it's critical to full transcriptional activation. Some aspects of CD8⁺ T-lymphocyte biology are directly regulated by IFN γ signaling. Importantly, IFN γ is required for the generation of CTLs' cytolytic ability. IL-2 receptor, the transcription factor T-bet, and granzyme are up-regulated after IFN γ influence CD8⁺ T-lymphocytes. IL-2 responsiveness is critical for the generation of cytotoxic CD8⁺ T-lymphocytes and granzyme is responsible for mediating target lysis. Meanwhile, it is known that IFN γ can either promote or suppress the proliferation of CD8⁺ T-lymphocyte following capturing activation signals (Siegel 1988; MaraskoVsky et al. 1989; Haring et al. 2005).

1.4.4 Interferon-gamma trafficking and secretion

Previous studies have shown that most cytokines are released through conventional secretion. In this form of secretion, cytokines might be packaged in the secretory vesicles or granules (SVs, or SGs) and then secreted only during the receptor-mediated release in a form of "regulated exocytosis" (Moqbel & Coughlin, 2006; Jolly & Sattentau, 2007; Stinchcombe & Griffiths, 2007), or they might be released continuously upon their synthesis through recycling endosomes (REs) and small SGs through "constitutive exocytosis" (Figure 9) (Stow et al., 2006 & 2009). Constitutive exocytosis involved the vesicular trafficking of freshly synthesized protein cargo, which might or might not be initiated by receptor stimulation of nuclear DNA transcription, directly to the plasma membrane and fusion there. The regulated secretory pathway existed in T-lymphocytes, NK cells, and DC cells to secrete specific cargo, such as cytokines, hormones, neurotransmitters, or enzymes (Stanley & Lacy, 2010). In these cells, SGs accumulated and concentrated their cargo through a process of retrograde movement through the Golgi. Once the vesicles are loaded to the correct concentration, they become transported via actin cytoskeleton or microtubule tracks near the site of secretion (Hunt & Stephens, 2011; Luo et al., 2013). After the vesicles had been trafficked to the correct location, the next step is tethering and docking with the plasma membrane, followed by membrane fusion. These steps are catalyzed by small GTPases from the Rab family, Rab-associated effectors, Munc proteins, and SNARE proteins.

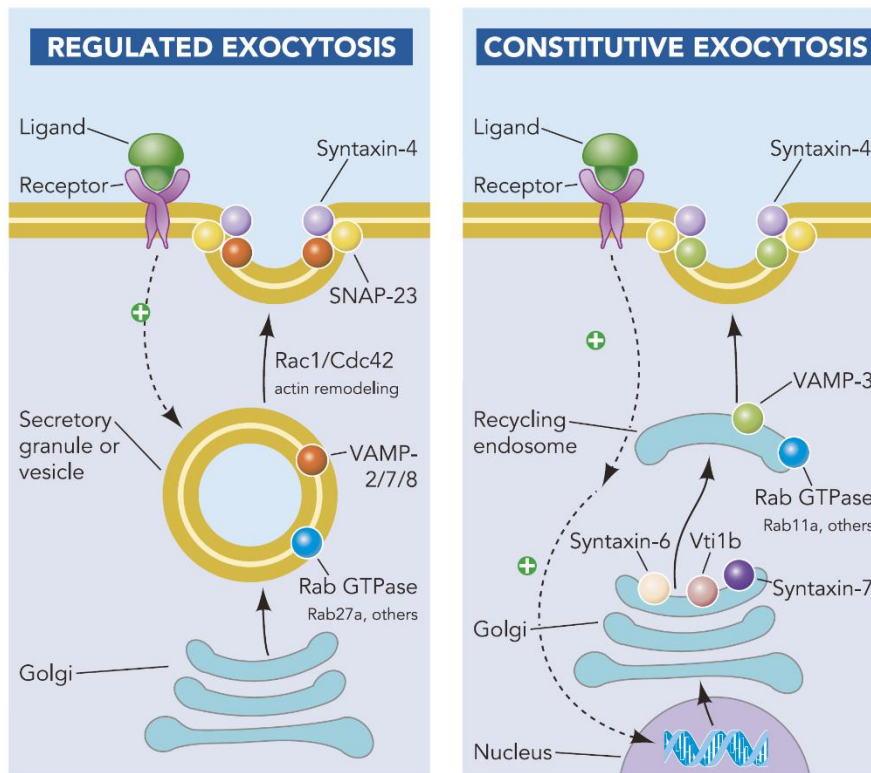


Figure 9. Regulated and constitutive exocytosis of cytokines.

Left: regulated exocytosis involves ligand-receptor signaling to secretory granules or vesicles, which contain preformed cytokines, that are mobilized to the cell surface for release. Right: constitutive exocytosis is instead dependent on receptor-mediated transcription events in the nucleus, leading to trafficking via Golgi through recycling endosomes to the cell surface. The pathway for regulated exocytosis is general for granulocytes, whereas the constitutive pathway shown here is an example of TNF release from macrophages. The v-SNAREs involved in regulated and constitutive exocytosis are distinct, with VAMP-2, -7, and -8 implicated in regulated secretion, whereas Vti1b and VAMP-3 are essential for the constitutive release of recycling endosomes. Several GTPases are also associated with cytokine release (from Stanley & Lacy, 2010).

Huse and his coworkers showed that activated Th cells use two directionally distinct pathways for the secretion of cytokines and chemokines, either “synaptic” (IL-2, IFN γ , and IL-10) or “multidirectional” (TNF, IL-4, and CCL3) pattern. IFN γ preferentially signals to the antigenic target cells contacted by T-lymphocytes at the IS. Rab3d and Rab19 were proteins associated with IFN γ trafficking compartments (Huse et al., 2006). Rab3d, a small GTPases of the Rab subfamily, enables myosin V binding activity, modulates a post-TGN trafficking step that is required for bone resorption (Pavlos et al., 2006) and positive regulation of regulated secretory pathway (Baldini et al., 1998; Schluter et al., 2002). Rab19, a small GTPase of the Rab subfamily (Lütcke et al., 1995), may enable GTPase activity and participate in intracellular protein transport. Sandersona and his colleagues developed live cell imaging to test the IFN γ secretion in CD8+ T-lymphocytes (Sandersona et al., 2012). They found that although the IFN γ secretion was synaptic, it could leak out from the synapse to stimulate bystander cells.

In both human primary NK cells and NK-like cell lines (YTS cells), VAMP7 is shown to be critical to CG exocytosis, the reduction of VAMP7 expression causes downregulation of CD107a expression and fewer CGs degranulation (Marcet-Palacios et al., 2008; Krzewski et al., 2011). Knockdown of VAMP7

doesn't affect IFN γ synthesis but will impair IFN γ secretion in NK cells (Krzewski et al., 2011). From previous reports, VAMP7 localized mainly in Golgi and late endosomes or lysosomes in most T-lymphocyte types. It might have a role in anterograde and retrograde trafficking from Golgi and endocytosis as well. Herda and his partners discovered that the polarized secretion of cytotoxic granules and IFN γ is controlled by the sorting receptor Sortilin (Herda et al., 2012). In murine Sortilin-deficient CTLs, regulated secretion of GzmA and cytotoxic killing were enhanced and correlated with increased expression of VAMP7. In contrast, IFN γ secretion was reduced in the absence of Sortilin which was required for IFN γ export from the Golgi apparatus. Furthermore, they tracked the transport route of IFN γ from the Golgi to the early endosome. In WT CTLs, IFN γ trafficking from the endosomal sorting platform to the plasma membrane proceeds independently of recycling endosomes, and IFN γ remains excluded from late endosomes.

1.5 Major goals of the thesis

The CTLs are the second main source of IFN γ besides Th1 cells in our body. When I started my thesis, little was known about the cell biology of IFN γ trafficking and release from this cell type. To reduce this knowledge gap, my task was to study interferon production, intracellular compartmentalization, and release by exocytosis in detail.

In my thesis, I demonstrate that IFN γ is not produced by naïve CTLs but in CTLs that reflect several effector and memory states. The release is exocytotic and regulated. Most interesting we found out that the majority of IFN γ comes with SCGs and MCGs that also contain cytotoxic substances respectively particles, like granzymes, perforin, and SMAPs. The signal for the release of IFN γ is the activation of T cell receptors. As a consequence, IFN γ is released by CTLs together with cytotoxic substances and only during direct cytotoxic action.

Data were obtained using a broad combination of techniques, including the use of marker mouse lines, transient overexpression in activated cells, flow cytometric analysis and sorting, super-resolution microscopy, TIRF-microscopy, electron microscopy, killing assay, multiplex assay, ELISA, and Western blot.

2. Material and Methods

2.1 Material

2.1.1 Chemicals

Chemical substance	Company (cat/order number)
Agar-Agar	Roth (5210.3)
Biozym Red HS Taq 2× Mix	Biozym (331126S)
Bovine Serum Albumin (BSA)	Sigma-Aldrich (A4503)
Bromophenol blue	Roth (A512.1)
β-Mercaptoethanol	Roth (4227.3)
Complete mini, EDTA-free Protease Inhibitor Cocktail	Roche (11836170001)
Coomassie Brilliant Blue G250	SERVA (17524.01)
Dithiothreitol	Sigma-Aldrich (10197777001)
Dodecyl sulfate Na-salt in pellets (SDS)	Roth (2326.2)
Dimethyl sulfoxide (DMSO)	Sigma-Aldrich (D8418)
dNTP-Mix	Fermentas (R0192)
Dulbecco's Phosphate Buffered Saline (DPBS (1×))	Thermo Scientific (14190-094)
λ-DNA	Roche (745782)
Easy ladder I	Meridian Bioscience (BIO-33046)
Ethanol (100%)	Roth (5054.1)
Ethidium bromide	Roth (2218.2)
Ethylenediamine tetraacetic acid disodium salt (EDTA)	Sigma-Aldrich (E6635)
Fetal Calf Serum (FCS)	Thermo Scientific (A4736401)
Glucose	Merck (1.08342.1000)
Glycerol	Sigma-Aldrich (G5516)
Glycine	Roth (56406)
Glutamax	Thermo Scientific (35050061)
HEPES	Thermo Scientific (15630080)
Hybond N+ nylon membrane	GE Healthcare (RPN119B)
Deoxyribonucleic acid from herring sperm	Merck (D3159)
HPLC water	Thermo Scientific (11307090)
Hydrochloric acid	Merck (9057.1000)
Interleukin-2 mouse recombinat	Thermo Scientific (10662264)
Ionomycin calcium salt	Merck (407952)
Isopropanol	Roth (AE73.1)
Kanamycin	Sigma-Aldrich (K-1377)

KCl	Merck (1049360500)
L-Glutamine 200 mM (100×)	Gibco (25030-024)
Methanol (100%)	Roth (HN41.1)
NaCl	Merck (1064040500)
NaHCO ₃	Merck
Na ₂ HPO ₄ × 2H ₂ O	VWR
NaH ₂ PO ₄ × H ₂ O	VWR
NE-2-buffer	Biolabs (B7002S)
N, N, N', N'- Tetramethyl ethylenediamine (TEMED)	Merck (1107320100) (TEMED)
Non-fat Dried Milk Powder	PanReac AppliChem
NuPAGE LDS sample buffer 4×	Thermo Scientific (NP0007)
NuPAGE MOPS SDS Running Buffer 20×	Thermo Scientific (NP0001)
NuPAGE Transfer Buffer 20×	Thermo Scientific (NP00061)
PCR Buffer	Sigma-Aldrich
Penicillin/streptomycin	Gibco (15140122)
Paraformaldehyde (PFA)	Merck (1040051000)
Phusion DNA polymerase	Thermo Scientific (F530S)
Phusion High-Fidelity DNA polymerase	Biolab (M05303)
5× pFusion HF Buffer (7.5 Mm MgCl ₂)	Thermo Scientific (F-518)
Poly-L-ornithine	Sigma-Aldrich (P4957)
pfu-Polymerase	Fermentas (EP0501)
Ponceau S solution 0.1%	Sigma-Aldrich (P7170)
Quick Start Bradford 1× Dye Reagent	Bio-Rad (500205)
Restore Western Blot Stripping buffer	Thermo Scientific (10057103)
Sigma H ₂ O	Sigma-Aldrich (W4502)
Sodium Pyruvate	Thermo Scientific (11360070)
Spectra Multicolor Broad Range Protein Ladder	Thermo Scientific (26634)
Super Signal West Dura Extended	Thermo Scientific (34075)
Super Signal West Pico Chemiluminescent Substrate	Thermo Scientific (34076)
Tryptone/Peptone	Roth (8952.3)
Trypan blue solution	Sigma-Aldrich (93595)
Triton X-100	Sigma-Aldrich (T8787)
Tris-hydrochloride	Roth (9090.3)
Tween-20	Roth (2727.1)
BamH I (FD)	Thermo Scientific (FD0054)
XbaI	Biolabs (RO145S)

2.1.2 Commercial Kits

Kits	Company (cat/order number)
EndoFree Plasmid Midi Kit	Qiagen (12143)
QIAquick PCR Purification Kit	Qiagen (28106)
Plasmid Midi Kit	Qiagen (10023)
QIAquick Gel Extraction Kit	Qiagen (28706)
Nucleofection kit for mouse T-lymphocytes	Lonza (VPA-1006)
Dynabeads™ FlowComp™ Mouse CD8 Kit	Thermo Scientific (11462D)
Dynabeads™ Mouse T-Activator CD3/CD28	Thermo Scientific (11453D)
Amersham Protran Premium 0.2 µm Nitrocellulose membrane	Cytiva (10600011)
NuPAGE™ 12% Bis-Tris Protein Gels, 1.0 mm, 12-well	Thermo Scientific (NP0342BOX)
BD Cytofix/Cytoperm™ Fixation/Permeabilization Kit	BD Bioscience (554714)
Mouse Th1 Panel (5-Plex) with V-bottom Plate V03	Biolegend (741050)
Legend Max ELISA Kit Mouse IFN γ	Biolegend (430807)

2.1.3 Antibodies

Antibodies	Host	Dilution	Company (cat/order)
Primary antibodies			
Anti-CD3 ϵ (145-2C11)	Hamster	30 µg/ml	BD Pharmingen (553057)
anti-mouse/rat/human IFN-gamma	Rabbit	WB: 1:1000-10,000	Abcam (ab133566)
Purified anti-mouse IFN-gamma (XM 1.2)	Rat	ICC & ICFC 1:200	BioLegend (505802)
Anti- IFN gamma alexa 488 (XM 1.2)	Rat	ICC & ICFC 1:200	BioLegend (505813)
Anti- IFN gamma PE (XM 1.2)	Rat	ICFC 1:200	BioLegend (505808)
Anti-granzyme B Alexa Fluor 647 (GB11)	Mouse	ICC 1:200	BioLegend (515406)
Anti-tRFP	Rabbit	WB 1:1000	Zchl/biocat evrogen
anti-GAPDH (14C10)	Rat	WB 1:5000	Sigma Aldrich (2118L)
Anti-cis Golgi GM 130	Mouse	ICC 1:100	BD bioscience (610823)
Anti-CD44 PE (IM7)	Rat	FC 1:1200	BD Bioscience (553134)
Anti-CD62L APC (MEL-14 (RUO))	Rat	FC 1:1600	BD Bioscience (553150)
Anti-CD8 α FITC	Rat	FC 1:200	BD Bioscience (553030)
Anti-IgG 2a PE (R35-95)	Rat	FC (same as interest)	BD Bioscience (553930)
Secondary antibodies			
Alexa 488 anti-mouse IgG (H+L)	Goat	1:1000	Thermo Scientific (A28175)
Alexa 568 anti-rat IgG (H+L)	Goat	1:1000	Thermo Scientific (A11011)
Alexa 647 anti-mouse IgG (H+L)	Goat	1:1000	Thermo Scientific (A32728)
Alexa 647 anti-rat IgG (H+L)	Chicken	1:1000	Thermo Scientific (A-

HRP-conjugated anti-mouse IgG	Goat	1:1000	Thermo Scientific (31430)
HRP-conjugated anti-rabbit IgG	Goat	1:10,000	Thermo Scientific (31460)

2.1.4 Medium and solution

Medium (Company (cat/order number))	Supplements
AIM V (for mouse primary CD8+ T-lymphocytes) (GIBCO) (12055-091)	10% FCS, 50 μ M 2-Mercaptoethanol
RPMI (GIBCO) (21875-034)	10% FCS, 50 μ M 2-Mercaptoethanol, 0.5% Pen/Strep, 10 mM HEPES
Erythrocyte lysis buffer (pH 7.3)	H ₂ O, 100 ml, NH ₄ Cl, 0.829 g, (155 mM), KHCO ₃ , 0.1 g, (10 mM), EDTA from 50 mM stock-260 μ l, pH 7.4 (0.1 mM) (Bzeih, 2016)
Extracellular buffer for TIRF measurements: 0 mM calcium buffer	155 mM NaCl, 4.5 mM KCl, 5 mM HEPES, 3 mM MgCl ₂ , (pH: 7.4 and Osmolarity: 300-310 mOsm) (Bzeih, 2016).
10 mM calcium buffer	140 mM NaCl, 4.5 mM KCl, 5 mM HEPES, 2 mM MgCl ₂ , 10 mM CaCl ₂ (Bzeih, 2016).
Isolation Buffer	58 mM Na ₂ HPO ₄ \times 2H ₂ O, 17 mM NaH ₂ PO ₄ \times H ₂ O, 0.1% BSA 0.5 g, (0.1%), 2 mM EDTA (Bzeih, 2016).
LB medium, 1 L	10 g Tryptone, 5 g yeast extract, 5 g NaCl, add H ₂ O to 1 L.
LB plate-medium	10 g Tryptone, 5 g yeast extract, 5 g NaCl, 12 g Agar-Agar, add H ₂ O to 1 L.
Mounting medium	6 g Glycerol, 2.4 g Mowiol 4-88, 6 mL H ₂ O, 12 ml of 0.2 M Tris-HCl buffer (pH 8.5).
Solutions for immunocytochemistry	
Fixation	4% PFA in DPBS (1 \times), pH 7.4
Permeabilization	0.1% Triton-X 100 in DPBS (1 \times)
Blocking	0.1% Triton-X 100 in DPBS (1 \times) + 2-5% BSA
Solutions for cloning	
TAE-buffer (50 \times) pH 8.5 (1 L)	242 g Tris base (M = 121.4 g/mol), 57.1 mL glacial acetic acid, 100 mL 0.5 M EDTA pH 8.0, add H ₂ O to 1000 mL.
6 x Loading buffer	4 g Sucrose, 10 mL H ₂ O, sterile filtered, and some drops of Bromophenol blue till the solution is blue.
Solutions for Western blot	
Lysis buffer	50 mM Tris-HCl (pH 7.5), 150 mM NaCl, 250 μ M PMSF, 1% Triton-X100, 1 mM Deoxycholate, 1 mM EDTA, 1 mM DTT and 1 protease inhibitor tablet (Roche), and H ₂ O.
TBS (10 \times)	87.7 g NaCl, 24 g Tris-Cl (pH 7.5), and H ₂ O up to 1 L
1 \times TBST (0.1%) (1L)	100 ml 10 \times TBS, 1 ml Tween-20, and add H ₂ O up to 1 L.

2.1.5 Mouse models

1. C57BL/6N wildtype (WT)
2. Homozygous Munc13-4 KO (Munc13-4 KO, official name C57BL/6J-Unc13d^{lⁱⁿx}/Mmucd)
3. Perforin gene KO (Perforin KO, official name C57BL/6-Prf1^{tm1Sdz/J})
4. Homozygous granzyme B-mTFP knock-in (GzmB-mTFP)

Crossbreeds

5. GzmB-mTFP × Munc13-4 KO
6. GzmB-mTFP × Perforin KO

2.2 Methods

2.2.1 Isolation of primary CD8⁺ T-lymphocytes

The mouse was anesthetized with CO₂ and killed by cervical dislocation (Figure 10). The stomach was opened at the left side and the spleen was carefully removed and crushed through a 70 μm cell strainer (Corning Life Sciences). RPMI medium (10 mL) was used to collect and wash the splenocytes by centrifugation (6 min, 1100 rpm without a break,). Washed splenocytes were incubated with erythrocyte lysis buffer (1 mL) for 30 s to lyse erythrocytes. The lysate was stopped by adding 10 mL ice-cold RPMI. Subsequently, erythrocyte debris was removed by immediate washing (centrifuge, 6 min, 1100 rpm) with RPMI once and once with isolation buffer. Primary CD8⁺ T-lymphocytes were positively isolated out of the splenocytes by using Dynabeads FlowComp Mouse CD8 Kit (Thermo Fisher Scientific) according to the manufacturer's protocol. In short: 25 μL of mouse anti-CD8 antibody were added to 475 μL of splenocyte solution and incubated for 10 min on ice followed by washing (centrifuge, 6 min, 1100 rpm) with isolation buffer. Subsequently, 75 μL of FlowComp™ Dynabeads were added to the cells and mixed gently on the rocker at 4 °C. In the next step, Dynabeads with bound CD8⁺ cells were fixed to the wall of the tube by a magnet and the supernatant was gently discarded. Finally, cells were detached from Dynabeads by using releasing buffer followed by washing with an isolation buffer. CD8⁺ T-lymphocytes were then collected by centrifugation and re-suspended in an AIM V culture medium supplemented with 10% FCS and 50 μM 2-mercaptoethanol (BME) (Figure 10).

2.2.2 Culture of primary CD8⁺ T-lymphocytes

The isolated cells were cultured at a density of 1×10^6 cells/mL in AIM V medium supplemented with 10% FCS, 50 μM BME, T activator dynabeads (number of cells: beads = 1 : 0.8, beads were CD3ε/CD28

coated, Thermo Fisher Scientific) and 100 U/mL recombinant IL-2 (Life technology) to generate activated CTLs. Cultivation was done in a 24-well plate in a cell culture incubator (37 °C, 5% CO₂, saturated humidity) according to a protocol from Bzeih et al. (2016). Cells were split after 2 days in culture and from then on daily (Figure 10). Therefore, fresh AIM V medium supplemented with 10% FCS, 50 µM BME, and 100 U/mL recombinant IL-2 was added. Usually, day4 to day6 cells were used for experiments.

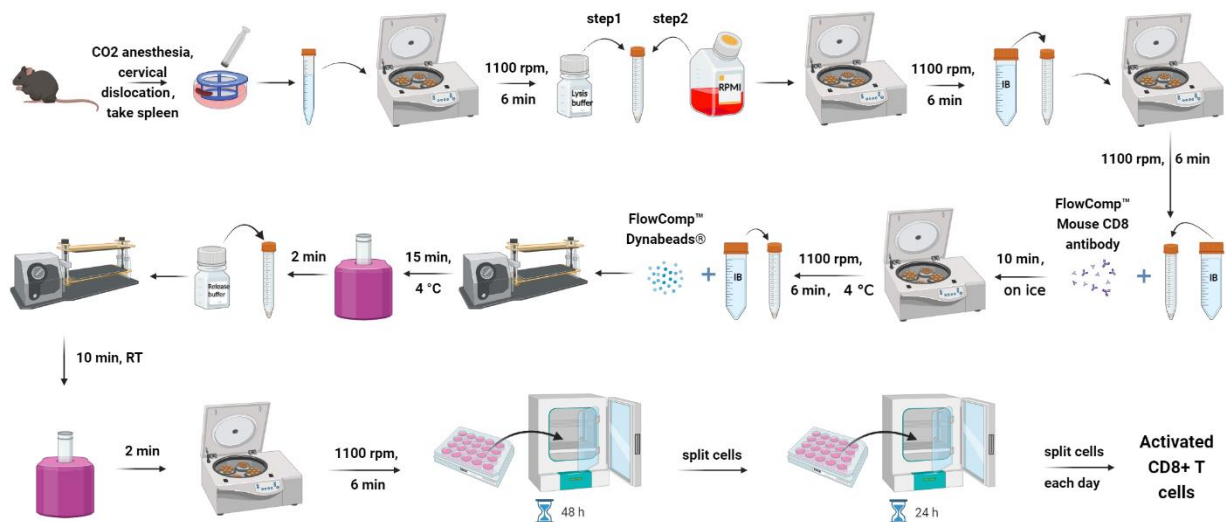


Figure 10. Positive isolation of CD8+ T-lymphocytes from mouse spleen and T-lymphocytes culture.

For some experiments, cells were used immediately after the CD28/CD3 ϵ activation beads had been removed. For most experiments, cells were allowed to recover for 2 h after CD28/CD3 ϵ beads had been removed. Those cells underwent a “re-stimulation” during the experiment. It is meant that by appropriate measures, the T-lymphocyte receptors have been acutely stimulated to trigger cytotoxic actions, such as the release of cytotoxic substances and IFN γ .

A. Re-stimulation protocols for FACS experiments:

1. For inducing intracellular IFN γ production, days 3-5 beads-activated WT CTLs were washed and restimulated with 10 µg/mL plate-bound anti-CD3 ϵ antibody for 0, 0.5, 1, 2, 3, and 4 h in a cell culture incubator.
2. For inducing the release of IFN γ to the supernatant and measuring it, we restimulated day5 beads-activated CTLs with 30 µg/mL plate-bound anti-CD3 ϵ antibody for 4 h in a cell culture incubator and used a LEGENDplexTM Multi-Analyte Flow Assay Kit.

B. Re-stimulation protocol for IFN γ measurements using ELISA:

For inducing the release of IFN γ to the supernatant which was measured by ELISA, we restimulated day5 beads-activated CTLs with 30 µg/mL plate-bound anti-CD3 ϵ antibody for 0,15 min, 30 min, and 60 min in a cell culture incubator.

C. Re-stimulation protocols for SIM colocalization experiments:

1. For inducing intracellular IFN γ production, day5 beads-activated WT CTLs were washed and restimulated either with 10 $\mu\text{g}/\text{mL}$ plate-bound anti-CD3 ϵ antibody for 2 h or with 30 $\mu\text{g}/\text{mL}$ plate-bound anti-CD3 ϵ antibody for 4 h in a cell culture incubator.
2. For understanding if the degree of IFN γ colocalization with GzmB is dependent on IS-formation, day5 beads-activated GzmB-mTFP CTLs overexpressing IFN γ were either restimulated or not with 10 $\mu\text{g}/\text{mL}$ plate-bound anti-CD3 ϵ antibody for 2 h in a cell culture incubator before displaying on poly-L-ornithine-coated or anti-CD3 ϵ -coated coverslips.

D. Re-stimulation protocol for TIRF experiments:

For measuring the exocytosis of GzmB-containing and/or IFN γ -containing vesicles, day5 beads-activated GzmB-mTFP CTLs overexpressing IFN γ were restimulated with 30 $\mu\text{g}/\text{mL}$ anti-CD3 ϵ antibody coated on a coverslip for 2-3 min in an extracellular solution to let them form IS.

2.2.3 Electroporation

Activated CTLs generated as described above were used for transfection with plasmid DNA by electroporation. Cells were transfected with several IFN γ plasmids using an Amaxa™ Mouse T-lymphocyte Nucleofector Kit (Lonza) and the corresponding Nucleofector. Briefly, cells were spun down and resuspended with a warm isolation buffer. After the second spun-down cells were resuspended into 100 μL nucleofection solution along with plasmid DNA and transferred to an electroporation cuvette. CTLs were then electroporated using Amaxa® Nucleofector® II Device (Lonza) and cultured in pre-warmed Amaxa™ Mouse T-lymphocyte nucleofector™ medium (Lonza) for 6 - 9 h to allow protein expression before the experiment started.

2.2.4 P815 cell culture

P815 (target cells for mouse CD8+ T-lymphocytes) cells were cultured in RPMI medium (Thermo Fisher Scientific) containing 10% FCS and 1% P/S antibiotics in an incubator (37 °C, 5% CO $_2$).

2.2.5 *pMax-IFN γ -linker-pHuji* Cloning

In my thesis, a pH sensor (*pMax-IFN γ -linker-pHuji*) was used and it was subcloned with the following procedures.

2.2.5.1 PCR amplification

Generation of the new vector started with digesting an existing *pMax-IFN γ -linker-mCherry* plasmid (Figure 11) with XbaI and BamHI to remove mCherry. *pHuji* was amplified from an existing *pMax-granzyme B-linker-pHuji* by using a forward primer with XbaI site 5'-TATATA CTAG TCTAGA ATGGTGAGCAAGGGCGAGGA-3' and a reverse primer with BamHI and a stop codon 5'-TATATA CGC GGATCC TTA CTTGTACAGCTCGTCCAT-3' (Table 1 & 2), followed by elution and digestion.

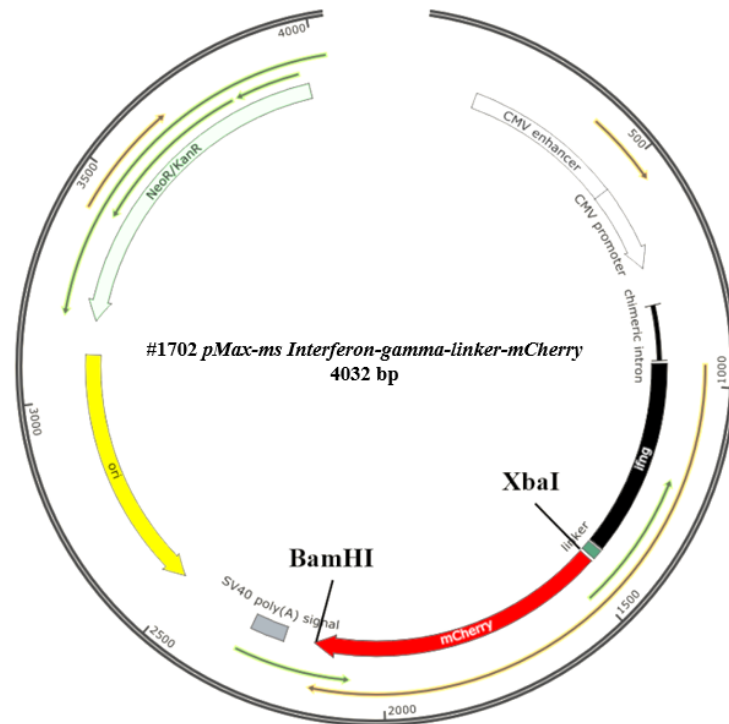


Figure 11. Vector map of *pMax-ifng-linker-mCherry* with restriction enzymes.

The linker sequence is GGTGGGAGCGGCGGAAGCGGCGGT and the amino acid is Gly-Gly-Ser-Gly-Gly-Ser-Gly-Gly.

Table 1. PCR mix for *pHuji* amplification

Component	50 μ L reaction	Final concentration
H ₂ O (Nucleus free)	36.25 μ L	
5 \times Phusion HF Buffer	10 μ L	1 \times
10 mM dNTPs	1.25 μ L	25 μ M/ μ L
Forward primer	0.5 μ L	50 pmol
Reverse primer	0.5 μ L	50 pmol
<i>pMax-granzyme B-linker-pHuji</i>	0.5 μ L	10 ng/ μ L
Phusion HF DNA polymerase	1 μ L	0.04 U/ μ L

Table 2. PCR program for *pHuji* amplification

Cycle step	Temperature	Time	Cycles
Initial Denaturation	98 °C	30 s	1
Denaturation	98 °C	10 s	30
Annealing	72 °C	20 s	
Extension	72 °C	15 s	
Final Extension	72 °C	5 min	1
End	4 °C	∞	

2.2.5.2 Sample elution and digestion

The size of the amplified PCR DNA product was checked on a 1.2 % agarose gel (with ethidium bromide). For that, 1 µL of PCR product with 1 µL 6× loading dye and 4 µL Sigma H₂O were loaded together with 4 µL of the 100-2000 bp Easy ladder I to the gel, and the electrophoresis was run for 40 minutes at 80 V. The PCR product was then purified with the QIAquick PCR Purification Kit following the manufacturer's protocol. DNA purification used a simple and fast bind-wash-elute procedure. The kit contained silica membrane columns for DNA binding in high-salt buffer and elution with low-salt buffer or water. After purification, the PCR product and the *pMax-ifng-linker-mCherry* plasmid were digested for 2 hours at 37 °C with the restriction enzymes BamHI and XbaI (Table 3). Restriction enzyme digestion generated compatible ends capable of being ligated together afterward.

Table 3. Restriction digestion mix for *pMax-ifng-linker-mCherry* and *pHuji*

Reagent	<i>pMax-IFNγ-linker-mCherry</i> (2.2 µg/µL)	PCR <i>pHuji</i> (400 ng/µL)
DNA	5 µL	5 µL
BamH I (FD)	2.5 µL	2.5 µL
Xba I (FD)	2.5 µL	2.5 µL
10× Cutsmart® Buffer	5 µL	5 µL
Sigma H ₂ O	35 µL	35 µL

2.2.5.3 Gel extraction and DNA ligation

Next, the loading buffer was added to the linearized DNA and loaded together with the 100-2000 bp Easy ladder I on a 1.2% agarose gel (with ethidium bromide). The gel was run for 10 minutes at 100 V and 40 min at 80 V. The DNA bands with the correct size for *pHuji* (~ 720 bp) and *pMax-ifng-linker*- (~ 3320 bp) were cut under the UV lamp and isolated from the agarose gel by using the QIAquick Gel Extraction Kit according to the manufacturer's protocol. To check the isolated DNA concentration, 3 µL of the sample with 1 µL 6× loading dye and 2 µL Sigma H₂O were loaded together with 4 µL of 100-2000 bp Easy ladder I on a 1.2% agarose gel (with ethidium bromide). The gel was run for 40 minutes at 80 V. Next, the two digested DNA fragments (*pHuji* and *pMax-ifng-linker*) were combined with the T4 DNA ligase. After calculation with a vector-to-insert ratio of 1:3, 150 ng of vector DNA was used

with 90 ng of insert DNA. The ligation control included the digested vector and the same components of the ligation reaction but without the insert (Table 4). The ligation reaction tube and the control tube were incubated for 2 h at 25 °C or overnight at 16°C.

$$\frac{150 \text{ ng Vector} \times 0.72 \text{ Kb Insert}}{90 \text{ ng Insert} \times 3.32 \text{ Kb Vector}} \approx 1:3$$

Table 4. Ligation mix for *pMax-ifng-linker-mCherry* and *pHuji*

Reagent	Reaction volume	Control volume
Vector DNA (<i>pMax-IFNγ-linker</i>), 300 ng/ μ L	0.5 μ L	0.5 μ L
Insert DNA (<i>pHuji</i>), 30 ng/ μ L	3 μ L	-
T4 DNA Ligase	2 μ L	2 μ L
10 \times T4 DNA Ligase Buffer	2 μ L	2 μ L
Sigma H ₂ O	12.5 μ L	15.5 μ L

2.2.5.4 Bacterial transformation using heat shock

An aliquot (50 μ L) of TOP10 competent *Escherichia coli* (C404010, Invitrogen) bacteria were thawed on ice and mixed with 10 μ L ligation mixture (120 μ g insert DNA attached to plasmid DNA). Afterward, heat shock was performed at 42 °C for 90 s. Subsequently, bacteria were mixed with 400 μ L LB medium under semi-sterile conditions and incubated at 37 °C with shaking at 150 rpm for 1 h. The content was streaked on preheated LB agar plates with the appropriate selection medium (LB medium with 30 μ g/mL kanamycin) and incubated overnight at 37 °C. Successfully transformed bacteria were picked as colonies and amplified overnight in the liquid LB selection medium with 30 μ g/mL kanamycin. Afterward, bacteria were harvested and DNA isolation was carried out using QIAGEN® Plasmid Midi Kits according to the manufacturer's instructions. The quantitative DNA determination was carried out by photometric measurement at 260 nm.

2.2.5.5 Plasmid digestion and sequencing

After retransformation, amplification, and isolation of the DNA, the cloning success was checked by digestion with BamHI and XbaI for the vector and insert. For that, 0.5 μ L isolated DNA was digested with 1 μ L BamHI and 1 μ L XbaI in the presence of 1.5 μ L 10 \times Cutsmart buffer and 11 μ L Sigma H₂O. The reaction mix was incubated for 1 hour at 37 °C. Loading buffer was added and samples were run on a 1.2% agarose gel (with ethidium bromide) for 40 minutes at 80 V. Clones with the correct digestion pattern were sequenced to eliminate the possibility of mutations.

2.2.6 Western blot

After activation and transfection, cells were homogenized with a syringe in lysis buffer on ice. Lysates were rotated on a rocker for 1 h at 4 °C, and insoluble material was removed by centrifugation at 10,000-13,000 rpm. Quick Start Bradford 1× Dye Reagent (5000205; Bio-Rad) was used to determine the protein concentration and proteins were diluted to 1 µg/µL. Samples were boiled with 1× loading buffer (Thermo Fischer Scientific) at 98 °C for 10 min. Subsequent, proteins within the samples were separated by SDS-PAGE (NuPAGE; Thermo Fisher Scientific), transferred to nitrocellulose membrane (0.2 µm, Amersham), blocked by incubation with 5% non-fat milk powder in TBST (1×) overnight at 4 °C, and then marked with specific antibodies. Blots were developed using enhanced chemiluminescence reagents (SuperSignal West Dura Chemoluminescent Substrate; Thermo Fisher Scientific) and imaged with a gel documenter. For densitometry analysis, the pixel area and mean fluorescence intensities (MFI) of protein bands were determined with Fiji (<https://imagej.net/>).

2.2.7 Immunocytochemistry

CTLs were stained with an anti-IFN γ antibody to detect endogenous IFN γ . Therefore, cells were fixed with freshly prepared ice-cold 4% paraformaldehyde in DPBS (1×) and washed in DPBS (1×) containing 0.1 M glycine (quenching of autofluorescence). After a second wash with DPBS (1×), cells were permeabilized for 20 minutes in DPBS (1×) containing 0.1% Triton-X 100 (Roth), then blocked for 20-30 minutes in a blocking buffer containing 5% BSA. Finally, cells were stained with primary rat anti-mouse IFN γ (1:200) and secondary anti-rat antibodies (1:1000), before they were mounted and imaged using high-resolution structured illumination microscopy (SIM).

2.2.8 Structured illumination microscopy (SIM)

2.2.8.1 Structured illumination microscopy setup

The structured illumination setup (SIM) setup was from Zeiss (ELYRA PS.1). Images were acquired using a 63× Plan-Apochromat (NA1.4) objective with excitation light of 488, 561, and 647 nm and then processed for SIM to obtain higher resolutions. Z-stacks of 200 nm step size were used to scan cells. Zen 2012 software (Zen 2012; Carl Zeiss) was used for the acquisition and processing of the images for higher resolutions.

2.2.8.2 Colocalization analysis

For colocalization analysis, the JACoP plugin (Bolte 2006) of Fiji (Johannes, 2012) was used. Pearson's and Manders' overlap coefficients (Manders et al., 1993) were used for the quantification of the degree of colocalization.

2.2.9 Total internal reflection fluorescence microscopy (TIRF-M)

2.2.9.1 Visualization of IFN γ and GzmB exocytosis

Mouse CD8⁺ T-lymphocytes isolated from granzyme B-mTFP knock-in mice were electroporated with *pMax-IFN γ -linker-pHuji*. The experiment was performed 6 - 9 h after transfection. 0.5×10^6 cells were resuspended in 30 μ L of extracellular buffer solution without Ca²⁺ and allowed to settle down for 2-3 min on anti-CD3 ϵ antibody (30 μ g/mL) coated coverslips. Subsequently, the acquisition was started with a frequency of 10 Hz for 1 min. Cells were then perfused with extracellular buffer containing 10 mM Ca²⁺ to trigger cytotoxic granule and cytokine exocytosis under continuing acquisition for another 6 minutes. Fluorescence was simultaneously excited with laser light of 450 nm (Spectra-Physics) and 561 nm (Melles Riot (model 85-YCA-615)) wavelength. TIRF illumination was set to an illumination angle allowing total reflection. The lightpath for illumination and imaging was guided by an Apochromat TIRF 100 \times NA 1.45 objective. Measurements were done at room temperature. The setup was operated by VisiView version 2.1.2 software from Visitron Systems. The acquisition frequency was 10 Hz and the exposure time was 100 ms.

2.2.9.2 Exocytosis analysis

Secreted cells with both a good signal of IFN γ -pHuji and GzmB-TFP were cropped, and analysis for IFN γ and GzmB exocytosis appeared at the TIRF plane using ImageJ V.18.0. The secretion of IFN γ and cytotoxic granules were analyzed using the plugin Time series Analyzer V3.2 in ImageJ V 18.0. In general, a sudden spark and subsequent fast drop of IFN γ -pHuji fluorescence within 300 ms (three acquisition frames) was defined as IFN γ secretion by SCG. The typical kinetic of a fusion event was produced by the pH-sensitivity of pHuji which, by the opening of the fusion pore, reaches the more basic extracellular environment leading to a sudden increase in fluorescence, while the subsequent drop is induced by diffusion of the pHuji away from the original point of fusion. Also, GrzmB fusion was typical in kinetics with a less pronounced initial increase (less pH sensitive) and a decrease of fluorescence induced by diffusion. The newly discovered MCG-type of lytic granule has much elongated kinetics because of its size and different internal organization. Granule-deposited particles on the coverslip after exocytosis lead to quite different rise and decay times of MCG exocytosis from SCG and can therefore be identified without doubt.

2.2.10 Correlative light and electron microscopy (CLEM)

Day5 activated CTLs were transfected with *pMax-ifng-linker-mCherry*. After 6 - 7 h, cells were washed, and re-suspended in AIM V containing 30% FCS and 10 mM Hepes. 1 μ L cell suspension (10^4 cells) was added to anti-CD3 ϵ coated sapphire coverslips and incubated for 5 - 10 min at 37 $^{\circ}$ C and 5% CO₂. Then

T-lymphocytes were cooled down (4 °C), transferred to the high-pressure freezing (HPF) system, and cooled down with a freezing rate of 20,000 °C/s guaranteeing the highest ultrastructural preservation. Thereafter, samples were embedded with increasing concentrations (30, 60, and 100 % for 1 h each) of Lowicryl (3:1 K11M/HM20 mixture) without uranyl acetate, to avoid background fluorescence during high-resolution SIM. After freeze-substitution, the samples were kept in the dark at 4 °C until further processing. 100 - 120 nm ultrathin sections were cut by using an EM UC7 (Leica). The sections were collected on carbon-coated 200 mesh copper grids (Plano). Fluorescence analysis (SIM) was performed within 1 d after sectioning to avoid loss of fluorescence signals. Therefore, grids were placed in a drop of water between two coverslips, sealed with silicone (picodent twinsil®). High-resolution SIM (ELYRA PS.1; Zeiss) images were acquired by using the 63× Plan-Apochromat (NA 1.4) with excitation light of 488 nm and 642 nm wavelengths and processed. After imaging in the bright-field mode for grid orientation, CellMask deep red images (642 nm) were recorded to identify both the image plane and the outline of CTLs by plasma membrane staining. In a z-stack analysis, 3 - 8 anti-RFP488 images (488 nm) and CellMask deep red images (642 nm) were recorded with a step size of 100 nm to scan the cells of interest. For data acquisition and image processing for higher resolution, ZEN 2010 software (Carl Zeiss Microscopy GmbH) was used.

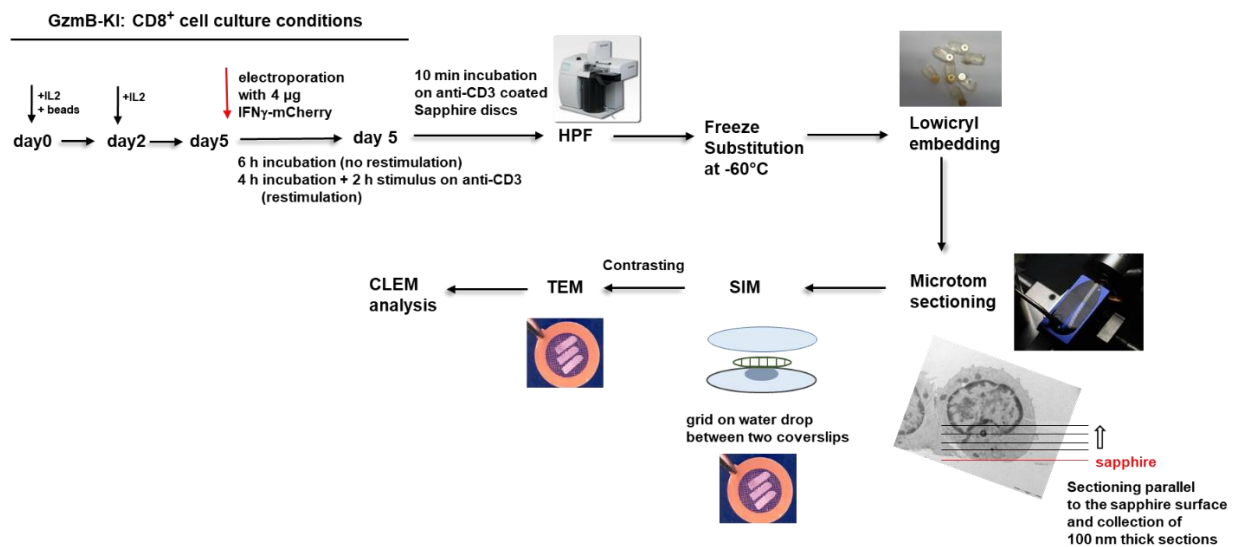


Figure 12. Sample preparation and operation procedure for the correlative light and electron microscopy.

After fluorescence analysis, the very same grids were stained with 2% uranyl acetate and lead citrate for TEM and analyzed with a Philips Tecnai12 Biotwin electron microscope (FEI). Only CTLs with well-conserved membranes, cell organelles, and nuclei were analyzed and used for correlation. For correlation, the CellMask deep red image, which shows the labeled plasma membrane of the cells, was used to find the optimal overlay with the EM image. The final alignment with the anti-RFP488 let me correlate

fluorescent vesicles with the respective TEM structures. Images were overlaid in Corel Draw (Chang et al., 2018). This experiment was performed with the help and guidance of Dr. Claudia Schirra.

2.2.11 Flow cytometry and enzyme-linked immunosorbent assay

2.2.11.1 Measurement of intracellular IFN γ

Day5 CTLs were washed with DPBS (1 \times) after restimulation for 0.5 h, 1 h, 2 h, 3 h, 4 h, 6 h, 8 h, 12 h, and 24 h with plate-bound anti-CD3 ϵ antibody (10 μ g/mL). The pellet (0.5×10^6 CTLs) was resuspended in 250 μ L fixation buffer and incubated on ice for 10 min using BD Cytotfix/CytopermTM Fixation/Permeabilization Kit (554714, BD Bioscience). Next, CTLs were centrifuged again and resuspended in 100 μ L wash buffer (1 \times) and stained on ice (1 h) for intracellular IFN γ and GzmB with respective fluorophore-conjugated antibodies (see 2.1.3). Cells were washed and analyzed by flow cytometry (FACS, BD FACSAria III). Data were analyzed by using FlowJo software (Celeza-Switzerland).

2.2.11.2 Measurement of surface markers

CD8+ T-lymphocytes either with or without (re)stimulation, were taken from cell culture and washed with cold-DPBS (1 \times). Next, they were stained for CD62L and CD25 using corresponding fluorescent Abs without fixation (live staining, 30 min on ice). Then cells were washed twice with cold-wash buffer (1 \times) and resuspended in cold-DPBS (1 \times) for FACS analysis.

2.2.11.3 Measurement of IFN γ in the supernatant

a. Legend Plex measurements

IFN γ concentration was measured in day5 CTL culture. The culture supernatant was collected from day5 CTLs after 4 hrs of plate-bound anti-CD3 ϵ (30 μ g/mL) restimulation by centrifugation and the IFN γ concentration was measured using LEGENDplexTM Multi-Analyte Flow Assay Kit for Mouse (Th1 Panel (5-Plex) with V-bottom Plate V03, 741050, BioLegend). The procedure was strictly performed as recommended by the manufacturer. Samples were read by our BD FACS ARIA3 (Figure 13). Only IFN γ was analyzed. Briefly, BioLegend's LEGENDplexTM assay is a bead-based immunoassay using the same basic principle as sandwich immunoassays. Beads are differentiated by size and internal fluorescence intensities on a flow cytometer. Each bead set is conjugated with a specific antibody on its surface and serves as the capture beads for that particular analyte. When a selected panel of capture beads is mixed and incubated with a sample containing target analytes specific to the capture antibodies, each analyte will bind to its specific capture beads. After washing, a biotinylated detection antibody cocktail is added, and each detection antibody in the cocktail will bind to its specific analyte bound on the capture beads, thus forming capture bead-analyte-detection antibody sandwiches. Streptavidin-phycoerythrin (SA-PE) is subsequently added, which will bind to the biotinylated detection antibodies, providing

fluorescent signal intensities in proportion to the number of bound analytes. Analyte-specific populations can be segregated and PE fluorescent signal quantified. The concentration of a particular analyte is determined using a standard curve generated in the same assay.

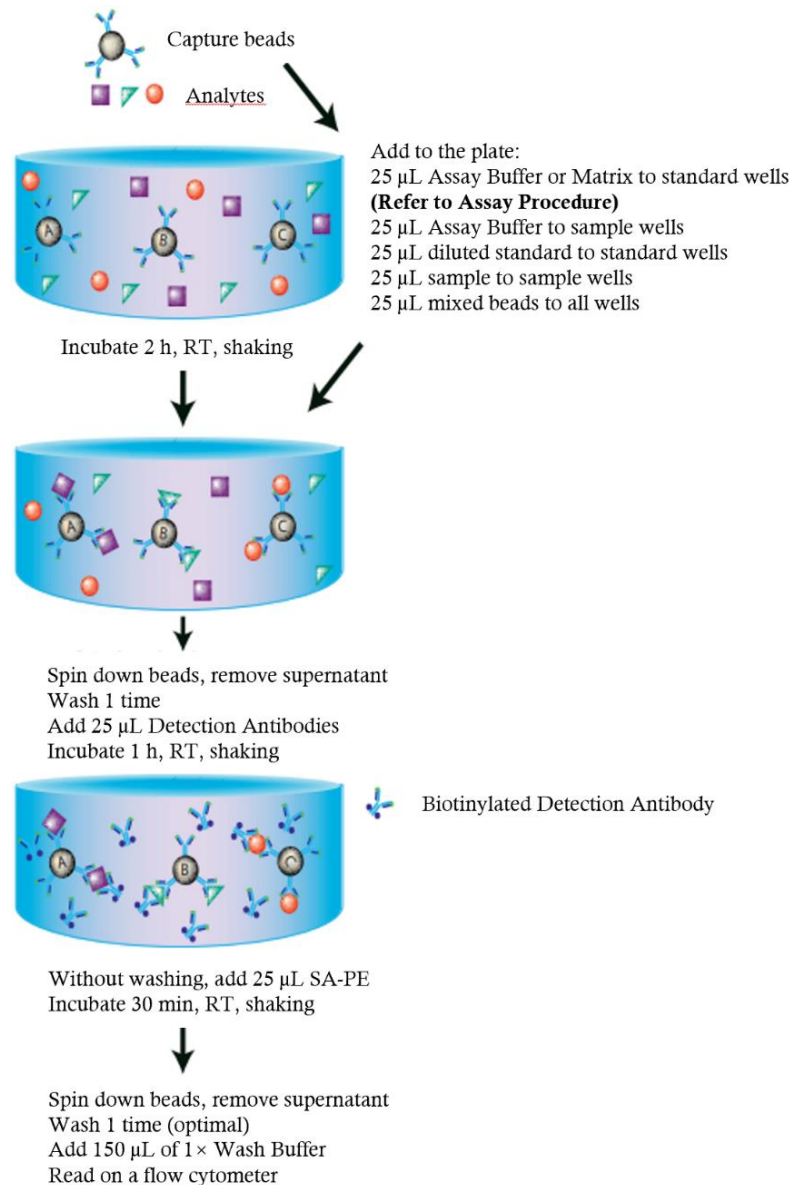


Figure 13. Assay procedure summary for supernatant IFN γ measurement.

This protocol was from the Mouse Th1 Panel (5-Plex) with V-bottom Plate V03 kit (741050, BioLegend).

b. Enzyme-linked immunosorbent assay (ELISA)

Alternatively, IFN γ concentration was measured in day5 CTLs culture with ELISA. Culture medium was collected from day5 CTLs after different times of restimulation (15 min, 30 min, and 60 min) with plate-bound anti-CD3 ϵ (30 μ g/mL) by centrifugation. The supernatant IFN γ was measured using LEGEND MAX Mouse IFN γ Enzyme-linked immunosorbent assay (ELISA) kit (430807, BioLegend) according

to the manufacturer's recommendations (Figure 14). The absorbance of the standard and each sample in the 96-well plate was read in the dual-wavelength mode (measuring at 450 nm, reference at 570 nm) using a Tecan Infinite M200 Plate Reader. The specific absorbance was calculated as the absorbance at 450 nm subtracted by the absorbance at 570 nm. A standard curve of known IFN γ concentration to absorbance was generated. The IFN γ concentration in samples was determined using this standard curve.

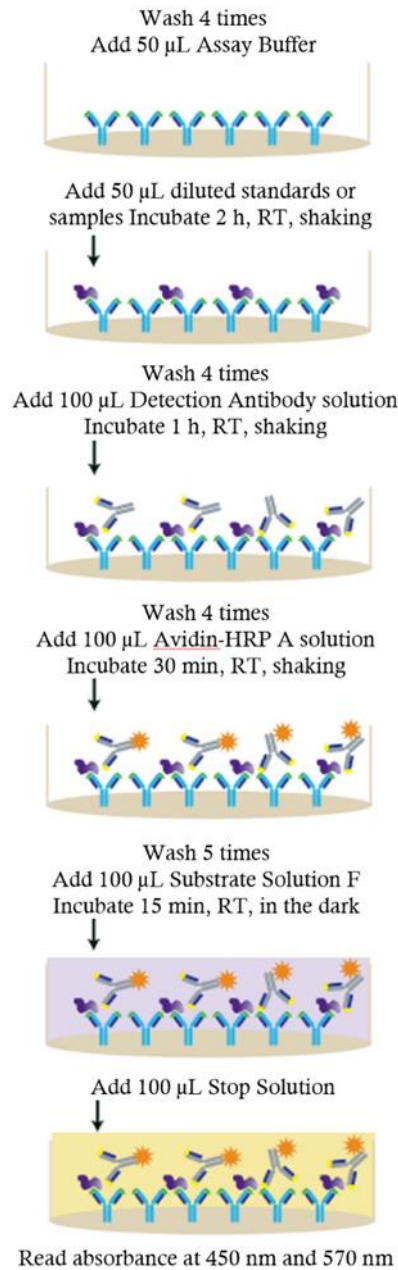


Figure 14. Assay procedure summary for supernatant IFN γ measurement.

This protocol was from the LEGEND MAX Mouse IFN γ ELISA kit (430807, BioLegend).

2.2.12 *In vitro* live cell imaging

Day5 activated CTLs were transfected with *pMax-ifng-linker-mCherry*. After 6 - 7 h, 0.125×10^6 T-lymphocytes were harvested and transferred to a measuring chamber on the top of a microscope which was prefilled with 0.025×10^6 P815 target cells. Before use, P815 targets were suspended in RPMI with 10 mM HEPES and either incubated with or without 30 $\mu\text{g}/\text{mL}$ anti-CD3 ϵ antibody at 37 °C with 5% CO₂ for 1 h. Live cell behavior was recorded by a confocal microscope (LSM780). The total volume of T-targets is 100 μL and the final concentration of anti-CD3 ϵ Ab is 10 $\mu\text{g}/\text{mL}$. Negative control was performed without the addition of anti-CD3 ϵ Ab. Finally, the killing events were processed by ImageJ.

2.2.13 Data analysis

For data analysis and to calculate the statistical significance, Fiji, ImageJ v1.8 (Rasband, W.S., ImageJ, U. S. National Institutes of Health, Bethesda, Maryland, USA, <https://imagej.nih.gov/ij/>, 1997-2018), Microsoft Excel (Microsoft), SigmaPlot 13 and GraphPad_Prism were used. The respective method to calculate statistical significance is given in the text for each figure. Figures were generated using CorelDRAW and PowerPoint and schemes were generated with Biorender.

Note: Figure 2 is from my data, and figure 3 and figure 10 are made from Biorender.

3. Results

3.1 IFN γ -production needs anti-CD3 ϵ restimulation in activated CTLs

To investigate whether IFN γ secretion in activated CTLs is constitutive or regulated, we first tried to measure the dynamic intracellular IFN γ -production upon CD3 ϵ /TCR restimulation using an anti-IFN γ antibody labeled with Alexa 488. Days 3-5 activated CTLs either with or without restimulation were fixed and permeabilized with BD Cytotfix/CytopermTM Buffer, washed with BD Perm/WashTM Buffer, and stained for intracellular IFN γ and GzmB. Finally, staining was quantified by FACS and the data were analyzed by FlowJo_V10_CL. IFN γ was barely detectable in beads-activated but resting CTLs (Figure 15A), while GzmB, as a marker for effector-like cells, was detectable (Figure 15B). The percentage of IFN γ ⁺ CTLs and the median cellular fluorescence intensity (MFI) of the IFN γ Ab signal increased within 2-3 hours of restimulation (Figure 15A, C). This meant that the amount of intracellular IFN γ was positively correlated with the duration of stimulation in culture. While the percentage of GzmB⁺ CTLs and its MFI of GzmB Ab were almost unaffected by restimulation and kept stable during 4 h restimulation (Figure 15B, C). After restimulation, IFN γ expression was significantly more in day5 CTLs when compared to in day3 CTLs, while it was comparable in day4 CTLs (Figure 15C). With prolonging the time of restimulation to 24 h, the amount of intracellular IFN γ reached the maximum at 12 h, while the amount of intracellular GzmB kept increasing for at least 24 h (Figure 15D). CTLs with 8 h and 12 h restimulation had significantly more intracellular IFN γ than CTLs with 24 h restimulation ($p = 0.036$ and $p = 0.020$ respectively).

Taken together, these results show that intracellular IFN γ synthesis is strongly dependent on TCR activation and starts after T-lymphocyte receptor activation within minutes, and reaches a maximum intracellular concentration after 12 h. In contrast, GzmB is constitutively present in unstimulated CTLs.

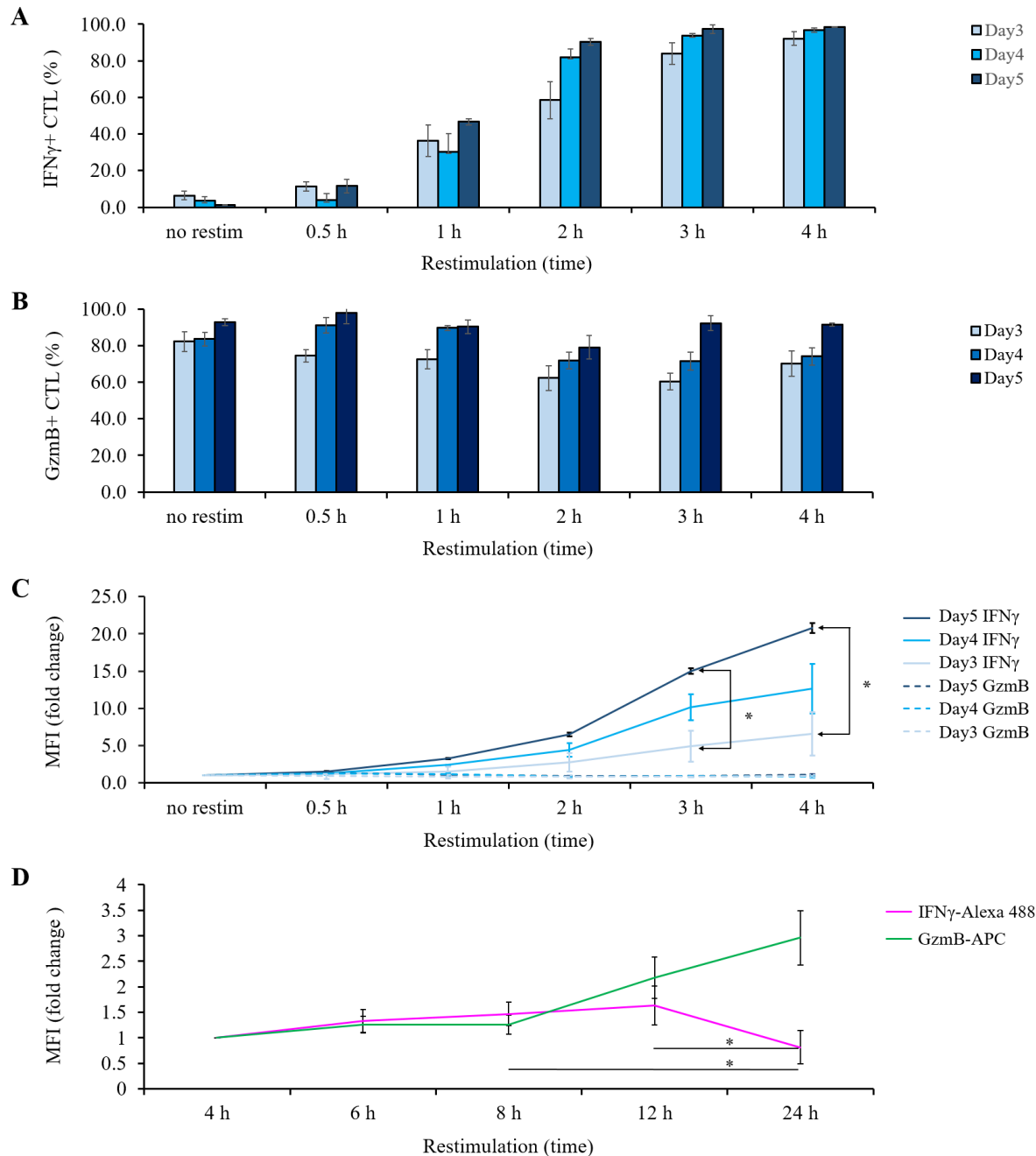


Figure 15. Intracellular IFN γ and GzmB in activated CTLs detected by flow cytometry.

Days 3-5 C57/BL6N CTLs were restimulated with 10 $\mu\text{g}/\text{mL}$ anti-CD3 ϵ antibody and stained for intracellular IFN γ and GzmB as indicated in the graphs. Data are expressed as mean \pm SEM and subjected to One Way ANOVA for comparison of differences, ns. $0.05 < p$, * $0.01 < p \leq 0.05$, ** $0.001 < p \leq 0.01$, *** $0.0001 < p \leq 0.001$. Experiments were repeated at least 3 times. **A-C**, 0-4 h restimulation. **A**, Percentage of IFN γ + CTLs **B**, Percentage of GzmB+ CTLs. **C**, Median fluorescence intensity change (the fold of start fluorescence) of anti-IFN γ -Alexa 488 and GzmB-APC. **D**, Median fluorescence intensity change (the fold of start fluorescence) of anti-IFN γ -Alexa 488 and GzmB-APC during 0-24 h restimulation.

3.2 Quantification of activated CTL subsets during restimulation

Many subtypes of CTLs have been identified. Most important are effector cells, effector-memory-, and central-memory-cells. To understand if IFN γ production is subtype-specific and if activation and

restimulation may change the subtype composition of the whole culture, we stained CTLs with subtype-specific surface markers, i.e CD44 (effector and effector-memory cells), CD62L (central-memory cell), using respective antibodies conjugated to a fluorophore and quantified them by FACS. When compared to no restimulation, the percentage of CD44 positive T-lymphocytes, as well as median fluorescence intensity (MFI) of CD44 Ab didn't vary significantly within 4 h restimulation no matter if day3, day4, or day5 CTLs were used (Figure 16A, C). It can be concluded that neither the day of culture nor restimulation changes the overall differentiation status in the culture. In contrast, the percentage of CD62L positive T-lymphocytes and MFI of CD62L Ab significantly declined upon initial restimulation, indicating a switch from central- to effector-memory cells (Figure 16B, C).

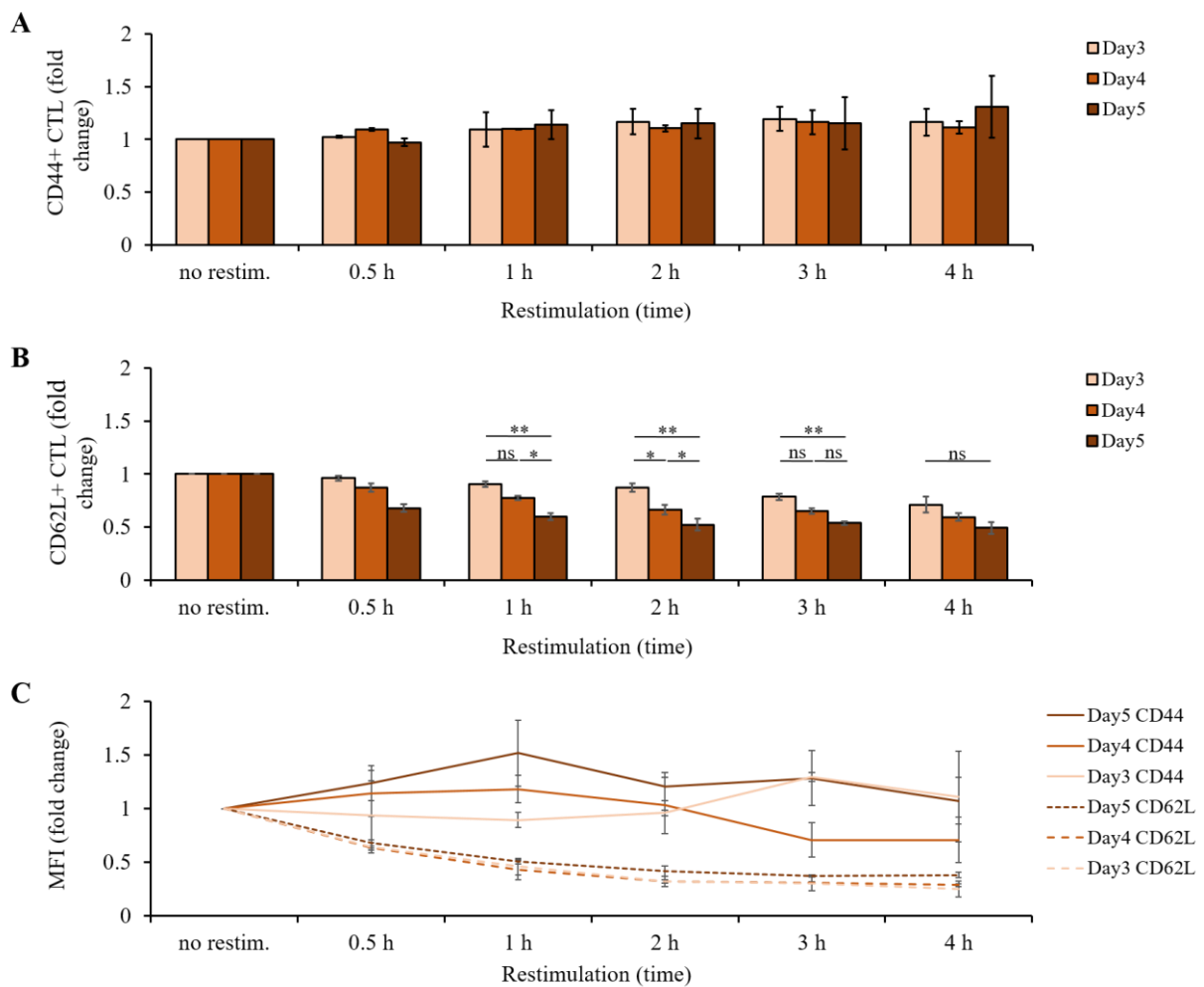


Figure 16. Effector- and central memory cell populations during restimulation.

Days 3-5 C57/BL6N CTLs were re-stimulated with 10 $\mu\text{g}/\text{mL}$ anti-CD3 ϵ antibody for 0-4 h and stained for CD44 and CD62L as indicated in the graphs. N=3. Data were shown as mean \pm SEM and subjected to One Way ANOVA for difference comparison, ns. $0.05 < p$, $* 0.01 < p \leq 0.05$, $** 0.001 < p \leq 0.01$, $*** 0.0001 < p \leq 0.001$. **A**, Fold change of CD44+ CTLs measurement. **B**, Fold change of CD62L+ CTLs measurement. **C**, Median fluorescence intensity (MFI) change of anti-CD44-PE and CD62L-FITC Abs. There was no significant difference in CD44 median FI change upon different hour restimulation no matter in day3 ($p = 0.798$), day4 ($p = 0.382$), or day5 CTLs ($p = 0.585$) CTLs. There was a significant difference in CD62L median FI change between no restim. and with restim in day3, day4 and day5 CTLs (In day3 CTLs: no restim. VS. 1-4 h restim. ($p \leq 0.001$), no restim. VS. 0.5 h restim. ($p = 0.004$), 0.5 h VS. 2-4 h ($0.001 < p < 0.05$), 0.5 h VS. 1 h (ns), 1-4 h (ns); In day4 CTLs: no restim.

VS. 0.5-4 h restim. ($p \leq 0.001$), 0.5 h VS. 1-4 h ($0.001 < p < 0.05$), 1-4 h (ns); In day5 CTLs: no restim. VS. 0.5-4 h restim. ($p < 0.001$), 0.5 h VS. 1-4 h ($p < 0.001$), 1 h VS. 2-4 h ($0.001 < p < 0.05$), 2-4 h (ns.)), indicating that CD62L was significantly reduced upon restimulation.

The more mature the CTLs had been, the more T_{EM} (CD62L^{low}) were generated upon restimulation (Figure 16B). Day5 cultures showed significantly more T_{EM} compared to day4 cultures in 2 h restimulation and day3 CTLs in 3 h restimulation (Figure 16B). Day4 cultures had significantly more T_{EM} in comparison to day3 cultures within 2 h restimulation. However, there was no significant difference in the percentage of T_{EM} and the MFI of CD62L after 3 h restimulation (Figure 16B, C).

3.3 Localization and trafficking of IFN γ in CTLs

3.3.1 Verification of a homemade *pMax-linker-IFN γ -mCherry* construct

To better understand IFN γ localization and to study its dynamics secretion in CTLs, we took advantage of a *pMax-linker-IFN γ -mCherry* construct (see material and methods) which we ectopically expressed in WT CD8⁺ T-lymphocytes. mCherry is a widely used red fluorescent protein variant that can be excited efficiently by the 561 nm laser. To follow IFN γ via fluorescence microscopy, we first performed control experiments to find a suitable time window in which IFN γ -mCherry was expressed as a secretion protein before proteolytic degradation occurs. For that purpose, we first transfected WT CD8⁺ T-lymphocytes with *pMax-linker-IFN γ -mCherry* and analyzed the cells at various time points (6 - 12 h) thereafter by immunoblotting with a mCherry detecting antibody. As expected, IFN γ -mCherry was detected as multiple bands with sizes around 46 kDa (Figure 17A). The appearance of three bands is the consequence of 0, 1, and 2 glycosylation sites within IFN γ . Over time, starting after 8 h, an additional band at 27 kDa appeared. We interpreted this band as mCherry-alone, due to the degradation of the full-length protein. The densitometric analysis revealed that the full-length protein makes 94.03 ± 0.03 %, 92.53 ± 0.02 %, 81.67 ± 0.05 %, and 73.82 ± 0.05 % of the total overexpressed proteins at 6 h, 8 h, 10 h, and 12 h after transfection, respectively (Figure 17B). At later time points, the amount of protein is reduced. There was no significant difference in the percentage of total full-length protein during 6-10 h after transfection.

We further performed immunostaining experiments. CTLs overexpressing IFN γ -mCherry were stained with aIFN γ -alexa488 at different time points (6 h, 8 h, and 10 h) after transfection, and observed with SIM (Figure 17C). A robust colocalization of aIFN γ Ab and mCherry was obtained at each time point, 6 h (PCC = 0.73 ± 0.02), 8 h (PCC = 0.78 ± 0.03), and 10 h (PCC = 0.69 ± 0.04) with the Pearson's correlation coefficient analysis (Figure 17D). There was no significant difference in colocalization of aIFN γ Ab and mCherry among 6 h, 8 h, and 10 h overexpression ($p = 0.166$). These results verify that overexpressed IFN γ -mCherry is intracellularly distributed as endogenous IFN γ (6 - 10 h).

Therefore, we suggested that 6 - 10 h of transfection was the optimal time window for morphological

and functional studies on CTLs overexpressing IFN γ .

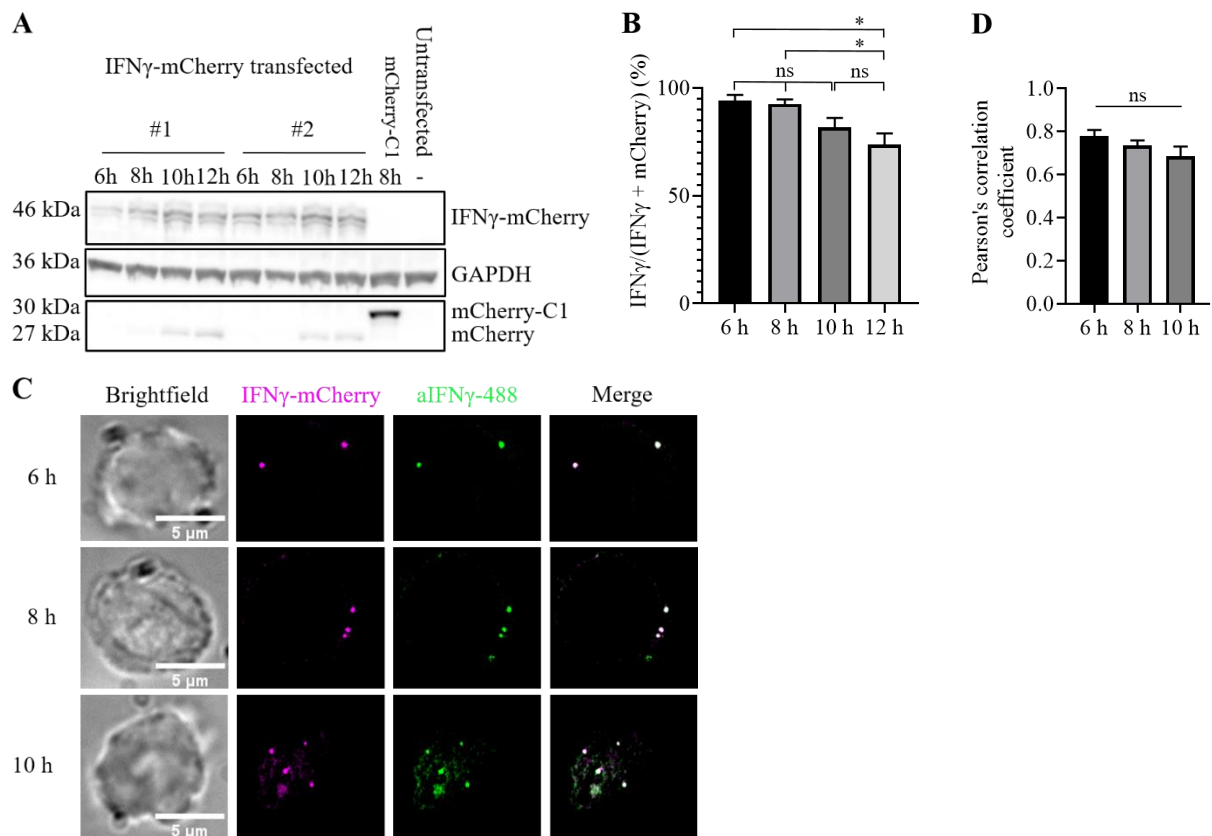


Figure 17. IFN γ -mCherry detection using Western Blot and immunocytochemistry.

A, B, Day5 CTLs were transfected with *pMax-IFN γ -linker-mCherry*. Cells were lysed at the indicated time points after electroporation. Denatured proteins were resolved on a 12% SDS-PAGE gel and transferred to 0.2 μ m nitrocellulose. IFN γ -mCherry secretion protein was detected by immunoblotting with a specific rabbit-anti-mRFP antibody at the expected size of 46 kDa. Cell lysates of untransfected cells and cells overexpressing mCherry-C1 alone were used as a negative and positive control, respectively. **A**, Lysates of CTLs were analyzed by immunoblotting 6 - 12 h after electroporation. GAPDH (36 kDa) was used as the loading control. A representative WB loading with CTLs lysates from two independent mice was shown. N = 4. **B**, Protein amounts of IFN γ -mCherry (secretion protein) and mCherry (degradation) were analyzed by densitometry in ImageJ and displayed as the percentage of total overexpressed protein (N = 4). **C**, One representative cell SIM imaging from each time point was shown here. Day4 WT CTLs were transfected and settled down on 0.005% poly-L-ornithine-coated coverslips, fixed and stained for IFN γ with rat anti-mouse IFN γ Ab coupled with Alexa 488. Cells were then mounted and imaged under SIM with ZEN software. **D**, Colocalization of endogenous IFN γ and overexpressed IFN γ -mCherry. The colocalization (Pearson's correlation coefficient, P) of endogenous and overexpressed IFN γ was analyzed by ImageJ and data were displayed in the histogram (n = 31, 22, 22). **B, D**, Data were shown in mean + SEM in the graph and subjected to One Way ANOVA for difference comparison, ns. 0.05 < p, * 0.01 < p \le 0.05, ** 0.001 < p \le 0.01, *** 0.0001 < p \le 0.001.

3.3.2 Live cell imaging of the conjugation between CTLs and P815 target cells

Since it has been shown that IFN γ is only produced following stimulation (Figure 15), where IFN γ is localized inside the cell and how its localization is related to cytotoxic granules (CGs) are interesting to discover. To get a qualitative answer, we performed live cell imaging with CTLs and P815 cells as targets. We took advantage of the GzmB-mTFP KI mice which endogenously expressed TFP marked GzmB in

CTLs. Activated GzmB-mTFP KI CTLs were transfected with IFN γ -mCherry. As a result, we could determine the localization of both IFN γ and GzmB intracellularly. CTLs and P815 together were put on the stage of a Laser Scanning Microscope and movies were recorded to capture CTL/P815 conjugates (Figure 18). Single CTLs showed a dispersed distribution of GzmB and IFN γ . Most of both markers could be identified in opposite the leading edge of a migrating CTL, as it is typical for intracellular vesicles. We could observe that after having formed an IS between CTLs and target cells, IFN γ and GzmB were trafficking together to the immunological synapse (IS). All these observations strongly argue for a joint transport of GzmB and IFN γ . Because of the limited optical resolution in the above-described microscopic assay, we were not able to conclude on the subcellular level from those experiments, if both proteins go together in one vesicle type. Further experiments were therefore carried out to clarify this question.

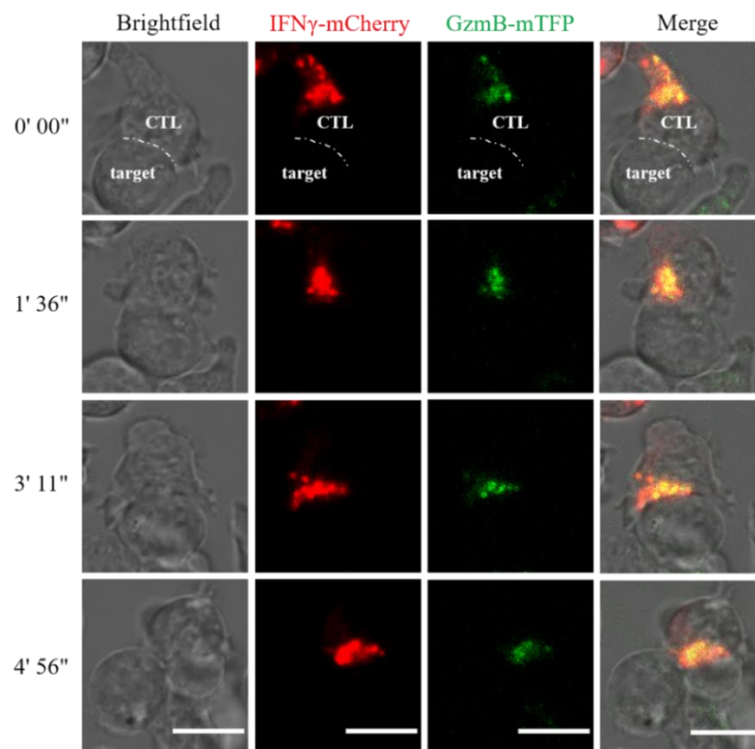


Figure 18. Conjugation of CTLs and P815 cells.

Confocal time-lapse imaging of CTLs (GzmB-mTFP KI CTLs overexpressing IFN γ -mCherry) conjugating to P815 cells and observation of IFN γ and GzmB trafficking. Scale bars: 10 μ m.

3.3.3 Super-resolution SIM analysis of IFN γ localization in CTLs

3.3.3.1 Overexpressed IFN γ partially colocalizes with GzmB and was found in identical cellular compartments when compared to endogenous IFN γ

Having validated that 6 to 10 h was the best time window to observe overexpressed IFN γ -mCherry, we next investigated the intracellular localization of IFN γ . This dataset has two goals. First, to verify if

overexpressed IFN γ can be found in the same compartments as endogenous IFN γ as figure 18 may imply, and the second aim is to find in which vesicle population IFN γ is. At present, it is not clear whether IFN γ has its class of vesicles or whether IFN γ is stored and released together with known vesicle classes such as cytotoxic granules (CGs), MVBs, and so on. To test for both possibilities, the degree of colocalization of IFN γ and CGs was measured in CTLs that were overexpressing IFN γ and those that expressed IFN γ endogenously. Moreover, we tested two combinations of the restimulation stimulus (2 h and 4 h) and DNA concentrations for transfection (2 μ g/3 $\times 10^6$ cells and 4 μ g/3 $\times 10^6$ cells) (Figure 19).

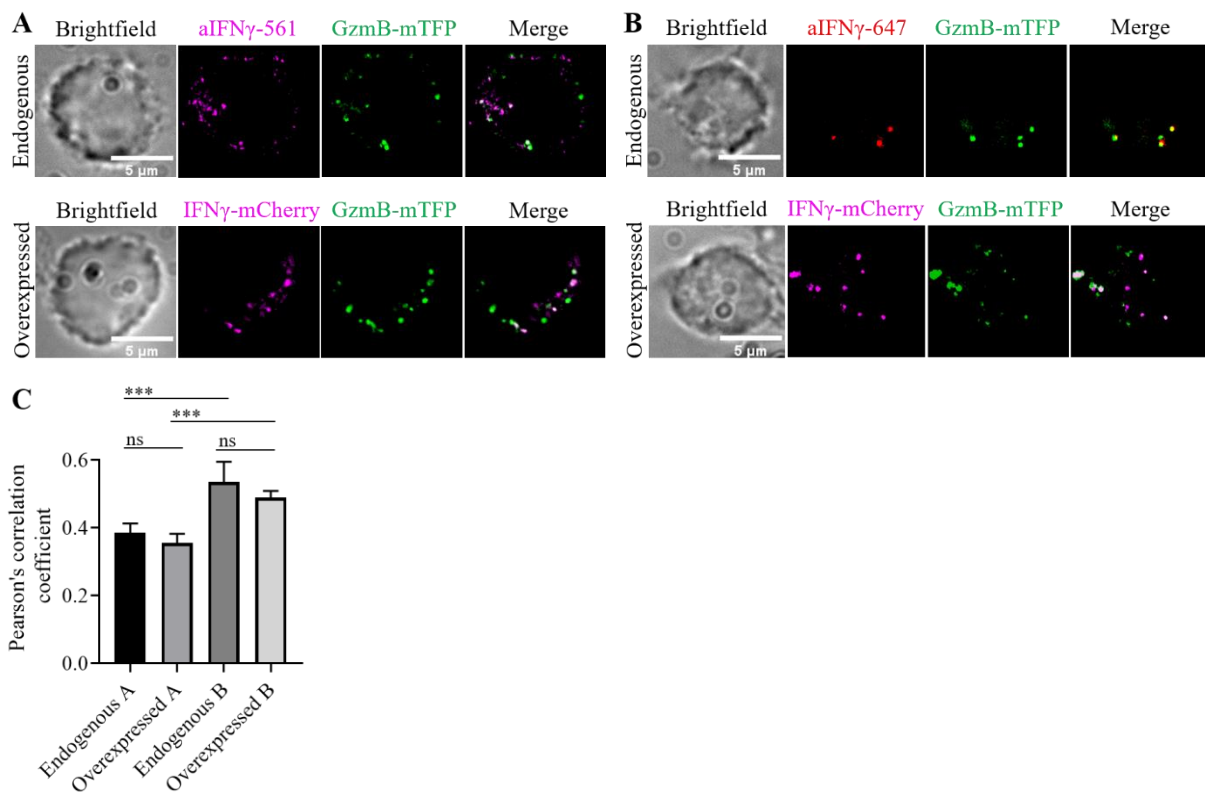


Figure 19. IFN γ partially colocalizes with GzmB.

Each cell SIM imaging was representative of at least 3 experiments. The GzmB and IFN γ were either indicated by fluorescence-linked target protein expression (GzmB-mTFP, IFN γ -mCherry) or by fluorescently conjugated antibodies (IFN γ -Alexa 561 or 647). Fluorescence colocalization was analyzed with Pearson's correlation coefficient in the Plugin of ImageJ. Data were subjected to t-test for statistical analysis and shown in median + SEM. **A**, Imaging of fluorescently conjugated GzmB and IFN γ from combination A. Combination A: Day5 GzmB-mTFP KI CD8 $^+$ T-lymphocytes were either re-stimulated for 2 h with anti-CD3 ϵ Ab (10 μ g/mL) (n=85) or transfected with *pMax-IFN γ -linker-mCherry* (2 μ g DNA/3 $\times 10^6$ CTLs, 6 h) for IFN γ expression. Cells with good fluorescence signals of GzmB and IFN γ were chosen for colocalization analysis, n=46, N=3. **B**, Imaging of fluorescently conjugated GzmB and IFN γ in combination B. Combination B: Day5 GzmB-mTFP KI CD8 $^+$ T-lymphocytes were either restimulated with plate-coated anti-CD3 ϵ (30 μ g/mL, 4 h, n=99) or transfected with *pMax-IFN γ -linker-mCherry* (4 μ g DNA/ 3 $\times 10^6$ cells, 7 h). Cells with good fluorescence signals of GzmB and IFN γ were chosen for colocalization analysis, n =38, N=4. **C**, Compared the colocalization of IFN γ with GzmB in two combinations. In cells overexpressing IFN γ , colocalization had no significant difference from endogenous (t-test, $p = 0.689$ for combination A, $p = 0.326$ for combination B). Prolonging the restimulation or increasing expressing time and overexpressed DNA amount could significantly improve the colocalization of IFN γ with GzmB (t-test, $p \leq 0.001$). Data were shown in median + 95% confidence interval (CI).

For both conditions, we could not find significant differences in Pearson's correlation coefficient between GzmB and endogenous resp. overexpressed IFN γ (Figure 19A: endogenous IFN γ = 0.39, overexpressing = 0.36; Figure 19B: endogenous IFN γ = 0.54, overexpressing = 0.47). From this result, we conclude that overexpression does not significantly change the broad distribution of IFN γ in CTLs (p = 0.689 and 0.326 respectively, Figure 19C). Remarkable is the finding that the correlation coefficient increased with a prolonged restimulation-phase significantly (Figure 19C). We believe that the longer time of stimulation leads to forming of new vesicles that preferably contain both IFN γ and GzmB. The observed partial colocalization between GzmB and IFN γ allows the surprising conclusion that a robust part of IFN γ is in compartments that also contain cytotoxic substances, and therefore it should be released by regulated secretion rather than constitutive. Further experiments will clarify in which vesicle types IFN γ can be found and to what degree these vesicles contribute to overall IFN γ release.

3.3.3.2 The degree of IFN γ colocalization with GzmB is independent of IS-formation

In this set of experiments, we proved that the colocalization of IFN γ with GzmB is dependent on the formation of an IS. As in the experiments above, we made use of functional anti-CD3 ϵ antibodies coated to the surfaces of coverslips. Activated T-lymphocytes make contact with this surface and the antibody activates the TCR, thereby building a functional artificial IS. As a negative control, the coverslips can be coated with poly-L-ornithine onto which CTLs also settle down mostly by unspecific ICAM binding but the TCR engagement is missing. Imaging was again done by structure illumination microscopy (SIM) and analyzed by ImageJ. CTLs either restimulated with 30 μ g/mL anti-CD3 ϵ antibodies (R) or non-restimulation (N) were settled down on 0.005 % poly-L-ornithine (P) or 10 μ g/mL anti-CD3 ϵ Ab-coated (C) coverslips.

We found a robust colocalization of IFN γ and GzmB at all conditions (Figure 20A). A slight but still significant difference could be observed between not-restimulated and restimulated CTLs on poly-L-ornithine (NP vers. RP and RP vers. NC, Figure 20 B). There was also a tendency of a higher colocalization, though the difference was not significant, between not-restimulated and restimulated cells on anti- CD3 ϵ . We interpreted the slight increases in colocalization as a result of enhanced IFN γ production by restimulation. Most interesting is the finding that the degree of colocalization is independent of the existence of an IS (NP and RP vers. NC and RC, Figure 20 B), since this finding makes it very unlikely that a specific vesicle type carrying only IFN γ or GzmB fuse before the other that should change the degree of colocalization. All of that data are counting for the idea of a common vesicle type transporting both IFN γ and GzmB to the IS and secreting it there together. Since SIM is a high-resolution microscopic technique, we can even discriminate single vesicles from each other and therefore count them (Figure 20 C, D). There was no significant difference in the vesicle number of IFN γ /GzmB among the 4 conditions (IFN γ vesicle number comparison, p = 0.856; GzmB vesicle number comparison, p = 0.903), suggesting that a CTL performs a stable equilibrium concerning production and release of

vesicles. Moreover, the absolute numbers of GzmB and IFN γ vesicles were similar (at least not statistically different), which is again an argument for a common vesicle class for both GzmB and IFN γ .

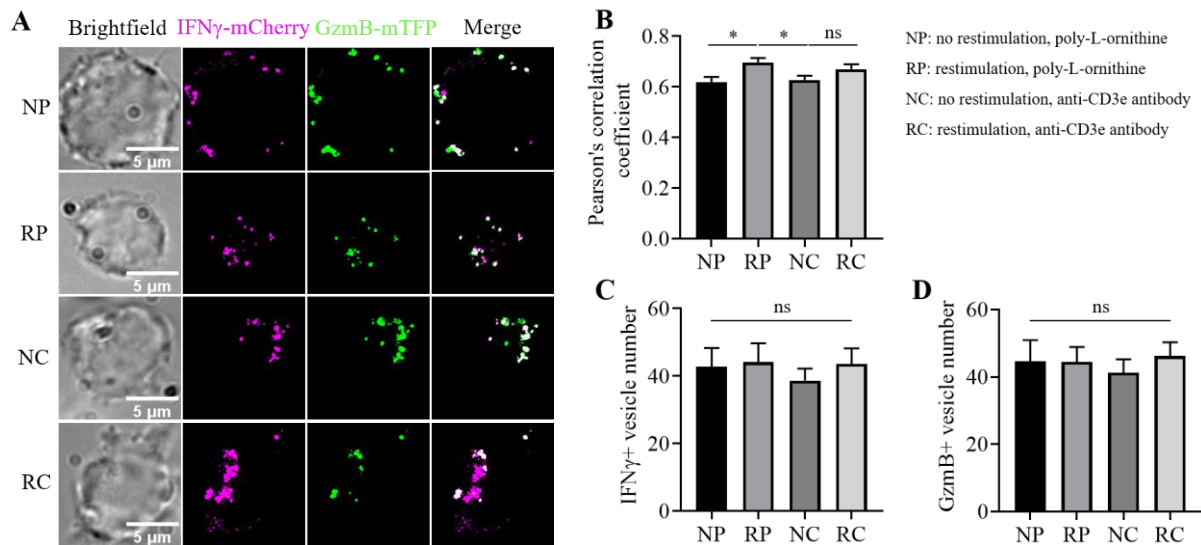


Figure 20. IFN γ robustly colocalizes with GzmB at different conditions.

DaDay 5zmB-mTFP KI CD8⁺ T-lymphocytes were transfected with *pMax-IFN γ -linker-mCherry* ($4 \mu\text{g DNA}/3 \times 10^6$ cells). 8 h resting/not-stimulated (N) or 6 h resting plus 2 h restimulated (R) CTLs were settled either on poly-L-ornithine-coated (P) or anti-CD3 ϵ antibody-coated (C) coverslips. NP: not-restimulated CTLs on poly-L-ornithine coated-coverslips. RP: restimulated CTLs on poly-l-ornithine-coated coverslips. NC: not-restimulated CTLs on anti-CD3 ϵ Ab-coated coverslips. RC: restimulated CTLs on anti-CD3 ϵ Ab-coated coverslips. Fluorescence colocalization of IFN γ -mCherry with GzmB-mTFP at 4 conditions was analyzed by Pearson's correlation coefficient in ImageJ. And IFN γ /GzmB vesicle number was counted in ZEN software. Data were from 3 independent experiments. **A**, SIM images of 4 conditions are representative. **B**, Colocalizations of IFN γ and GzmB. Data were shown in mean + SEM. NP: PCC = 0.62 ± 0.02 , number of cells (n) = 32. RP: PCC = 0.70 ± 0.17 , n = 46. NC: PCC = 0.63 ± 0.17 , n = 52. And RC: PCC = 0.67 ± 0.19 , n = 41. Data were shown in mean + SEM in the graph and subjected to the t-test to confirm significance. **C**, **D**, Data were shown in median + 95% CI and subjected One Way ANOVA analysis to confirm significance. **C**, Intracellular IFN γ vesicle number in CTLs was counted at each condition. Median numbers of IFN γ and GzmB vesicles per cell: 30 (NP), 37 (RP), 33 (NC), and 39 (RC). Cell number for analyzing IFN γ vesicle number at each condition: $n_{NP}=17$, $n_{RP}=19$, and $n_{NC}=18$, and $n_{RC}=18$. **D**, Intracellular GzmB vesicle number in CTLs was counted at each condition. The median number of GzmB vesicles per cell: 38 (NP), 43 (RP), 36 (NC), and 46 (RC). N=3. Cell number for analyzing GzmB vesicle number at each condition: $n_{NP}=17$, $n_{RP}=19$, $n_{NC}=18$, and $n_{RC}=18$.

3.4 Subcellular morphology of IFN γ compartments – TEM and CLEM

All data that were shown so far are compatible with the assumption that IFN γ is localized in the same vesicle types as cytotoxic granules but perhaps also in so far unidentified vesicles. To identify the actual morphological structures containing IFN γ , transmission electron microscopic studies were performed in combination with light microscopic analyses (so-called CLEM, see Material and Methods). The principle of the technique is to identify IFN γ - and/or GzmB-containing structures by light microscopy in the first

step. Subsequently, the identified structures become morphologically resolved by transmission electron microscopy (TEM).

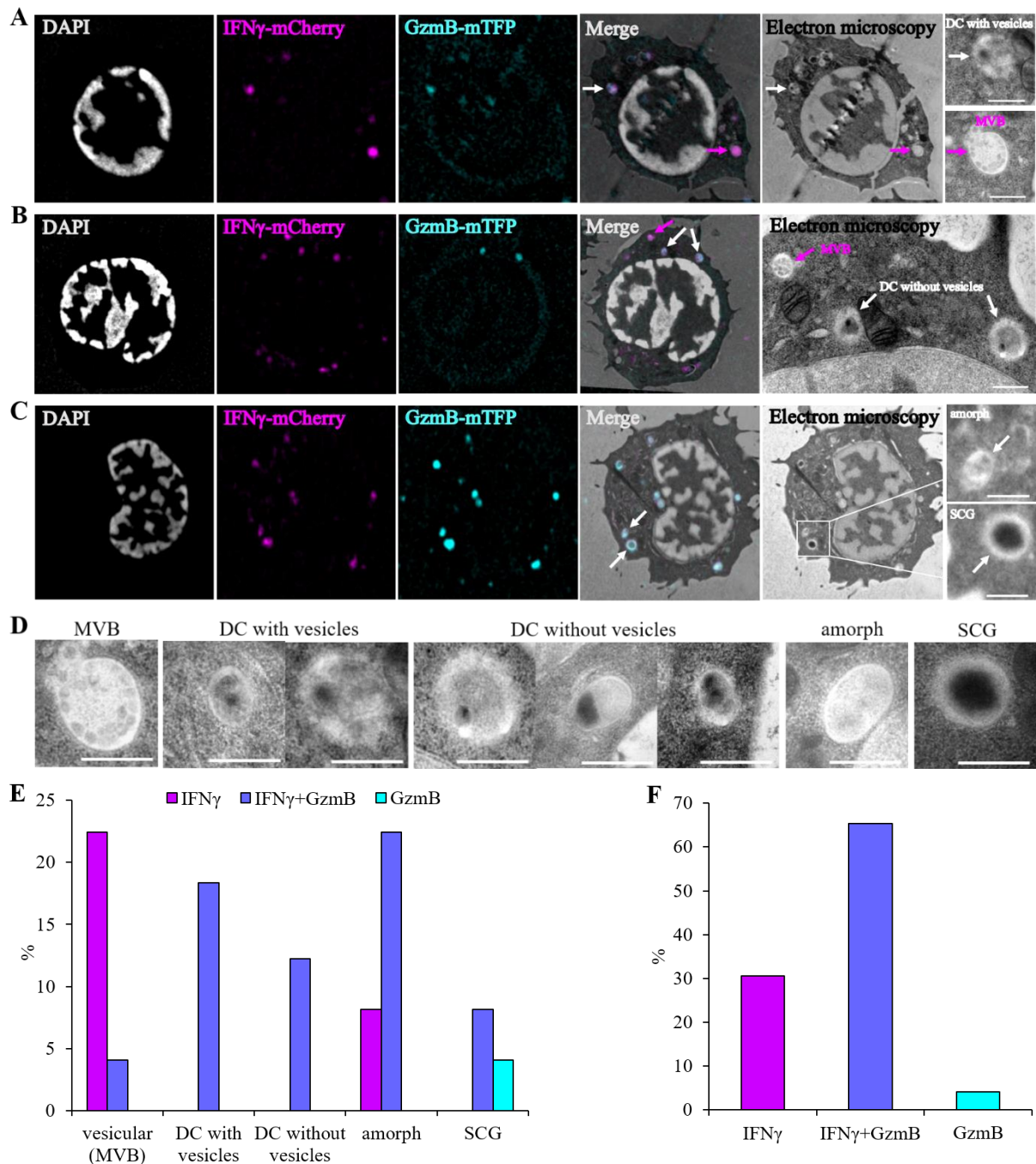


Figure 21. IFN γ and GzmB exist in the same compartments.

Day5 GzmB-mTFP KI CD8⁺ T-lymphocytes were transfected with *pMax-IFN γ -linker-mCherry* (4 μ g DNA/3 \times 10⁶ cells, 6.5 h) and CTLs (1 μ L, 1 \times 10⁵ cells/coverslip) were settled on anti-CD3 ϵ (30 μ g/mL) coated sapphire coverslips. The fluorescence of IFN γ -mCherry and GzmB-mTFP were analyzed by CLEM. Images were representative of N = 2 animals, n = 13 cells, 49 fluorescent organelles, and 3.76 organelles per cell section. **A-C**, CTLs displayed IFN γ and GzmB in different organelles according to their morphology. Scale bar, 0.5 μ m. **A**, A CTL showing one IFN γ ⁺GzmB⁺MVB (indicated by magenta arrows) and two IFN γ ⁺GzmB⁺ DC with vesicles (indicated by white arrows). **B**, A CTL showing one IFN γ ⁺GzmB⁺MVB (magenta arrows) and two IFN γ ⁺GzmB⁺ DC without vesicles (white arrows). **C**, A CTL showing one IFN γ ⁺GzmB⁺ amorph and one IFN γ ⁺GzmB⁺ SCG. **D**,

Morphological diversity of different types of organelles. **E**, Classification of the organelles by their morphology and content. IFN γ ⁺GzmB⁻ organelles were mainly MVBs and some were amorph vesicles. IFN γ ⁺GzmB⁺ organelles made up 22.5% amorph vesicles, 31% DC vesicles with or without intravesicular vesicles, and others were MVBs and SCGs. **F**, Percentage of all vesicles related to content. The percentage was calculated by counting the number of organelles carrying either IFN γ or GzmB, or both. IFN γ ⁺GzmB⁻, IFN γ ⁺GzmB⁺, and IFN γ ⁻GzmB⁺ organelles made up 30%, 66%, and 4% of populations respectively.

As a result, an unexpected variety of structures could be found. In most cases, IFN γ and GzmB were localized together but in different vesicle populations as classical cytotoxic granules (CGs), multivesicular bodies (MVB), single core granules (SCGs), and recently identified multicore granules (MCGs) (Figure 21A-D). For quantitative analyses, we group the variety of vesicles as MVB/MCG, dark core granules (DC) with or without vesicles, amorph vesicles (amorph), and single core granules (SCG), according to their morphology (Figure 21D). Among the different vesicle types, the distribution of IFN γ and GzmB is discrete, meaning that in all DCs both substances coexist while most MVBs carry IFN γ only. Amorph vesicles are just the opposite. Most of them carry both IFN γ and GzmB. The only vesicle population that can carry GzmB alone is SCG (Figure 21E, from left to right 22.5%, 4%, 18%, 12.5%, 8%, 22.5%, 8%, 4%, respectively). Taking all vesicle types together 66% of them contain both IFN γ and GzmB while in 30% IFN γ and in 4% GzmB exist alone (Figure 21F). These results were in good agreement with what was shown before in our colocalization studies (Figure 20). Also there, with some variation from sample to sample around 60 % of the GzmB and IFN γ signals were colocalized.

3.5 Live cell imaging of IFN γ secretion with TIRF-M

3.5.1 Usability of a pH-sensitive IFN γ -pHuji expression construct

So far, we collected indirect evidence for a joint secretion of GzmB and IFN γ by a common population of vesicles at the immunological synapse. To directly demonstrate the joint fusion, we now wanted to use TIRF-M, which allows precise observations at the plasma membrane/coverslip interface down to a depth of 200 nm by a special illumination technique. A prerequisite for TIRF is a clear and specific staining of the vesicles of interest. Before starting the experiments, we made use of the GzmB-mTFP KI mouse which specifically marks respective vesicles. In former experiments, we used IFN γ -mCherry as an IFN γ marker. Since mCherry is not pH sensitive, therefore described feature is missing making mCherry a bad choice for TIRF. While pHuji is well-suited for TIRF since its pH sensitivity lets it highlight the moment when a fusion pore opens. Therefore, we decided to clone a new, better-suited construct (see Material and Methods) leading to the expression of the fusion-protein IFN γ -pHuji. As a first step, we optimized protocols and characterized the new fusion construct to verify its usability. We first optimized the DNA concentration for electroporation (Figure 22 A, B) and analyzed the colocalization of IFN γ -pHuji and GzmB (Figure 22 C-E). 3×10^6 GzmB-mTFP CTLs were electroporated with 2 μ g or 4 μ g *pMax-*ifng-linker-pHuji** and expression were quantified after 6 and 8 h.

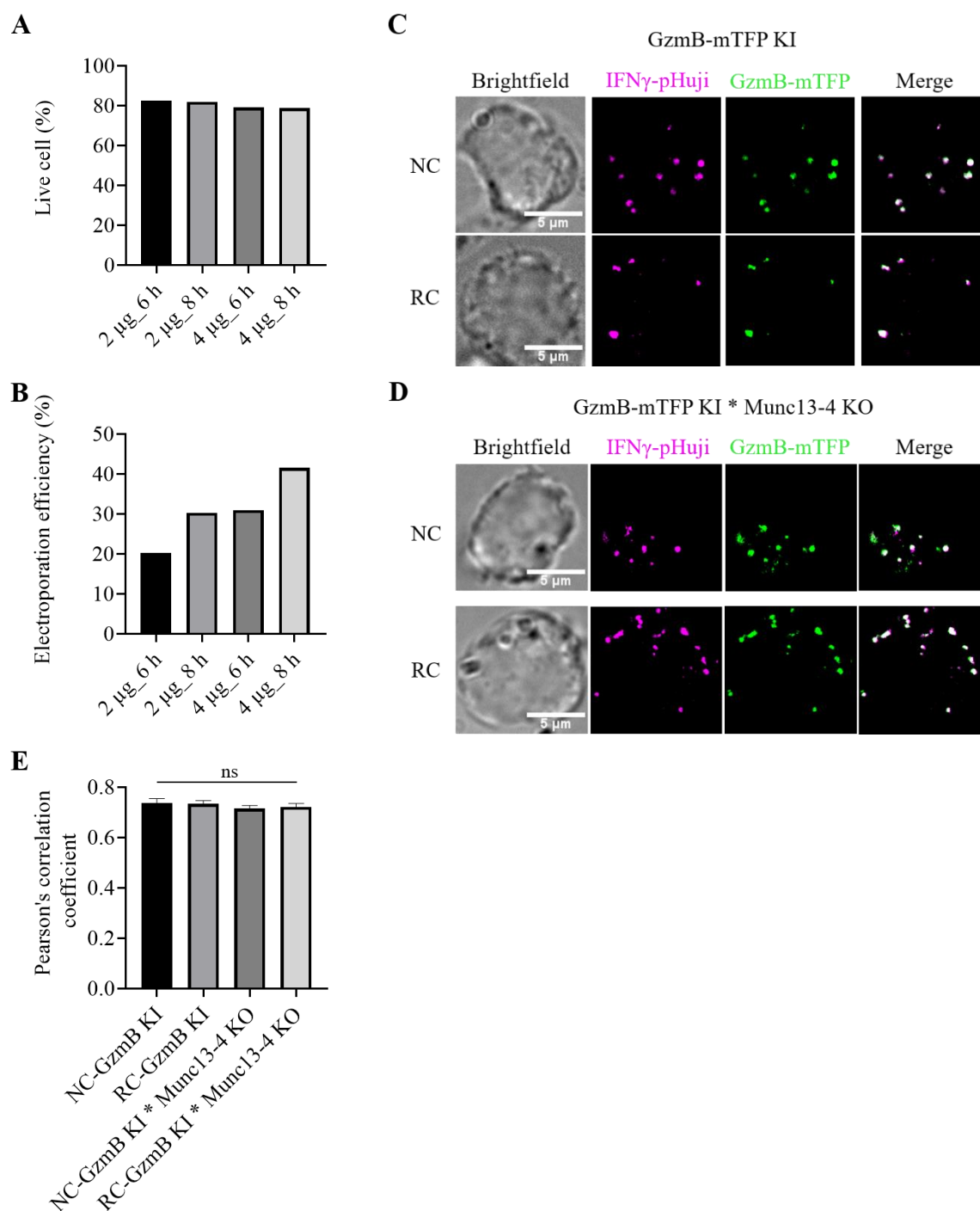


Figure 22. Validation of a *pMax-ifng-linker-pHuji* construct.

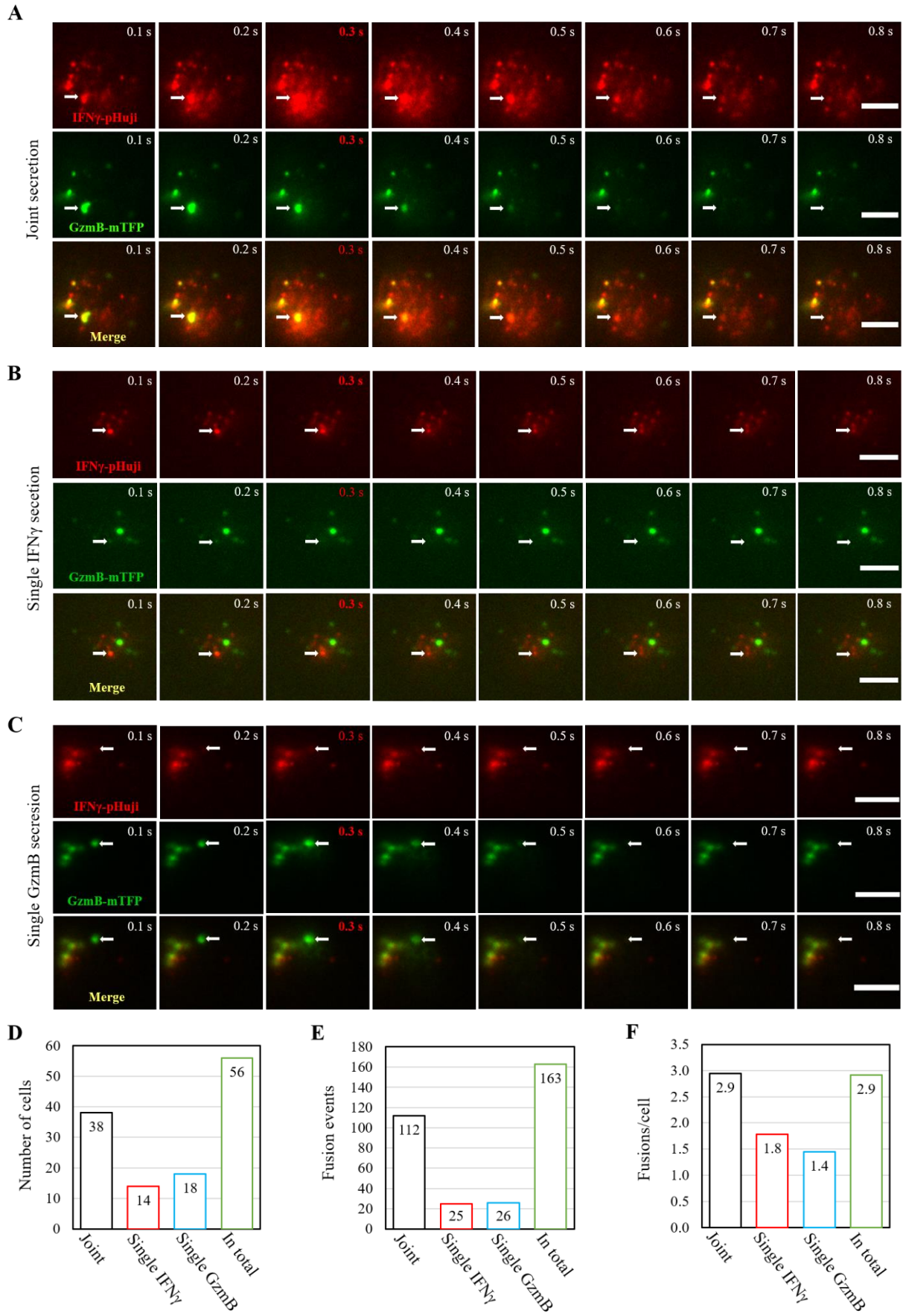
A-B, Optimization of DNA amount and expression time of a *pMax-ifng-linker-pHuji* construct. Day5 GzmB-mTFP KI CTLs were electroporated with *pMax-ifng-linker-pHuji* either in an amount of 2 or 4 μ g/ 3×10^6 CTLs. After 6 h and 8 h expression, T-lymphocytes were centrifuged down, re-suspended in DPBS (1 \times), and analyzed for the percentage of living cells (**A**) and the transfection rate (**B**) by FACS. Data were shown in mean. **C, D**, Day5 GzmB-mTFP KI (**C**) or GzmB-mTFP KI \times Munc13-4 KO (**D**) CD8 $^+$ T-lymphocytes were transfected with *pMax-IFN γ -linker-pHuji* (4 μ g DNA/ 3×10^6 cells). IFN γ -pHuji and GzmB-mTFP were observed with 561 nm and 488 nm laser excitation with SIM (7.5 h resting, N = 2). **E**, Colocalization of IFN γ and GzmB in cells from GzmB-mTFP (NC, n=64; RC, n=51) and GzmB-mTFP KI * Munc13-4 KO (NC, n=59; RC, n= 56). Data were shown in median + 95% CI and subjected One Way ANOVA analysis to confirm significance. No significant difference was found in IFN γ and GzmB colocalization between GzmB-mTFP KI CTLs and GzmB-mTFP KI * Munc13-4 KO CTLs ($p = 0.167$).

Essentially, the DNA concentration did not affect the cell viability significantly, but higher DNA concentration increased the transfection rate (Figure 22 A, B). Colocalization studies on cells from both GzmB KI animals and the later used GzmB KI × Munc13-4 KO crossbreed animals resemble the high colocalization (PCC) between IFN γ and GzmB that was described earlier (Figures 22 C-E). The results verify that the *pMax-ifng-linker-pHuji* construct in CTLs is very similar to the mCherry construct in terms of cell compatibility, expression rate, and cellular distribution.

3.5.2 The majority of fusion events at the IS are IFN γ /GzmB joint fusions

Having demonstrated a robust colocalization of IFN γ and GzmB with overexpressed IFN γ -pHuji in GzmB-mTFP KI CD8⁺ T-lymphocytes, we next used that construct to analyze the secretion process in living cells. For experiments, IFN γ -mCherry transfected CTLs from GzmB KI animals were settled onto anti-CD3 antibody-coated coverslips in a Ca²⁺-free medium to stop secretion. Ca²⁺ (10 mM) which is added to the medium after 1 - 2 min starts the secretion and the observation of the cells was continued for another 5 - 6 min. Single vesicle secretion was in general characterized by a sudden increase in fluorescence (opening of the fusion pore and neutralization of the vesicle content) followed by a loss in fluorescence when vesicular cargo (IFN γ and/or GzmB) diffused away. Figure 23A-C shows vesicle secretion events representing joint fusion (IFN γ +GzmB⁺), single IFN γ fusion (IFN γ +GzmB⁻), and single GzmB fusion (IFN γ -GzmB⁺). Out of 56 cells, 38 showed joint fusions and 14 resp. 18 single fusion events of GzmB and IFN γ respectively (Figure 23D), meaning that most cells were able to perform joint fusions in addition to single ones. In terms of total fusion events, joint fusion events made up the majority (112 out of 163) of fusions (Figure 23E). Same as the total fusions per cell, joint fusions were also 2.9 per cell, while single-IFN γ - and single-GzmB-fusions were 1.8 and 1.4 per cell respectively (Figure 23F).

To examine if the ratios of the different fusion events could change depending on the day of culture, we repeated measurements and directly compared the results of day5 to day7 CTLs. The percentage of secreting cells from days 5-7 did not differ significantly (55.78 ± 7.50 %, 42.14 ± 5.71 %, 40.93 ± 5.50 % on respective days 5, 6 and 7) (Figure 23G). Changes in the three types of fusion, single IFN γ , single GzmB, and joint fusion could be detected (Figure 23H). When the fusion rate of double positive vesicles stayed constant over days 5-7 (approximately 70 % of all fusions), the fusion rate of single IFN γ vesicles decreased dramatically (15 %, 1%, 0,5% on respective days) while single GzmB vesicles fusion rate increased (16%, 29%, 30% on respective days), indicating that more matured CTLs had more single GzmB- and less single IFN γ -containing vesicles.



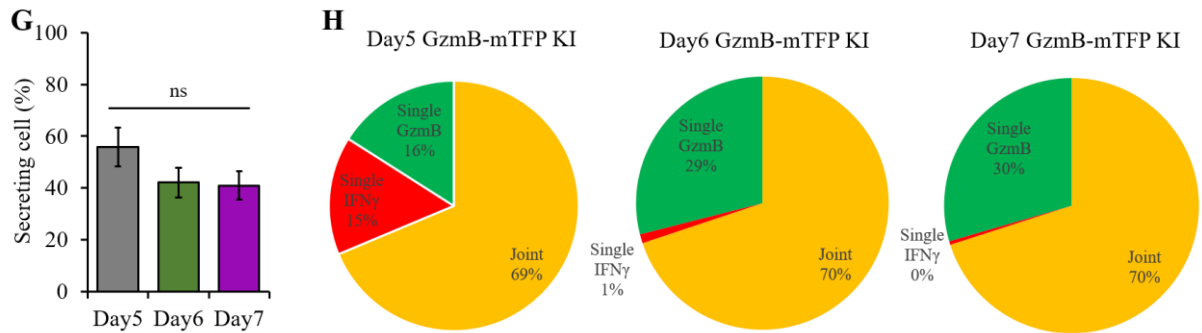
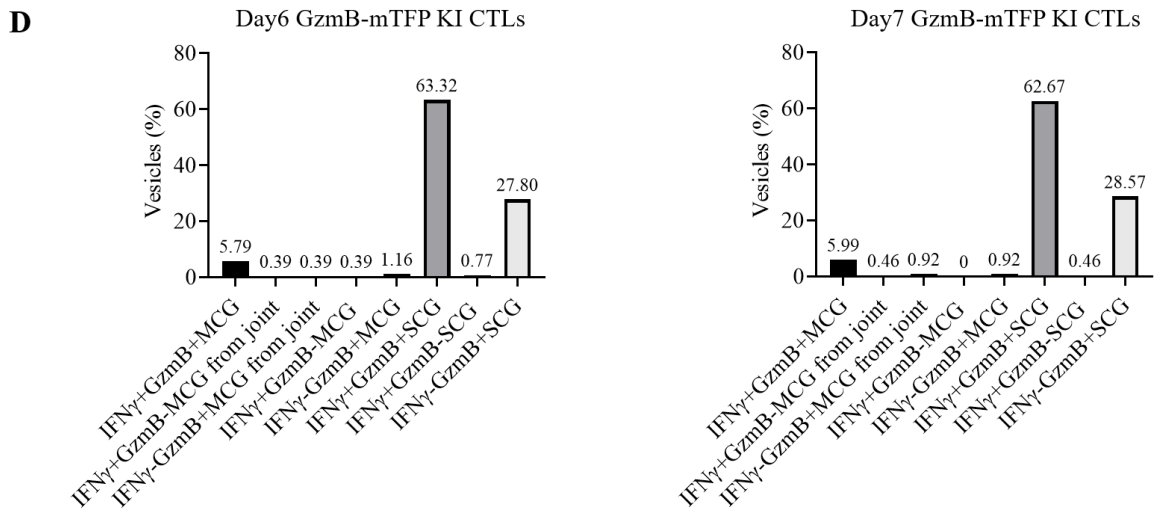
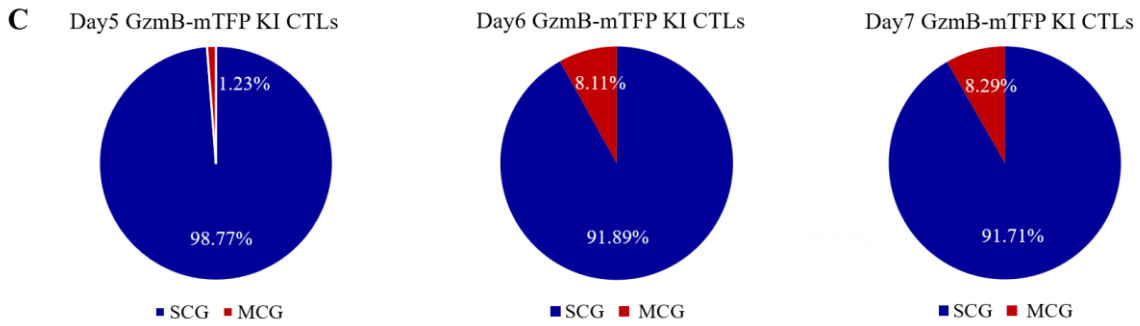
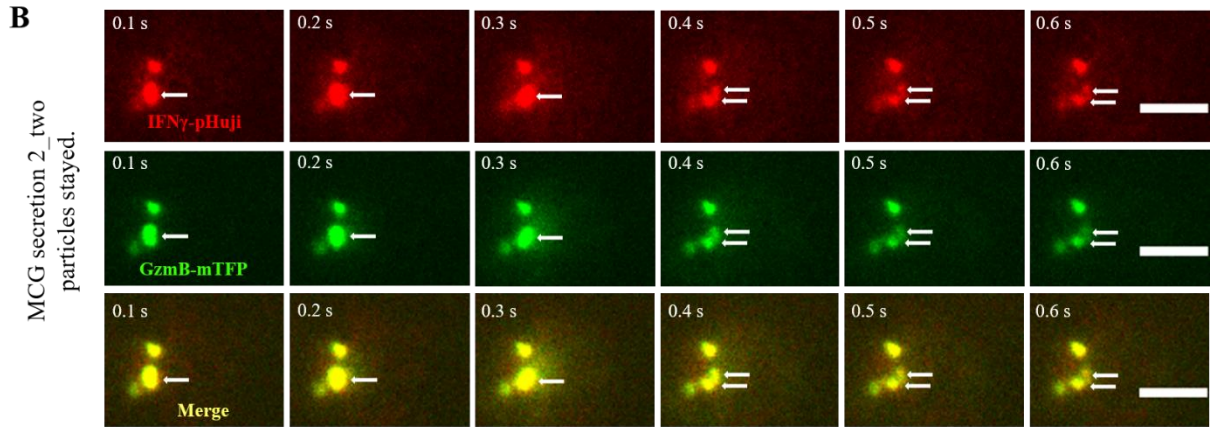
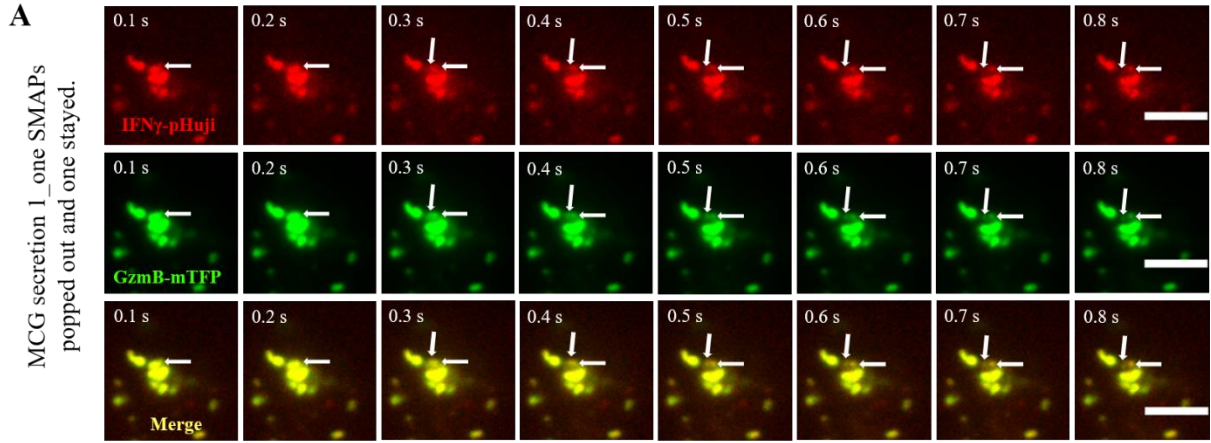


Figure 23. IFN γ and GzmB secretion observed by TIRF-M.

Day5 (A-F) or days 5-7 (G, H) activated GzmB-mTFP KI CD8⁺ T-lymphocytes were transfected with *pMax-IFN γ -linker-pHuji*. IFN γ - and GzmB-containing vesicles were observed in the TIRF field as described in the text. A-C, Joint (IFN γ and GzmB in one vesicle) and single secretion events (IFN γ or GzmB in separate vesicle) are shown in three exemplary cells. Fusing vesicles are indicated by white arrows. The time marked in red in the third image is the vesicle fusion moment which shows the brightest fluorescence of secreted proteins. D-E, 56 cells with 163 secretion events from 4 independent experiments were observed and analyzed. Three classes of secretion events were defined: joint secretion (IFN γ and GzmB in a common vesicle), single secretion of IFN γ , and single secretion of GzmB. D, Most T-lymphocytes (38/56) performed joint secretions of IFN γ and GzmB. E, On the level of fusion events, joint fusion was also dominant (112 out of 163 fusion events) F, Fusion events per cell of the respective class of fusion event. G, The fraction of secreting cells from all cells was independent of the day of culturing between day5 and day7 cells (Data were shown in mean \pm SEM, and significance was tested with One Way ANOVA). H, Interestingly, from day5 to day7 of culturing, single IFN γ secretion events nearly completely disappear and IFN γ is exclusively secreted together with GzmB (joint) from day7 cells.

3.5.3 IFN γ and GzmB are released at the IS by both SCGs and MCGs

In the previous chapter, we clarified to which ratio GzmB and IFN γ are released together, resp. separately from CTL. Now we are trying to add morphological aspects to our analysis. Recently, it is known that vesicular content from CTLs is not only released by single core granules but also by multi-core granules (presumably multivesicular bodies). With TIRF it is possible to discriminate both modes of secretion by their kinetics and appearance. While the fluorescence changes of SCG fusion are typically finished within less than a second, a MCG fusion needs several seconds up to 30 s. Morphologically, a MCG fusion can be identified by vesicles that become unmasked exactly at the area of the fusion of the MCG, such events are called multi-core granule-fusion (MCG-fusion) and can be seen in Figure 24A, B. Note that at the end of the time curve, there is no longer a single vesicle at the marked location, but several vesicles can be seen from which it is believed that they are released content (vesicles and/or protein deposits like SMAPS) from MCGs. We found that the ratio of MCGs/SCGs fusions increased from day5 to day7, which might also positively associate with CTLs maturation. There were nearly 1 % MCG and 99 % SCG fusions at day5 CTLs, while around 8% MCG and 92 % SCG fusions could be detected up to day7 (Figure 24C). The TIRF dataset we had, also allowed us to further split up the population of MCGs and SCGs at the end into 8 subpopulations dependent on what was deposited after fusion (Figure 24D).



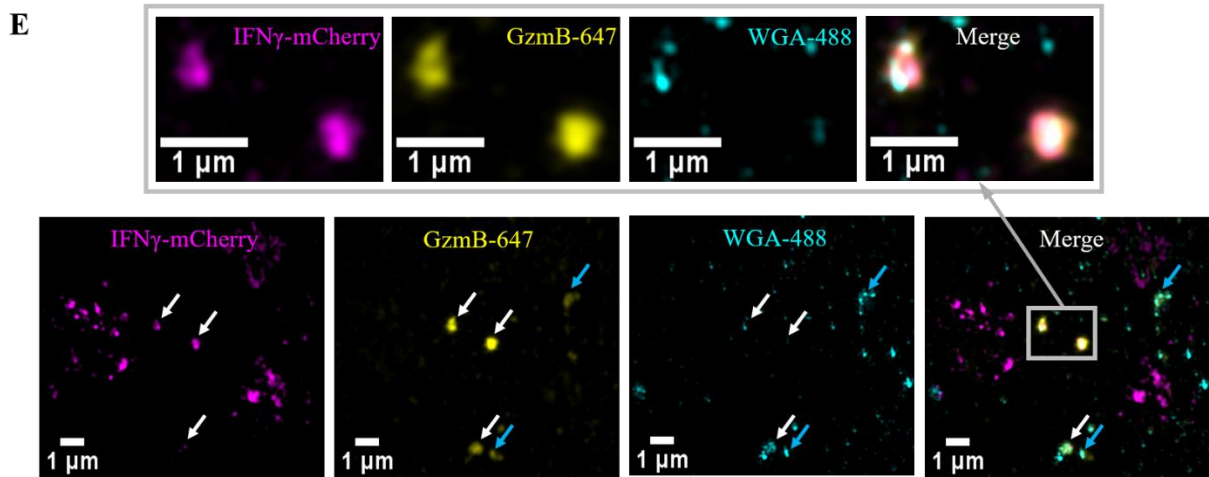


Figure 24. IFN γ and GzmB are released from both SCGs and MCGs.

Days 5-7 GzmB-mTFP KI CTLs were electroporated with *pMax-IFN γ -linker-pHuji*. After 6 h resting, cells were settled down on 30 $\mu\text{g}/\text{mL}$ anti-CD3 ϵ coated coverslips and exocytosis was induced by a change of the extracellular solution from Ca^{2+} free to 10 mM Ca^{2+} . Data were acquired with TIRF-M. **A, B**, Two representative SMAPs were secreted from MCGs. **C**, The percentage of SCGs and MCGs in total secretion events. **D**, Further classification of fused IFN γ and GzmB vesicles. **E**, One example of SMAPs on top of SLBs was shown. Secreted materials on lipids were stained for WGA and GzmB. Colocalization of all three indicated by the white arrow argued for IFN γ being an integral constituent of SMAPs. The colocalization of GzmB and WGA was indicated by the blue array.

Concerning MCGs, we could discriminate IFN γ^+ GzmB $^+$ -MCGs which were depositing double positive vesicles. Complicated cases were double positive (joint) before fusion which did deposit only IFN γ or GzmB MCG, while the other content became lost with the MCG fusion meaning that part of the cargo was not only loaded to included structures of a MCG but also the intravesicular lumen and got lost immediately via fusion. Moreover, as expected IFN γ^+ GzmB $^-$ MCGs and IFN γ^- GzmB $^+$ MCGs exist. The SCG population splits up into 3 subpopulations, namely IFN γ^+ GzmB $^+$ SCG which were double positive before fusion, IFN γ^+ GzmB $^-$ SCG, and IFN γ^- GzmB $^+$ SCGs. Interestingly, IFN γ^+ GzmB $^+$ vesicles accounted for around 70 % of secretion events, which is consistent with the percentage of double-positive vesicles detected with CLEM (Figure 21F). Some of the described populations especially in the group of MCGs were very rare with percentages around or below 1 %. Therefore, we are not sure that these populations are real or if methodological inadequacies as subthreshold fluorescence intensities lead to misinterpretations of results. If these low percentage populations are artifacts, it would mean that MCGs without exception release both IFN γ and GzmB.

Recently, a new class of secretion product of MCGs was identified in CTLs which was named supramolecular-attack-particles (SMAPs) and was believed to be cytotoxic itself since it contained granzyme B (Balint et al. 2020). We wanted to test if SMAPs also contain IFN γ . Therefore, we used a protocol allowing us to identify SMAPs on supported lipid bilayers (SLBs) by specific markers as a carbon-dense shell that specifically could be stained with fluorophore-coupled wheat germ agglutinin (WGA) (Balint et al., 2020). To confirm that IFN γ was also contained in SMAPs, we overexpressed IFN γ -mCherry in CTLs, let them settle down on SLBs, and washed the cells away by intensive rinsing

with cold PBS after 15 min. We expected SMAPs to be resistant to washing and remain on the SLBs. Consequently, we could identify a colocalization of granzyme B, IFN γ , and WGA signals on the SLBs (Figure 24E). Importantly, these results demonstrated that IFN γ was not only released by MCGs but was also a constituent of SMAPs.

3.6 IFN γ release from CTLs is strongly regulated by TCR activation and dependent on the SNARE-associated protein Munc13-4.

3.6.1 IFN γ secretion is abrogated in Munc13-4 deficient CTLs

Munc13-4 is a SNARE-associated protein that mediates the priming process of secretory vesicles in both mouse and human CTLs. Consequently, any release of CG is abrogated but exocytosis of other vesicle types seems to be unaffected in a Munc13-4 KO mouse. Here we compare IFN γ vesicle fusion from CTLs from Munc13-4 KO and WT-mice. From the data that we have collected so far, we assumed that IFN γ vesicle fusion is disturbed in Munc13-4 KO cells. To prove that hypothesis, we quantified the secretion of IFN γ in Munc13-4 KO mice by TIRF and compared the results to WT and Perforin KO mice as controls, from which we know that a cytotoxic defect is independent of disturbed fusion.

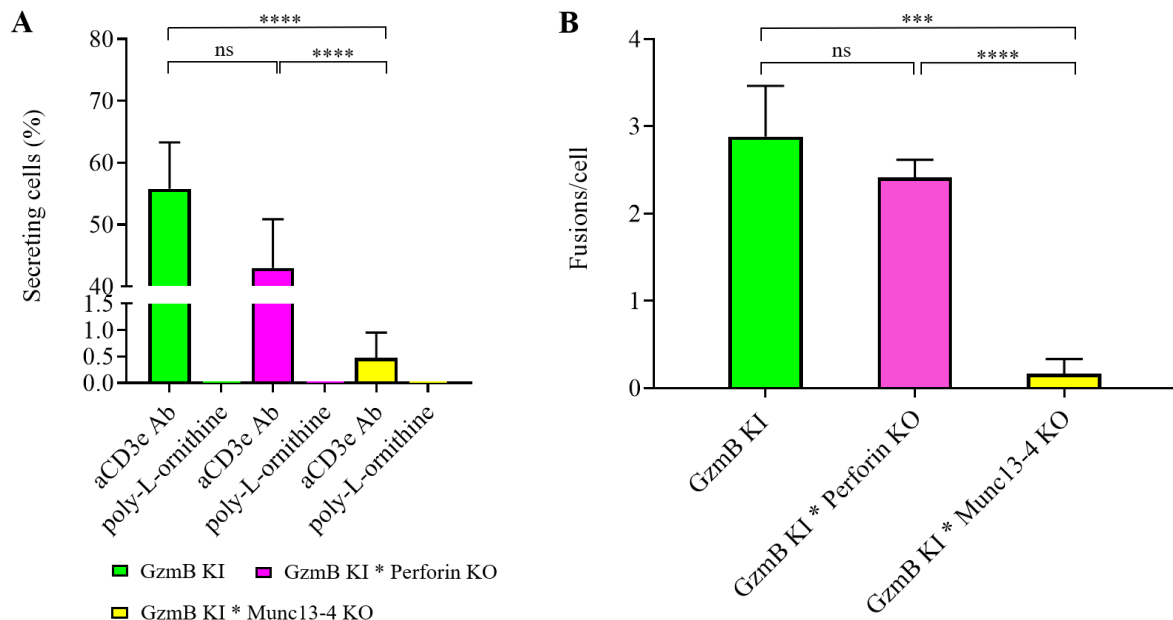


Figure 25. The exocytosis of IFN γ - and GzmB-containing vesicles is abrogated in Munc13-4 KO CTLs.

A-B, Day5 CTLs from GzmB-mTFP KI, Perforin KO \times GzmB-mTFP KI, and Munc13-4 KO \times GzmB-mTFP KI mice were transfected with *pMax-IFN γ -linker-pHuji* (4 μ g DNA/ 3×10^6 cells, 6-9 h resting). The secretion of IFN γ - and GzmB-containing vesicles at the IS was observed in the TIRF field as described previously. **A**, 55.78 ± 7.50 % GzmB-mTFP KI CTLs (N = 4) showed secretion, while 43.78 ± 7.90 % of Perforin KO \times GzmB-mTFP KI CTLs (N = 3) and only 0.5 ± 0.5 % of Munc13-4 KO \times GzmB-mTFP KI CTLs (N = 6) had secretion. **B**, Perforin KO \times GzmB-mTFP KI CTLs had 2.9 ± 0.6 fused vesicles per cell which were comparable to the GzmB-mTFP KI CTLs

which had 2.9 ± 0.2 fused vesicles. While deletion of Munc13-4 almost abrogated the vesicle secretion in Munc13-4 KO \times GzmB-mTFP KI CTLs (0.17 ± 0.17). Data are presented as mean + SEM in the graph. *p*-values are determined by the t-Test.

For these experiments, we overexpressed IFN γ -pHuji in GzmB-mTFP CTLs, GzmB-mTFP KI \times Perforin KO CTLs, and GzmB-mTFP KI \times Munc13-4 KO CTLs. The exocytosis of IFN γ and GzmB at the IS was compromised in GzmB-mTFP KI \times Munc13-4 KO but not in GzmB-mTFP KI and GzmB-mTFP KI \times Perforin KO mice. The number of secreting cells showed no significant decrease among Perforin KO CTLs compared to GzmB-mTFP KI CTLs, but a dramatic decrease in secreting cells in Munc13-4 KO CTLs was observed (Figure 25A, 43.78 %, 55.78 %, and 0.5 % respectively). In terms of secretion events per secreting cell (Figure 25B), it was found that a Munc13-4 KO cell secreted only 0.17 fusion event per cell in contrast to 2.9 resp. 2.4 events per cell for GrzmB KI and Perforin KO respectively. The results let us suggest that the release of IFN γ at the IS required Munc13-4. Since Munc13-4 is believed to be specific for cytotoxicity, both pathways are interconnected.

There is another aspect that can be deduced from the experiments in Figure 25A. For fusion of IFN γ , stimulation of TCR is an indispensable prerequisite, as can be demonstrated by the missing of any secretion, if poly-L-ornithine-coated coverslips were used.

3.6.2 Quantification of IFN γ in the surrounding environment

To date, IFN γ release from CTLs has been determined as secretory events (fusions) from single cells at the IS. This leaves the possibility that we have overlooked some IFN γ secretion that may have occurred outside the IS of a CTL. Therefore, in the last set of experiments, we performed measurements of released IFN γ to test if any constitutive IFN γ component exists that could not be found with TIRF. Therefore, we performed a cytokine beads array assay (LegendPlex™ Multi-Analyte Flow Assay Kit, Mouse Th1 Panel (5-plex) with V-bottom plate) or IFN γ specific ELISA to measure the released IFN γ in the culture medium (supernatant) of CTLs either without restimulation or with restimulation for variable times in 30 μ g/mL anti-CD3 ϵ antibody-coated 96-well plates. We compared the supernatant IFN γ secreted by day0 and day5 C57/6N (WT), Perforin KO, and Munc13-4 KO CTLs. In agreement with our FACS and TIRF data, day0 (naïve) CTLs did not show any secretion of IFN γ neither constitutive (unstimulated) or (re)stimulated during 4 h. Also, day5 CTLs (effector CTLs) did not show any secretion when unstimulated but significant secretion within 4 h of stimulation (Figure 26A). Secretion didn't differ for the three tested animal strains and just a little higher secretion in Perforin KO. More surprising was the finding that Munc13-4 KO did show comparable IFN γ release when compared to WT after 4 h stimulation. From the results of our TIRF experiments, we predicted a reduced IFN γ release. This could mean two things. First, IFN γ is regulatorily secreted outside the IS and this secretion is not Munc13-4 dependent. Secondly, the long restimulation induces mechanisms compensating the Munc13-4 KO effect

we observe in short-term TIRF.

To discriminate between both possibilities, we performed additional measurements with shorter restimulation times (Figure 26B). Indeed, a significant reduction of IFN γ release in Munc13-4 KO cells could be found within the first 60 min.

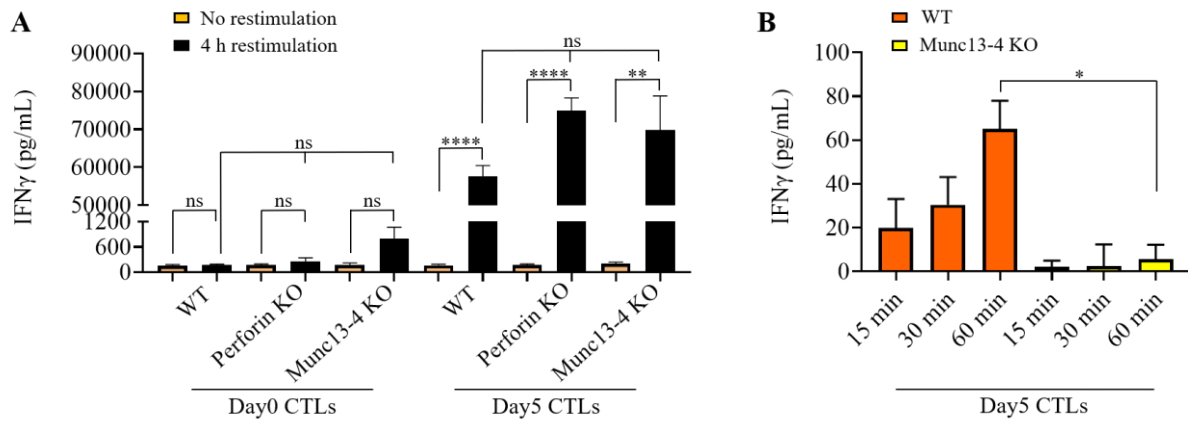


Figure 26. Quantification of IFN γ concentration in CTLs culture.

Day0 or 5 CTLs from WT, Perforin KO, and Munc13-4 KO mice were restimulated or not for different times with plate-bound anti-CD3 ϵ antibody (30 μ g/mL) and the supernatant was collected. **A**, IFN γ analysis was performed in V-bottom 96-well plates by using Mouse Th1 Panel LegendPlexTM 5-Plex. Analysis was performed with a FACS ARIA3 flow cytometer. Data for each condition were collected from 3 independent experiments. **B**, IFN γ analysis was performed by IFN γ ELISA Kit (Legend MAXTM) and analyzed with a M200 microplate reader. Therefore, day5 CTLs were restimulated with 30 μ g/mL anti-CD3 ϵ antibody in a 96-well plate for 15 min, 30 min, and 60 min respectively.

IFN γ concentrations in the culture medium of CTLs are displayed in mean + SEM. The data were subjected to the t-test and One Way Analysis of Variance for comparison. There was a statistical difference in IFN γ secretion between WT and Munc13-4 KO CTLs after 1 h restimulation ($p = 0.015$). ns. $0.05 < p$, * $0.01 < p \leq 0.05$, ** $0.001 < p \leq 0.01$, *** $0.0001 < p \leq 0.001$, **** $p \leq 0.0001$.

4. Discussion

4.1 IFN γ expression and release from CTLs are TCR dependent and its release takes place at the IS

The main objectives of the present work are to investigate IFN γ production, localization, and secretion in CD8+ T-lymphocytes.

Our studies demonstrated a regulated secretion pathway for IFN γ in CD8+ T-lymphocytes. We showed that not only the IFN γ production but also the secretion was regulated by TCR stimulation. Similarly, concerning IFN γ production it was shown earlier that without TCR stimulation, IFN γ could not be detected in naïve CD8+ T-lymphocytes at all and was only mildly expressed in activated CD8+ T-lymphocytes. A small portion of IFN γ +CTLs (usually less than 10%) was probably induced by cytokine stimulation, such as exogenous or autocrine IL-2 in T-lymphocyte culture (Freeman et al., 2012). However, with plate-bound anti-CD3 ϵ stimulation, naïve CD8+ T-lymphocytes could produce a certain amount of IFN γ in a couple of hours. IFN γ production lasted till the end of initial activation and central memory T-lymphocyte (T_{CM}) became formed (Sallusto et al., 1999, 2004). The T_{CM} were re-active upon plate-bound anti-CD3 ϵ restimulation and differentiated into effector (T_E) or effector memory T-lymphocyte (T_{EM}) which could produce a high level of intracellular IFN γ . This considerable intracellular IFN γ got saturated when T_E died and the remaining CTLs differentiated to T_{CM}.

In contrast to the already known fact of receptor-dependent IFN γ production in CTLs, it has not been shown to our knowledge that a significant amount of IFN γ is released only in a regulatory manner and that this release is coupled to the release of cytotoxic substances. We have demonstrated the latter with a combination of microscopic techniques, mainly TIRF-M, colocalization studies with SIM, and biochemical detection of IFN γ (ELISA or multiplex bead assay). From TIRF-M experiments we learned, that IFN γ and GzmB were only secreted by cells with activated TCRs but not from CTLs simply sitting on a poly-L-ornithine-coated surface. Direct measurements of IFN γ release to the medium also showed that IFN γ could only be released after TCR stimulation. Our results not only allow the interpretation that IFN γ is released at the IS by TCR stimulation. Moreover, we also proved, that a robust fraction of IFN γ could be found in the same compartments as GzmB by colocalization studies. The degree of colocalization positively correlated to the strength of restimulation and expression of IFN γ , suggesting that IFN γ uses a similar vesicular trafficking pathway as GzmB in CTLs. The more acute and strong the stimulation was, the more overlap they had. The colocalization in the overexpressing system was comparable with the endogenous system, which suggested that an overexpression artifact can be excluded. The degree of colocalization of IFN γ and GzmB was the same no matter whether CTLs were settled down on poly-L-ornithine or anti-CD3 ϵ coated coverslips (10 min) but increased after 2 h

restimulation, suggesting that the colocalization of IFN γ and GzmB is not dependent of short-time but longer-time TCR stimulation.

Finally, by observing the dynamic secretion of IFN γ and GzmB in GzmB-mTFP KI CTLs with TIRF-M, we found that IFN γ does not only colocalize with GzmB in the same compartments but is also secreted together with GzmB from CTLs at the IS, suggesting that IFN γ shared the similar trafficking and secretion pathway with GzmB in CTLs. Detailed analysis of TIRF data indicated that part of IFN γ was found in MCGs. MCGs are a new class of granules in mice CTLs, which have a different diameter, morphology, protein composition, and killing ability than classical SCGs. Moreover, MCGs are the source of only recently described SMAPs (Balint et al., 2020, Chang et al., 2022). SMAPs, which were discovered in human CTLs and further studied in human NK cells in recent years, were particles with a shell of TSP1 and a core of cytotoxic substances (mainly granzymes, perforin, and serglycin), with cytokines like CCL5 and IFN γ and with autonomous extracellular killing function (Ambrose et al., 2020; Balint et al., 2020).

A further argument for common transport vesicles for IFN γ and cytotoxic substances are results that were obtained with Munc13-4 KO mice. Munc13-4 is a protein participating in CGs trafficking and priming before secretion (Ménager et al., 2007; Dudenhöffer-Pfeifer, 2013). In Munc13-4 KO mice, not only GzmB release was absent but also IFN γ release in both TIRF-M and ELISA assays.

If the observation that IFN γ is secreted at the IS along with cytotoxic agents is correct, there should be a benefit associated with this. The general functions of IFN γ are systemic. Thus, IFN γ acts on macrophages, Th cells, and B cells for which focal release is not necessary. However, it has also been shown, and this is the first function assigned to IFN γ , that activation of IFN γ receptors activates antiviral processes in the corresponding cell (Kang et al., 2018). Perhaps the focally released amount of IFN γ at the IS may be sufficient to activate underlying IFN γ receptors and put the target cell into an antiviral mode regardless of the success of the direct cytotoxic agents. Only in a second step after the so-called detachment of the CTL (Xiao et al., 2017) would IFN γ become released from the dissolving synaptic cleft and become systemically active.

4.2 Implications on familial haemophagocytic lymphohistiocytosis (FHL)

Familial haemophagocytic lymphohistiocytosis (FHL) is a rare (1 patient/100,000-500,000 newborns) autosomal recessive disorder of immune dysregulation associated with uncontrolled activation of immune cells (T-lymphocytes, natural killer cells, B cells, and macrophages) and hypercytokinaemia (Suleman et al., 2021). Five specific genetic defects are having been identified, which account for approximately 90% of all patients. Type 1 is due to an as-yet unidentified gene defect located on

chromosome nine. Type 2 is caused by mutations in the perforin (PRF1) gene, type 3 by mutations in the Munc-13-4 (UNC13D) gene, type 4 by mutations in the STX11 gene, and type 5 due to mutations in the gene encoding syntaxin binding protein 2 (STXBP-2) (Gholam et al., 2011). Common to all of these individual defects is that they lead to drastically reduced cytotoxicity of CTLs, which is why the CTL-based immune defenses of affected carriers are unable to control viral and/or bacterial infections. However, the affected individuals do not suffer primarily from the difficult-to-control infections, but, unexpectedly, from overstimulation of the immune system, as evidenced by the appearance of high concentrations of cytokines and, among them, IFN γ . This phenomenon is called cytokine storm (Zhang et al., 2022). The general activation triggered by the cytokine storm, especially of the non-specific immune system, leads to side effects such as the eponymous hemophagocytic lymphohistiocytosis and other symptoms (high fever, hepato-splenomegaly, cytopenia, hypertriglyceridemia, and hyperferritinemia), which, if left untreated, lead to death in diseased children at an early age (Brisse et al., 2016). The development of the cytokine storm is imagined to be due to the lack of function of cytotoxic cells leading to reduced or missing attenuating signals that limit the cytokine release of e.g., helper cells, but also the IFN γ release of the CTLs themselves. Since CTLs themselves are a major source of IFN γ , and we have shown here that IFN γ secretion continues in a mouse model for FHL2 (Perforin KO), whereas it does not in a mouse model for FHL3 (Munc13-4 KO), one might expect that the exact course of a cytokine storm would occur in FHL2 patients with more elevated IFN γ levels than in FHL3 patients. Unfortunately, because of the small number of cases on FHL, we are not aware of quantitative data supporting our hypotheses. However, we can read that the course of the disease in FHL3 patients is somewhat milder (although also fatal) than in FHL2 patients (Zhang et al., 2020). Nevertheless, in our opinion, it is conceivable that knowledge of the different IFN γ release rates in different FHL types could provide approaches to diagnosis and therapy of the disease.

4.3 IFN γ expression in the endogenous and overexpressing system

IFN γ production is induced by cytokines (mainly IL-12 and IL-18) (Berg et al., 2002) or antigen-peptides (Huse et al., 2008) binding to their receptors on T-lymphocytes in vivo. In this study, endogenous IFN γ was produced by CTLs with anti-CD3 ϵ (re)stimulation, and overexpressing IFN γ was from CTLs transfected with *ifng* constructs: *pMax-ifng-linker-mCherry* or *pMax-ifng-linker-pHuji* under the control of an early and enhancer-promoter, cytomegalovirus (CMV) promoter in vitro (Figure 11). The cloning and expression of human and murine IFN γ cDNA were completed in the early 1980s by Gray & Goeddel (Gray et al., 1982; Gray & Goeddel, 1982 & 1983). They obtain the murine IFN γ cDNA by using RNA from both mitogen-induced murine spleens and the transfected monkey COS-1 cells under the control of the simian virus 40 early promoters. IFN γ cDNA is expressed in *Escherichia coli* under *trp* promoter control. The encoded mature murine IFN γ is 136 AA long, 10 AA shorter than human IFN γ , and showed 40% homologous with human IFN γ . In our experiments, the size of the IFN γ gene was 465 bp. This gene

encoded 155 AA with a predicted molecular weight of 18.9 kDa. The IFN γ protein possesses two different N-glycosylation sites at 38 (Asn-Ser-Ser) and 90 (Asn-Ile-Ser). N-glycosylation is the most common glycosylation which is formed by the attachment of oligosaccharides to a nitrogen atom, usually, the N4 of asparagine residues (Asn), and occurs at specific amino acid motifs Asn-X-Ser/Thr or Asn-X-Cys. In WT CTLs, the overexpressed secretion protein IFN γ -mCherry was extensively expressed from 6 h and displayed three bands on SDS-PAGE and Western blot (Figure 17A), the molecular weight was around 46, 49, and 54 kDa, separately representing 0, 1, and 2 N-glycosylation sites according to the previous study on human IFN γ (PAN et al., 1987). IFN γ -mCherry was a transient stable protein in a narrow time window, it was 100% full length before 8 h and appeared to proteolytic degradation after as it's shown in western blot (Figures 17A, B). To some extent, there was no significant difference in the amount of secretion protein during 6-10 h according to the densitometric analysis from western blotting (Figure 17B) and an extensive colocalization of anti-IFN γ Ab and mCherry signals using immunocytochemistry (Figure 17C, D) in CTLs overexpressing *pMax-ifng-linker-mCherry*. From SIM, no matter in the condition of normal restimulation (10 μ g/mL anti-CD3 ϵ restimulation, 2 h) (Figure 19A, upper channel) and overexpression (2 μ g DNA/ 3×10^6 GzmB-mTFP KI CTL) (Figure 19A, lower channel) or strong restimulation (30 μ g/mL anti-CD3 ϵ restimulation, 4 h) (Figure 19B, upper channel) and overexpression (4 μ g DNA / 3×10^6 GzmB-mTFP KI CTLs) (Figure 19B, lower channel), the colocalization of IFN γ and GzmB in the overexpressing system was equivalent to endogenous expression system (Figures 19 C). Investigating IFN γ trafficking and secretion in an overexpressing system could be taken as the same effect as an endogenous system. Here, we used the overexpressing system in analyzing the IFN γ localization and compartmentalization, observing the dynamic process of IFN γ secretion at the IS.

The IFN γ produced in vitro T-lymphocytes stimulation can be detected long after T-lymphocyte activation ended for it was not significantly consumed by the cells in the culture (Schreiber et al., 1983). In contrast, IFN γ is rarely detected in the circulation of humans or mice undergoing immunologic stimulation. This apparent discrepancy between in vitro and in vivo levels of fluid phase IFN γ is most likely due to the rapid removal of IFN γ from the circulation by IFN γ receptors that are ubiquitously expressed in nearly all cells (Langer & Pestka, 1988).

4.4 IFN γ localization in immune cells

IFN γ localizes together with two of the Rab GTPases, Rab3d and Rab19 at the synapse but shows little overlap with the scattered pool of TNF-containing compartments. Rab3d locates in cytoplasmic microtubules and secretory granules (Valentijn et al., 1996; Pavlos et al., 2011) and Rab19 may locate in the extracellular exosome (Lütcke et al., 1995). In contrast, the SNARE protein syntaxin 6 which locates in trans-Golgi and endosomes (Bock et al., 1996 & 1997), overlaps extensively with TNF-containing

compartments in the cytoplasm but shows little localization together with the synaptic cytokines. These data show that IFN γ localizes together with a different pool of trafficking proteins with TNF α , suggesting that the synaptic and multidirectional secretion pathways use distinct compartments for cytokine release (Huse et al., 2006). In human NK cells, IFN γ and TNF α localize and traffick in different compartments and vesicles that don't overlap with perforin or other late endosome granule markers (Reefman et al., 2010). In murine Sortilin-deficient CTLs, the release of IFN γ was reduced upon infections and in autoimmune colitis, suggesting that sortilin attended the exit of IFN γ from the Golgi apparatus. In WT CTLs, IFN γ from the Golgi was transported to the early endosome, however IFN γ trafficking from the endosomal sorting platform to the plasma membrane proceeded independently of recycling endosomes, and IFN γ remained excluded from late endosomes (Herda, et al., 2012). IFN γ was compartmentalized within SGs and can be released with SGs in response to cell activation in human eosinophils (Carmol, 2018).

We could visualize the IFN γ localization and compartmentalization by SIM by overexpressing an IFN γ -mCherry construct in GzmB-mTFP KI CTLs. Our results, for the first time, showed that IFN γ was extensively colocalized with GzmB-containing vesicles (Figure 19-21), revealing that they shared a common trafficking and secretion pathway in murine CTLs. The colocalization of IFN γ and GzmB increased if cells were upon 2 h restimulation in our experiments (Figure 20B). But the vesicle number of IFN γ or GzmB was comparable among 4 conditions (Figures 20C, D). The re-stimulated CTLs here had stronger fluorescence intensity of IFN γ and fewer healthy cells and more dead cells when compared to not restimulated CTLs. This might be that more short-live effector CTLs were generated after restimulation thus promoting the IFN γ -producing and sorting to the GzmB-containing vesicles. The IFN γ and GzmB-containing compartments in CTLs (Day5) were further observed by CLEM (Figures 21A-C). There were five identified compartments consisting of MVBs, DC with vesicles, DC without vesicles, amorph, and SCGs (Figure 21D). Most MVBs contained only IFN γ except some contained both IFN γ and GzmB, all DC no matter with or without vesicles were IFN γ +GzmB+, most amorphs were IFN γ +GzmB+ and some were only IFN γ +, and only GzmB+ only existed in SCG which also contained a big portion of IFN γ +GzmB+ (Figure 21E). In conclusion, the majority of compartments were IFN γ +GzmB+, the second was IFN γ + and the least was GzmB+ (Figure 21F). The CLEM data again strengthened that IFN γ and GzmB shared the same trafficking compartments thus they probably also shared the secretion pathway in activated murine CTLs.

5. Outlook

Further experiments are required to better understand IFN γ -containing vesicle trafficking and secretion, we can analyze the colocalization of IFN γ with trafficking proteins (such as Rab3d, Rab19, Rab27a, and so on), SNARE-associated proteins (Munc13 and Syt7) and SNAREs (VAMP2/7/8 and SNAP23) at first, and verify Munc13-4 function and the associated protein-protein interactions, from the endosome to vesicle exocytosis. To analyze the colocalization of IFN γ with trafficking molecules, we can perform immunostaining at different time points after T-target cells form conjugates. These different trafficking organelles together with IFN γ can be stained with their fluorescent antibodies. To verify Munc13-4 function on the trafficking and priming process of IFN γ -containing vesicles, we can use a Munc13-4 construct and stain for upstream and downstream proteins which participate in vesicle exocytosis in Munc13-4 KO CTLs.

To clarify whether IFN γ is localized in MCGs, we can overexpress IFN γ -mCherry in GzmB-mTFP KI CTLs, either settle CTLs on anti-CD3 ϵ antibodies-coated coverslips or the sapphire coverslips, and do immunocytochemistry or immunogold staining for WGA, TSP1, and IFN γ , check cells under SIM or CLEM. To further confirm IFN γ is secreted from the MCGs and contained in SMAPs, we can visualize the dynamic secretion of IFN γ at IS between CTLs and the supported lipid bilayer (SLB). For visualizing dynamic IFN γ secretion from MCGs, *pMax-IFN γ -linker-pHuji* will be expressed in CTLs. To confirm IFN γ is on the SMAPs, we can incubate CTLs on the SLB for 1-2 hours, they will secrete endogenous IFN γ on the SLB, then cells are washed away with 4 °C DPBS (1 \times), then we stain the SMAPs on the SLB for WGA, TSP1, and IFN γ .

6. Reference

- Akondy RS, Fitch M, Edupuganti S, Yang S, Kissick HT, Li KW, Youngblood BA, Abdelsamed HA, McGuire DJ, Cohen KW, Alexe G, Nagar S, McCausland MM, Gupta S, Tata P, Haining WN, McElrath MJ, Zhang D, Hu B, Greenleaf WJ, Goronzy JJ, Mulligan MJ, Hellerstein M, Ahmed R (2017) Origin and differentiation of human memory CD8 T cells after vaccination. *Nature* 552: 362-367.
- Alspach E, Lussier DM, Schreiber RD (2019) Interferon γ and its important roles in promoting and inhibiting spontaneous and therapeutic cancer immunity. *Cold Spring Harbor perspectives in biology* 11: a028480.
- Ambrose AR, Hazime KS, Worboys JD, Niembro-Vivanco O, Davis DM (2020) Synaptic secretion from human natural killer cells is diverse and includes supramolecular attack particles. *Proceedings of the National Academy of Sciences* 117: 23717-23720.
- Balaji KN, Schaschke N, Machleidt W, Catalfamo M, Henkart PA (2002) Surface cathepsin B protects cytotoxic lymphocytes from self-destruction after degranulation. *The Journal of experimental medicine*, 196: 493-503.
- Baldini G, Baldini G, Wang G, Weber M, Zweyer M, Bareggi R, Witkin JW, Martelli AM (1998) Expression of Rab3D N135I inhibits regulated secretion of ACTH in AtT-20 cells. *The Journal of cell biology* 140: 305-313.
- Bálint Š, Müller S, Fischer R, Kessler BM, Harkiolaki M, Valitutti S, Dustin ML (2020) Supramolecular attack particles are autonomous killing entities released from cytotoxic T-lymphocytes. *Science* 368: 897-901.
- Betts MR, Koup RA (2004) Detection of T-lymphocyte degranulation: CD107a and b. *Methods in cell biology*. Academic Press 75: 497-512.
- Bhat P, Leggatt G, Waterhouse N, Frazer IH (2017) Interferon- γ derived from cytotoxic lymphocytes directly enhances their motility and cytotoxicity. *Cell death & disease* 8: e2836-e2836.
- Bock JB, Lin RC, Scheller RH (1996) A new syntaxin family member implicated in targeting of intracellular transport vesicles. *Journal of Biological Chemistry*, 271: 17961-17965.
- Bock JB, Klumperman J, Davanger S, Scheller RH (1997) Syntaxin 6 functions in trans-Golgi network vesicle trafficking. *Molecular biology of the cell* 8: 1261-1271.
- Bossi G, Griffiths GM (1999) Degranulation plays an essential part in regulating cell surface expression of Fas ligand in T cells and natural killer cells. *Nature medicine* 5: 90-96.
- Brisse E, Matthys P, Wouters CH (2016) Understanding the spectrum of haemophagocytic lymphohistiocytosis: update on diagnostic challenges and therapeutic options. *British journal of haematology* 174: 175-187.
- Bzeih H (2016) The Role of Synaptobrevin2 in Exo-Endocytosis in Primary Mouse Cytotoxic lymphocytes.
- Carmo LA, Bonjour K, Spencer LA, Weller PF, Melo RC (2018) Single-cell analyses of human eosinophils at high resolution to understand compartmentalization and vesicular trafficking of Interferon-gamma. *Frontiers in immunology* 9: 1542.
- Chang HF, Mannebach S, Beck A, Ravichandran K, Krause E, Frohnweiler K, Fecher-Trost C, Schirra C, Pattu V, Flockerzi V, Rettig J (2018) Cytotoxic granule endocytosis depends on the Flower protein. *Journal of Cell Biology* 217(2): 667-683.
- Chang HF, Schirra C, Ninov M, Hahn U, Ravichandran K, Krause E, Becherer U, Bálint Š, Harkiolaki M, Urlaub H, Valitutti S, Baldari CT, Dustin ML, Jahn R, Rettig J (2022) Identification of distinct cytotoxic granules as the origin of supramolecular attack particles in T lymphocytes. *Nature communications* 13(1): 1-15.
- Chitirala P, Ravichandran K, Galgano D, Sleiman M, Krause E, Bryceson YT, & Rettig J (2019) Cytotoxic granule exocytosis from human cytotoxic T lymphocytes is mediated by VAMP7. *Frontiers in immunology* 10: 1855.
- Costa-Pereira AP, Williams TM, Strobl B, Watling D, Briscoe J, Kerr IM (2002) The antiviral response to gamma Interferon. *Journal of virology*, 76: 9060-9068.
- Cox, M. A., Harrington, L. E., Zajac AJ (2011) Cytokines and the inception of CD8 T-cell responses. *Trends in immunology* 32: 180-186.

- Cruz-Guilloty F, Pipkin ME, Djuretic IM, Levanon D, Lotem J, Lichtenheld MG, Groner Y, Groner Y, Rao A (2009) Runx3 and T-box proteins cooperate to establish the transcriptional program of effector CTLs. *Journal of Experimental Medicine* 206: 51-59.
- Curtsinger JM, Johnson CM, Mescher MF (2003) CD8 T cell clonal expansion and development of effector function require prolonged exposure to antigen, costimulation, and signal 3 cytokine. *The Journal of Immunology* 171: 5165-5171.
- Curtsinger JM, Valenzuela JO, Agarwal P, Lins D, Mescher MF (2005). Cutting edge: type I IFNs provide a third signal to CD8 T cells to stimulate clonal expansion and differentiation. *The Journal of Immunology* 174: 4465-4469.
- Czarniecki CW, Sonnenfeld G (1993) Interferon-gamma and resistance to bacterial infections. *Apmis* 101: 1-17.
- Deeths MJ, Kedl RM, & Mescher MF (1999) CD8⁺ T cells become nonresponsive (anergic) following activation in the presence of costimulation. *The Journal of Immunology* 163: 102-110.
- Dudenhöffer-Pfeifer M, Schirra C, Pattu V, Halimani M, Maier-Peuschel M, Marshall MR, Matti U, Becherer U, Dirks J, Jung M, Lipp P, Hoth M, Sester M, Krause E, Rettig J (2013) Different Munc13 isoforms function as priming factors in lytic granule release from murine cytotoxic T lymphocytes. *Traffic* 14: 798-809.
- Dupuis M, Schaerer E, Krause KH, Tschopp J (1993) The calcium-binding protein calreticulin is a major constituent of cytotoxic granules in cytolytic T lymphocytes. *The Journal of experimental medicine* 177: 1-7.
- Dustin ML, Chakraborty AK, & Shaw AS (2010) Understanding the structure and function of the immunological synapse. *Cold Spring Harbor perspectives in biology* 2: a002311.
- Elstak ED, Neeft M, Nehme NT, Voortman J, Cheung M, Goodarzifard M, Gerritsen HC, van Bergen en Henegouwen PMP, Callebaut I, de Saint Basile G, Van Der Sluijs P (2011) The munc13-4-rab27 complex is specifically required for tethering secretory lysosomes at the plasma membrane. *Blood, The Journal of the American Society of Hematology* 118: 1570-1578.
- Feldmann J, Callebaut I, Raposo G, Certain S, Bacq D, Dumont C, Lambert N, Ouachée-Chardin M, Chedeville G, Tamary H, Minard-Colin V, Vilmer E, Blanche S, Le Deist F, Fischer A, Basile G, de Saint Basile G (2003) Munc13-4 is essential for cytotoxic granules fusion and is mutated in a form of familial hemophagocytic lymphohistiocytosis (FHL3). *Cell* 115: 461-473.
- Fischer A, Latour S, de Saint Basile G (2007) Genetic defects affecting lymphocyte cytotoxicity. *Current opinion in immunology* 19: 348-353.
- Froelich CJ, Orth K, Turbov J, Seth P, Gottlieb R, Babior B, Shah GM, Bleackley RC, Dixit VM, Hanna W (1996) New paradigm for lymphocyte granule-mediated cytotoxicity: target cells bind and internalize granzyme B, but an endosomolytic agent is necessary for cytosolic delivery and subsequent apoptosis. *Journal of Biological Chemistry* 271: 29073-29079.
- Freeman BE, Hammarlund E, Raué HP, Slifka MK (2012) Regulation of innate CD8⁺ T-cell activation mediated by cytokines. *Proceedings of the National Academy of Sciences* 109: 9971-9976.
- Fuchs YF, Sharma V, Eugster A, Kraus G, Morgenstern R, Dahl A, Reinhardt S, Petzold A, Lindner A, Löbel D, Bonifacio, E. (2019). Gene expression-based identification of antigen-responsive CD8⁺ T cells on a single-cell level. *Frontiers in immunology* 10: 2568.
- Fukuda M (1991) Lysosomal membrane glycoproteins: structure, biosynthesis, and intracellular trafficking. *The Journal of biological chemistry* 266: 21327-21330.
- Gao J, Shi LZ, Zhao H, Chen J, Xiong L, He Q, Chen T, Roszik J, Bernatchez C, Woodman S, Chen PL, 3 Hwu P, Allison J, Futreal A, Wargo J, Sharma, P (2016) Loss of IFN- γ pathway genes in tumor cells as a mechanism of resistance to anti-CTLA-4 therapy. *Cell*, 167: 397-404.
- Gerber SA, Sedlacek AL, Cron KR, Murphy SP, Frelinger JG, & Lord EM (2013) IFN- γ mediates the antitumor effects of radiation therapy in a murine colon tumor. *The American journal of pathology* 182: 2345-2354.
- Gholam C, Grigoriadou S, Gilmour KC, Gaspar HB (2011) Familial haemophagocytic lymphohistiocytosis: advances in the genetic basis, diagnosis and management. *Clinical & Experimental Immunology* 163: 271-283.
- Gray PW, Leung DW, Pennica D, Yelverton E, Najarian R, Simonsen CC, Derynck R, Sherwood PJ, Wallace DM, Berger SL, Levinson AD, Goeddel DV (1982) Expression of human immune Interferon cDNA in *E. coli* and monkey cells. *Nature* 295: 503-508.

- Gray PW, Goeddel DV (1982) Structure of the human immune Interferon gene. *Nature* 298: 859-863.
- Gray PW, Goeddel DV (1983) Cloning and expression of murine immune Interferon cDNA. *Proceedings of the National Academy of Sciences* 80: 5842-46
- Griffiths GM, Tsun A, Stinchcombe JC (2010) The immunological synapse: a focal point for endocytosis and exocytosis. *Journal of Cell Biology* 189: 399-406.
- Halimani M, Pattu V, Marshall MR, Chang HF, Matti U, Jung M, Becherer U, Krause E, Hoth M, Schwarz EC, Rettig J (2014) Syntaxin11 serves as at-SNARE for the fusion of cytotoxic granules in human cytotoxic T lymphocytes. *European journal of immunology* 44: 573-584.
- Hamann D, Baars PA, Rep MH, Hooibrink B, Kerkhof-Garde SR, Klein MR, Lier, RAV (1997) Phenotypic and functional separation of memory and effector human CD8+ T cells. *The Journal of experimental medicine* 186: 1407-1418.
- Haring JS, Corbin GA, & Harty JT (2005) Dynamic regulation of IFN- γ signaling in antigen-specific CD8+ T cells responding to infection. *The Journal of Immunology* 174: 6791-6802.
- Herda S, Raczkowski F, Mittrücker HW, Willimsky G, Gerlach K, Kühl AA, Breiderhoff T, Willnow TE, Dorken B, Höpken UE, Rehm A (2012) The sorting receptor Sortilin exhibits a dual function in exocytic trafficking of Interferon- γ and granzyme A in T-lymphocytes. *Immunity* 37: 854-866.
- Hu X, Ivashkiv LB (2009) Cross-regulation of signaling pathways by Interferon- γ : implications for immune responses and autoimmune diseases. *Immunity* 31: 539-550.
- Hunt SD, Stephens DJ (2011) The role of motor proteins in endosomal sorting. *Biochemical Society Transactions* 39: 1179-1184.
- Huppa JB, Davis MM (2003) T-lymphocyte-antigen recognition and the immunological synapse. *Nature Reviews Immunology* 3: 973-983.
- Huse M, Lillemeier BF, Kuhns MS, Chen DS, Davis MM (2006) T cells use two directionally distinct pathways for cytokine secretion. *Nature immunology* 7: 247-255.
- Huse M, Quann EJ, Davis MM (2008) Shouts, whispers and the kiss of death: directional secretion in T cells. *Nature immunology* 9: 1105-1111.
- Huster KM, Busch V, Schiemann M, Linkemann K, Kerksiek KM, Wagner H, Busch DH (2004) Selective expression of IL-7 receptor on memory T cells identifies early CD40L-dependent generation of distinct CD8+ memory T cell subsets. *Proceedings of the National Academy of Sciences* 101: 5610-5615.
- Ihle JN, Witthuhn BA, Quelle FW, Yamamoto K, Thierfelder WE, Kreider B, Silvennoinen O (1994). Signaling by the cytokine receptor superfamily: JAKs and STATs. *Trends in biochemical sciences* 19: 222-227.
- Ivashkiv LB (2018) IFN γ : signalling, epigenetics and roles in immunity, metabolism, disease and cancer immunotherapy. *Nature Reviews Immunology* 18: 545-558.
- Jameson SC, Masopust D (2009) Diversity in T cell memory: an embarrassment of riches. *Immunity* 31: 859-871.
- Janeway Jr CA, Travers P, Walport M, Shlomchik MJ (2001) The complement system and innate immunity. *Immunobiology: The Immune System in Health and Disease*. 5th edition. Garland Science.
- Rettig J, Stevens DR (2017) Synaptic Transmission in the Immune System. *e-Neuroforum* 23: A167-A174.
- Johnson JL, Hong H, Monfregola J, Kiosses WB, Catz SD (2011) Munc13-4 restricts motility of Rab27a-expressing vesicles to facilitate lipopolysaccharide-induced priming of exocytosis in neutrophils. *Journal of Biological Chemistry* 286: 5647-5656.
- Jolly C, Sattentau QJ (2007) Regulated secretion from CD4+ T cells. *Trends in immunology* 28: 474-481.
- Kaech SM, Wherry EJ, & Ahmed R (2002) Effector and memory T-lymphocyte differentiation: implications for vaccine development. *Nature Reviews Immunology*, 2: 251-262.
- Kaech SM, Wherry EJ (2007) Heterogeneity and cell-fate decisions in effector and memory CD8+ T-lymphocyte differentiation during viral infection. *Immunity* 27: 393-405.
- Kambayashi T, Assarsson E, Lukacher AE, Ljunggren HG, Jensen PE (2003) Memory CD8+ T cells provide an early source of IFN- γ . *The Journal of Immunology* 170: 2399-2408.
- Kang S, Brown HM, Hwang S (2018) Direct antiviral mechanisms of interferon-gamma. *Immune network* 18.

- Kay JG, Murray RZ, Pagan JK, Stow JL (2006) Cytokine secretion via cholesterol-rich lipid raft-associated SNAREs at the phagocytic cup. *Journal of Biological Chemistry*, 281: 11949-11954.
- Knop M, Aareskjold E, Bode G, Gerke V (2004) Rab3D and annexin A2 play a role in regulated secretion of vWF, but not tPA, from endothelial cells. *The EMBO Journal* 23: 2982-2992.
- Krzewski K, Gil-Krzewska A, Watts J, Stern JN, Strominger JL (2011). VAMP4-and VAMP7 expressing vesicles are both required for cytotoxic granule exocytosis in NK cells. *European journal of immunology* 41: 3323-3329.
- Krzewski K, Coligan JE (2012) Human NK cell cytotoxic granules and regulation of their exocytosis. *Frontiers in immunology* 3: 335.
- Krummel M, Mahale JN, Uhl LF, Hardison EA, Mujal AM, Mazet JM, Weber RJ, Gartner ZJ, Gérard A (2018) Paracrine costimulation of IFN- γ signaling by integrins modulates CD8 T-lymphocyte differentiation. *Proceedings of the National Academy of Sciences* 115: 11585-11590.
- Kuramochi M, Fukuhara H, Nobukuni T, Kanbe T, Maruyama T, Ghosh HP, Pletcher M, Isomura M, Onizuka M, Kitamura T, Sekiya T, Reeves RH, Murakami Y (2001) TSLC1 is a tumor-suppressor gene in human non-small-cell lung cancer. *Nature genetics* 27: 427-430.
- Lanzavecchia A, Sallusto F (2000) Dynamics of T lymphocyte responses: intermediates, effectors, and memory cells. *Science* 290: 92-97.
- Larkin JM, Woo B, Balan V, Marks DL, Oswald BJ, LaRusso NF, McNiven MA (2000) Rab3D, a small GTP-binding protein implicated in regulated secretion, is associated with the transcytotic pathway in rat hepatocytes. *Hepatology* 32: 348-356.
- Lieberman J (2003) The ABCs of granule-mediated cytotoxicity: new weapons in the arsenal. *Nature Reviews Immunology* 3: 361-370.
- Liu H, Golji J, Brodeur LK, Chung FS, Chen JT, deBeaumont RS, Bullock CP, Jones MD, Kerr G, Li L, Rakiec DP, Schlabach MR, Sovath S, Growney JD, Pagliarini RA, Ruddy DA, MacIsaac KD, Korn JM, McDonald ER (2019) Tumor-derived IFN triggers chronic pathway agonism and sensitivity to ADAR loss. *Nature medicine* 25: 95-102.
- Lock JG, Hammond LA, Houghton F, Gleeson PA, Stow JL (2005) E-cadherin transport from the trans-Golgi network in tubulovesicular carriers is selectively regulated by golgin-97. *Traffic*, 6: 1142-1156.
- Luo W, Yu CH, Lieu ZZ, Allard J, Mogilner A, Sheetz MP, Bershadsky AD (2013) Analysis of the local organization and dynamics of cellular actin networks. *Journal of Cell Biology* 202: 1057-1073.
- Luo XY, Takahara T, Kawai K, Fujino M, Sugiyama T, Tsuneyama K, Tsukada K, Nakae S, Zhong L, Li XK (2013) IFN- γ deficiency attenuates hepatic inflammation and fibrosis in a steatohepatitis model induced by a methionine-and choline-deficient high-fat diet. *American Journal of Physiology-Gastrointestinal and Liver Physiology* 305: G891-G899.
- Lütcke A, Olkkonen VM, Dupree P, Lütcke H, Simons K, Zerial M (1995) Isolation of a murine cDNA clone encoding Rab 19, a novel tissue-specific small GTPase. *Gene* 155: 257-260.
- Manders EMM, Verbeek FJ, Aten JA (1993) Measurement of co-localization of objects in dual-colour confocal images. *Journal of microscopy*, 169: 375-382.
- Maraskovsky E, Chen WF, Shortman K (1989) IL-2 and IFN-gamma are two necessary lymphokines in the development of cytolytic T cells. *The Journal of Immunology* 143: 1210-1214.
- Marcet-Palacios M, Odemuyiwa SO, Coughlin JJ, Garofoli D, Ewen C, Davidson CE, Ghaffaria M, Kanec KP, Lacya P, Logan MR, Befusa AD, Bleackley RC, & Moqbel R (2008) Vesicle-associated membrane protein 7 (VAMP-7) is essential for target killing in a natural killer cell line. *Biochemical and biophysical research communications* 366: 617-623.
- Matti U, Pattu V, Halimani M, Schirra C, Krause E, Liu Y, Weins L, Chang HF, Guzman R, Olausson J, Freichel M, Schmitz F, Pasche M, Becherer U, Bruns D, Rettig J (2013) Synaptobrevin2 is the v-SNARE required for cytotoxic T-lymphocyte lytic granule fusion. *Nature communications* 4: 1-8.
- Masopust D, Vezys V, Marzo AL, Lefrançois L (2001) Preferential localization of effector memory cells in nonlymphoid tissue. *Science* 291: 2413-2417.
- Ménager MM, Ménasché G, Romao M, Knapnougel P, Ho CH, Garfa M, Raposo G, Feldmann J, Fischer A, de Saint Basile G (2007) Secretory cytotoxic granule maturation and exocytosis require the effector protein hMunc13-4. *Nature immunology* 8: 257-267.
- Merino-Gracia J, García-Mayoral MF, Rapali P, Valero RA, Bruix M, Rodríguez-Crespo I (2015) DYNLT (Tctex-1) forms a tripartite complex with dynein intermediate chain and RagA, hence

- linking this small GTPase to the dynein motor. *The FEBS Journal* 282: 3945-3958.
- Metkar SS, Wang B, Aguilar-Santelises M, Raja SM, Uhlin-Hansen L, Podack E, Trapani JA, Froelich, CJ (2002) Cytotoxic cell granule-mediated apoptosis: perforin delivers granzyme B-serglycin complexes into target cells without plasma membrane pore formation. *Immunity* 16: 417-428.
- Miller JD, van der Most RG, Akondy RS, Glidewell JT, Albott S, Masopust D, Murali-Krishna K, Mahar PL, Edupuganti S, Lalor S, Germon S, Del Rio C, Mulligan MJ, Staprans SI, Altman JD, Feinberg MB, Ahmed R (2008) Human effector and memory CD8⁺ T cell responses to smallpox and yellow fever vaccines. *Immunity* 28: 710-722.
- Mimura K, Teh JL, Okayama H, Shiraishi K, Kua LF, Koh V, Smoot DT, Ashktorab H, Oike T, Suzuki Y, Fazreen Z, Asuncion BR, Shabbir A, Yong WP, So J, Soong R, Kono K (2018) PD-L1 expression is mainly regulated by Interferon-gamma associated with JAK-STAT pathway in gastric cancer. *Cancer science* 109: 43-53.
- Moqbel R, Coughlin JJ (2006) Differential secretion of cytokines. *Science's STKE* 2006: pe26-pe26.
- Munder M, Mallo M, Eichmann K, Modolell M (1998) Murine macrophages secrete Interferon γ upon combined stimulation with interleukin (IL)-12 and IL-18: a novel pathway of autocrine macrophage activation. *The Journal of experimental medicine* 187: 2103-2108.
- Nakamura N, Fukuda H, Kato A, Hirose S (2005) MARCH-II is a syntaxin-6-binding protein involved in endosomal trafficking. *Molecular biology of the cell*, 16:1696-1710.
- Paley MA, Kroy DC, Odorizzi PM, Johnnidis JB, Dolfi DV, Barnett BE, Bikoff EK, Robertson EJ, Lauer GM, Reiner SL, Wherry EJ (2012) Progenitor and terminal subsets of CD8⁺ T cells cooperate to contain chronic viral infection. *Science*, 338: 1220-1225.
- Pavlos NJ, Cheng TS, Qin A, Ng PY, Feng HT, Ang ES, Carrello A, Sung CH, Jahn R, Zheng MH, Xu J (2011) Tctex-1, a novel interaction partner of Rab3D, is required for osteoclastic bone resorption. *Molecular and cellular biology* 31: 1551-1564.
- Pavlos NJ, Xu J, Riedel D, Yeoh JS, Teitelbaum SL, Papadimitriou JM, Jahn R, Ross FP, Zheng MH (2005) Rab3D regulates a novel vesicular trafficking pathway that is required for osteoclastic bone resorption. *Molecular and cellular biology* 25: 5253-5269.
- Perdomo-Celis F, Tabora NA, Rugeles MT (2019) CD8⁺ T-cell response to HIV infection in the era of antiretroviral therapy *Frontiers in immunology* 10: 1896.
- Peters PJ, Borst J, Oorschot V, Fukuda M, Krähenbühl O, Tschopp J, Slot JW, Geuze HJ (1991). Cytotoxic T lymphocyte granules are secretory lysosomes, containing both perforin and granzymes. *The Journal of experimental medicine* 173: 1099-1109.
- Poggi A, Giuliani M (2016) Mesenchymal stromal cells can regulate the immune response in the tumor microenvironment. *Vaccines* 4: 41.
- Pollard AJ, Bijker EM (2021) A guide to vaccinology: from basic principles to new developments. *Nature Reviews Immunology*, 21: 83-100.
- Pollizzi KN, Powell JD (2014) Integrating canonical and metabolic signalling programmes in the regulation of T cell responses. *Nature Reviews Immunology* 14: 435-446.
- Qu B, Pattu V, Junker C, Schwarz EC, Bhat SS, Kummerow C, Marshall M, Matti U, Neumann F, Pfreundschuh M, Becherer U, Rieger H, Rettig J, Hoth M (2011) Docking of cytotoxic granules at the immunological synapse in human CTL requires Vti1b-dependent pairing with CD3 endosomes. *The Journal of Immunology* 186: 6894-6904.
- Reefman E, Kay JG, Wood SM, Offenhäuser C, Brown DL, Roy S, Stanley AC, Low PC, Manderson AP, Stow JL (2010) Cytokine secretion is distinct from secretion of cytotoxic granules in NK cells. *The Journal of Immunology* 184: 4852-4862.
- Reinhardt RL, Khoruts A, Merica R, Zell T, & Jenkins MK (2001) Visualizing the generation of memory CD4 T-lymphocytes in the whole body. *Nature* 410: 101-105.
- Rhein BA, Powers LS, Rogers K, Anantpadma M, Singh BK, Sakurai Y, Bair T, Miller-Hunt C, Sinn P, Davey RA, Monick MM, Maury W (2015) Interferon- γ inhibits Ebola virus infection. *PLoS pathogens* 11: e1005263.
- Riggs KA, Hasan N, Humphrey D, Raleigh C, Nevitt C, Corbin D, Hu C (2012) Regulation of integrin endocytic recycling and chemotactic cell migration by syntaxin 6 and VAMP3 interaction. *Journal of cell science* 125: 3827-3839.
- Sallusto F, Geginat J, Lanzavecchia A (2004) Central memory and effector memory T-lymphocyte subsets: function, generation, and maintenance. *Annual review of immunology* 22: 745.

- Sallusto F, Lenig D, Förster R, Lipp M, Lanzavecchia A (1999) Two subsets of memory T lymphocytes with distinct homing potentials and effector functions. *Nature* 401: 708-712.
- Sánchez-Díaz R, Blanco-Dominguez R, Lasarte S, Tsilingiri K, Martín-Gayo E, Linillos-Pradillo B, de la Fuente H, Sánchez-Madrid F, Nakagawa R, Toribio ML, Martín P (2017) Thymus-derived regulatory T cell development is regulated by C-type lectin-mediated BIC/microRNA 155 expression. *Molecular and cellular biology* 37: e00341-16.
- Sanderson NSR, Puntel M, Kroeger KM, Bondale NS, Swerdlow M, Iranmanesh N, Yagita H, Ibrahim A, Castro MG, Lowenstein PR (2012) Cytotoxic immunological synapses do not restrict the action of Interferon- γ to antigenic target cells. *Proceedings of the National Academy of Sciences* 109: 7835-7840.
- Schluter OM, Khvotchev M, Jahn R, Sudhof TC (2002) Localization versus function of Rab3 proteins: evidence for a common regulatory role in controlling fusion. *Journal of Biological Chemistry* 277: 40919-40929.
- Schroder K, Hertzog PJ, Ravasi T, Hume DA (2004) Interferon- γ : an overview of signals, mechanisms and functions. *Journal of leukocyte biology*, 75: 163-189.
- Shtrichman R, Samuel CE (2001) The role of gamma Interferon in antimicrobial immunity. *Current opinion in microbiology* 4: 251-259.
- Siegel JP (1988) Effects of Interferon- γ on the activation of human T lymphocytes. *Cellular immunology*, 111: 461-472.
- Sleiman M, Stevens DR, Chitirala P, Rettig J (2020) Cytotoxic granule trafficking and fusion in synaptotagmin7-deficient cytotoxic T-lymphocytes. *Frontiers in immunology* 11: 1080.
- Stanley AC, Lacy P (2010) Pathways for cytokine secretion. *Physiology* 25: 218-229.
- Stenger S, Hanson DA, Teitelbaum R, Dewan P, Niazi KR, Froelich CJ, Ganz T, Thoma-Uszynski S, Melian A, Bogdan C, Porcelli SA, Bloom BR, Krensky AM, Modlin RL (1998) An antimicrobial activity of cytolytic T cells mediated by granulysin. *Science* 282: 121-125.
- Stemberger C, Huster KM, Koffler M, Anderl F, Schiemann M, Wagner H, Busch DH (2007) A single naive CD8⁺ T cell precursor can develop into diverse effector and memory subsets. *Immunity* 27: 985-997.
- Stinchcombe JC, Majorovits E, Bossi G, Fuller S, Griffiths GM (2006) Centrosome polarization delivers secretory granules to the immunological synapse. *Nature* 443: 462-465.
- Stinchcombe JC, Griffiths GM (2007) Secretory mechanisms in cell-mediated cytotoxicity. *Annual Review of Cell and Developmental Biology* 23: 495-517.
- Stinchcombe JC, Salio M, Cerundolo V, Pende D, Arico M, Griffiths GM (2011) Centriole polarisation to the immunological synapse directs secretion from cytolytic cells of both the innate and adaptive immune systems. *BMC biology* 9: 1-8.
- Stow JL, Manderson AP, Murray RZ (2006) SNAREing immunity: the role of SNAREs in the immune system. *Nature Reviews Immunology* 6: 919-929.
- Stow JL, Low PC, Offenhäuser C, Sangermani D (2009) Cytokine secretion in macrophages and other cells: pathways and mediators. *Immunobiology* 214: 601-612.
- Suleman N, Ozdemirli M, Weisman D (2021) Lamotrigine-associated hemophagocytic lymphohistiocytosis. *BMJ Case Reports CP* 14: e238183.
- Tewari K, Nakayama Y, Suresh M (2007) Role of direct effects of IFN- γ on T cells in the regulation of CD8 T cell homeostasis. *The Journal of Immunology* 179: 2115-2125.
- Tham EL, Shrikant P, Mescher MF (2002) Activation-induced nonresponsiveness: a Th-dependent regulatory checkpoint in the CTL response. *The Journal of Immunology* 168: 1190-1197.
- Valentijn JA, Sengupta D, Gumkowski FD, Tang LH, Konieczko EM, Jamieson JD (1996) Rab3D localizes to secretory granules in rat pancreatic acinar cells. *European journal of cell biology* 70: 33-41.
- Villarino AV, Kanno Y, O'Shea JJ (2017) Mechanisms and consequences of Jak-STAT signaling in the immune system. *Nature immunology* 18: 374-384.
- Weninger W, Manjunath N, Von Andrian UH (2002) Migration and differentiation of CD8⁺ T-lymphocytes. *Immunological reviews* 186: 221-233.
- Wheelock EF (1965) Interferon-like virus-inhibitor induced in human leukocytes by phytohemagglutinin. *Science* 149: 310-311.
- Wherry EJ, Ahmed R (2004) Memory CD8 T-lymphocyte differentiation during viral infection. *Journal*

- of virology, 78: 5535-5545.
- Whitmire JK, Tan JT, Whitton, JL (2005) Interferon- γ acts directly on CD8+ T cells to increase their abundance during virus infection. *The Journal of experimental medicine* 201: 1053-1059.
- Williams MA, Bevan MJ (2007) Effector and memory CTL differentiation. *Annual review of immunology* 25: 171-192.
- Wolint P, Betts MR, Koup RA, Oxenius A (2004) Immediate cytotoxicity but not degranulation distinguishes effector and memory subsets of CD8+ T cells. *The Journal of experimental medicine* 199: 925-936.
- Xiao J, Yordanova Z, Miao M (2017) 2nd international symposium on phytochemicals in medicine and food (2-ISPMF). *Phytochemistry Reviews* 16: 375-377.
- Yiu HH, Graham AL, Stengel RF (2012) Dynamics of a cytokine storm. *PLOS ONE* 7: e45027.
- Zhang HQ, Yang SW, Fu YC, Chen MC, Yang CH, Yang MH, Liu XD, He QN, Jiang H, Zhao MY (2022) Cytokine storm and targeted therapy in hemophagocytic lymphohistiocytosis. *Immunologic Research*: 1-12.
- Zhang N, Bevan MJ (2011) CD8+ T-lymphocytes: foot soldiers of the immune system. *Immunity* 35: 161-168.
- Zhang J, Sun Y, Shi X, Zhang R, Wang Y, Xiao J, Cao J, Gao Z, Wang J, Wu L, Wei W, Wang Z (2020) Genotype characteristics and immunological indicator evaluation of 311 hemophagocytic lymphohistiocytosis cases in China. *Orphanet journal of rare diseases* 15: 1-13.

7. Publication

1. **Li X**, Schirra C, Pattu V, Chang HF, Ravichandran K, Becherer U, Krause E (2023) Interferon-gamma trafficking and secretion in CD8+ T lymphocytes, in preparation.
2. Estl M, Blatt P, **Li X**, Becherer U, Chang HF, Rettig J, Pattu V (2020) Various stages of immune synapse formation are differently dependent on the strength of the TCR stimulus. *International journal of molecular sciences* 21: 2475.

8. Curriculum Vitae

Aus datenschutzrechtlichen Gründen wird der Lebenslauf in der elektronischen Fassung der Dissertation nicht veröffentlicht.

For data protection reasons, the curriculum vitae is not published in the electronic version of the dissertation.